

INFORMATION TO USERS

This manuscript has been reproduced from the microfilm master. UMI films the text directly from the original or copy submitted. Thus, some thesis and dissertation copies are in typewriter face, while others may be from any type of computer printer.

The quality of this reproduction is dependent upon the quality of the copy submitted. Broken or indistinct print, colored or poor quality illustrations and photographs, print bleedthrough, substandard margins, and improper alignment can adversely affect reproduction.

In the unlikely event that the author did not send UMI a complete manuscript and there are missing pages, these will be noted. Also, if unauthorized copyright material had to be removed, a note will indicate the deletion.

Oversize materials (e.g., maps, drawings, charts) are reproduced by sectioning the original, beginning at the upper left-hand corner and continuing from left to right in equal sections with small overlaps. Each original is also photographed in one exposure and is included in reduced form at the back of the book.

Photographs included in the original manuscript have been reproduced xerographically in this copy. Higher quality 6" x 9" black and white photographic prints are available for any photographs or illustrations appearing in this copy for an additional charge. Contact UMI directly to order.



**Bell & Howell Information and Learning
300 North Zeeb Road, Ann Arbor, MI 48106-1346 USA
800-521-0600**

**An Investigation to Predict the Sub-Atmospheric
Pressure on High Spillways**

Hassan Kiamanesh

A Thesis
in
The Department
of
Civil Engineering

Presented in Partial Fulfillment of the Requirements
for the Degree of Doctor of Philosophy at
Concordia University
Montreal, Quebec, Canada

May 1996

© Hassan Kiamanesh, 1996



National Library
of Canada

Acquisitions and
Bibliographic Services

395 Wellington Street
Ottawa ON K1A 0N4
Canada

Bibliothèque nationale
du Canada

Acquisitions et
services bibliographiques

395, rue Wellington
Ottawa ON K1A 0N4
Canada

Your file Votre référence

Our file Notre référence

The author has granted a non-exclusive licence allowing the National Library of Canada to reproduce, loan, distribute or sell copies of this thesis in microform, paper or electronic formats.

The author retains ownership of the copyright in this thesis. Neither the thesis nor substantial extracts from it may be printed or otherwise reproduced without the author's permission.

L'auteur a accordé une licence non exclusive permettant à la Bibliothèque nationale du Canada de reproduire, prêter, distribuer ou vendre des copies de cette thèse sous la forme de microfiche/film, de reproduction sur papier ou sur format électronique.

L'auteur conserve la propriété du droit d'auteur qui protège cette thèse. Ni la thèse ni des extraits substantiels de celle-ci ne doivent être imprimés ou autrement reproduits sans son autorisation.

0-612-44872-X

Canada

ABSTRACT

AN INVESTIGATION TO PREDICT THE SUBATMOSPHERIC PRESSURE ON HIGH SPILLWAYS

Hassan Kiamanesh, Ph. D.
Concordia University. 1996

In the past few decades, spillways have attraction significant as flow measuring devices as well as for release of flood discharges for dams.

Severe cavitation damage has occurred on many high spillways around the world, including Russia, Pakistan, Venezuela, and Iran. In Iran, this phenomena caused serious damage to the Karun I dam spillway. Many studies and investigations related to cavitation effects were performed on different scale models and prototypes.

Presently, standard shape spillways are designed based on previous experiences. Every case is subjected to a physical model study. It seemed necessary to systematize the evaluation of the flow field and the pressure distribution on the crests of spillways. The investigation of the subatmospheric pressure which is the main cause of cavitation was primary objective of the thesis. Consequently, a functional numerical model for design purposes was developed. Since viscous effects can be negligible, a two-dimensional irrotational flow was assumed. Comparable results between numerical and experimental spillway models validated this assumption.

The developed numerical model was based on Navier-Stokes equations and the Bernoulli equation for Boundary-Fitted Curvilinear Coordinates (BFCC). The discretizations and computations were executed on a fixed, square grid regardless of the shape of the physical boundary. Equations were discretized using the finite difference method. The results show that the BFCC system is capable of treating Navier-Stokes equations for a wide range of Reynolds numbers with free surface boundary.

In order to validate the numerical results of the problem, they were compared with WES¹ experimental data from the U. S. Army (1952). Also a small lab model was built to determine the free surface and pressure over an existing spillway. The investigation demonstrated agreement between the numerical, lab-scale and other researchers results.

WES spillways are shaped knowing the design head. New shapes and pressures can easily be predicted by executing the BFCC program and introducing a optimal head for reiterated designs.

The developed model can predict the formation of subatmospheric pressure at the early stage of spillway design. This model can also be applicable to flow in partially filled tunnels and in the design of supercritical slopes.

While the BFCC model is a significant step forward in the development of numerical methods for predicting flow behavior on spillways, the flow patterns can often defy present analytical techniques.

The thesis also contains several recommendations about spillway design in order to avoid damage due to the cavitation.

1. The Waterway Engineering Station.

DEDICATION

This thesis is dedicated to my mother: my support in life

In the name of "Allah", the most gracious, the merciful

ACKNOWLEDGEMENTS

The author is deeply grateful to his supervisors. Prof. M. Elektorowicz and Prof. H. Poorooshab for their continued guidance and encouragement during the course of this work.

The author is grateful to Dr. G. H. Vatistas for consultations and discussions related to fluid dynamics topics.

Financial support of the Iranian Ministry of Water and Power Authority (MWPA) is gratefully acknowledged.

Finally, the author would like to express his appreciation to his wife during the course of this undertaking.

TABLE OF CONTENTS

	page
List of Figures.....	xiii
List of Tables.....	xvi
List of Photographs.....	xviii
Notations	xix

Chapter 1.0

INTRODUCTION	1
1.1 General	1
1.2 Physics of the problem	4
1.3 World experience of cavitation occurrence	5
1.4 Literature review.....	14
1.4.1 Numerical models	14
1.4.2 Physical models	19
1.5 Scope of the study.....	29

Chapter 2.0

MATHEMATICAL MODELLING OF FLOW OVER SPILLWAYS	32
2.1 General	32
2.2 Methods of spillway design	33
2.2.1 Spillway layout.....	33
2.2.2 Hydraulic and structural design	33
2.2.3 Crest design	34
2.2.4 Point of tangency	39
2.2.5 Numerical methods	40
2.3 Mathematical modelling the spillway.....	41
2.3.1 Background	41
2.3.2 Numerical generation of Boy-Fitted Curvilinear Coordinate systems	45
2.3.3 Governing Equations.....	49
2.4 Application to potential flow	55
2.5 Transformation of governing partial differential equations	56
2.6 Boundary conditions.....	59
2.6.1 Transformation of boundary conditions in Fitted Boundary Coordinate ...	61
2.7 Tangent and normal velocity components to lines of constant ξ and η	62

2.8	Coordinate transformation	64
2.9	Determination of pressure on the solid boundary	66
2.10	Spillway configuration.....	69
2.10.1	Influence of spillway profile and crest alignment	69
2.10.2	Approach conditions at the spillway crest	74
2.10.3	Spillway toe.....	74
2.11	Cavitation phenomenon	74
2.11.1	Inception and initial growth	74
2.11.2	Continued growth and collapse	75
2.11.3	Factors contributing to cavitation	76
2.11.3.1	Geometric factors.....	76
2.11.3.2	Hydrodynamic factors.....	77
2.11.3.3	Other factors	77
2.12	Prediction of cavitation	78

Chapter 3.0

POTENTIAL FLOW SOLVER	85
3.1 General	85

3.2	Governing equations	86
3.3	Finite difference approximations in the transformed plane	88
3.4	Discretization	89
3.4.1	Derivative approximation.....	90
3.4.2	Transformation parameters	92
3.5	Boundary discretization	96
3.5.1	General boundary conditions	96
3.5.2	Additional boundary condition on free surface	97
3.6	Computer program for spillway design	99

Chapter 4.0

EXPERIMENTAL STUDY	103
4.1 General	103
4.2 Experimental methodology	104
4.2.1 Physical modelling	104
4.2.1.1 Reynold's number	104
4.2.1.2 Frounde's number	104
4.3 Similitude-scale relationships for hydraulic similarity	107

4.4	Objectives of physical modelling	109
4.5	Model specification	110
4.6	Experimental set-up	116
4.7	Methodology of measurements.....	118
4.7.1	Calibration of the crest model.....	118
4.7.2	Water surface profiles on the spillway.....	122
4.7.3	Pressure measurements.....	128
4.8	Determination of the mean flow velocity along the spillway.....	130
4.9	Discussion of experimental results.....	139

Chapter 5.0

COMPARISON OF NUMERICAL AND EXPERIMENTAL STUDIES.....		142
5.1	General	142
5.2	Comparison of Numerical and Lab Models	143
5.3	Comparison with U. S Army experimentation	151
5.4	Comparison with Sivakumaran <i>et al.</i> results	152
5.5	Discussion and analysis	152
5.5.1	Discussion on physical and numerical models	152

5.5.1.1 Physical model.....	154
5.5.1.2 Numerical BFCC model	155
5.6 Application of model to spillway design.....	159
5.6.1 Design criteria.....	159

Chapter 6.0

CONCLUSIONS AND RECOMMENDATIONS	162
6.1 General.....	162
6.2 Conclusions	163
6.3 General recommendation for spillway design.....	166
6.5.1 Velocities $V < 30 \text{ m/s}$	167
6.5.2 Velocities $V > 30 \text{ m/s}$	168
6.4 Recommendations for future work	169
6.5 General recommendation to prevent cavitation damage	171
REFERENCES	177

LIST OF FIGURES

Figure	Page
1.1 Development of flow on a chute spillway	6
1.2 Incipient cavitation for flow over offsets into flow	20
1.3 Incipient cavitation with into-the flow chamfers	20
1.4 Water surface, pressure, and chute floor profiles in Karun model	23
2.1 Crest shape for a spillway	35
2.2 Curves for determination of velocity at the toe of spillway	38
2.3 Spillway crest tangent ordinates	39
2.4 Pressure variation in straight and curved flows	42
2.5 Determination of the transformed domain from the physical domain	44
2.6 Field transformation-single body	46
2.7 Piecewise spatial view of spillway channel geometry	51
2.8 Spillway crest characteristic.....	53
2.9 Boundary conditions, physical and computational domains	60
2.10 Tangent and normal unit vectors	63
2.11 WES spillway crest upstream quadrant	71

2.12	WES spillway crest downstream quadrant	72
2.13	Non-dimensional crest of WES spillway	73
2.14	Important factors effecting bubble collapse models.....	80
2.15	Boundary layer development on a spillway crest	83
3.1	Computational field of spillway flow in Domain D^*	90
3.2	Schematic diagram showing the steps in an iteration	101
3.3	Subroutine of SUR for determination of water surface profile	102
4.1	Side view dimensions of experimental model	112
4.2	Perspective view of experimental model	113
4.3	Plan view of experimental WES spillway model.....	115
4.4	Experimental set-up	117
4.5	V-notch weir measuring the output flow of flume.....	120
4.6	Non-dimensional free surface at $H/H_d = 0.5, 1.0$, and 1.33	127
4.7	Bed pressure reading	128
4.8	Non-dimensional pressure measured over spillway	132
4.9	Measured velocity field inside spillway domain for $H/H_d = 0.5$	136
4.10	Measured velocity field inside spillway domain for $H/H_d = 1.0$	137
4.11	Measured velocity field inside spillway domain for $H/H_d = 1.33$	138

5.1	Comparison of numerical and experimental free surface	144
5.2	Comparison of numerical and experimental crest pressure	146
5.3	Comparison of numerical and experimental $\sigma_z(x)$	150
5.4	Comparison of present model with U. S. Army and Sivakumaran <i>et al.</i> ...	153
5.5	Design criteria algorithm for cavitation detection	161
6.1	Types of aeration facilities	176

LIST OF TABLES

Table	Page
1.1 High velocity spillways damaged during operation.....	7
2.1 Vertical weir lower nappe coordinates	35
2.2 Experimentally determined coefficient C	37
2.3 Boundary conditions and numerical equivalent in physical domain D	61
2.4 Effective factors for the rate of collapse	76
3.1 Boundary conditions in computational domain D^*	97
4.1 Comparison of measured discharge coefficient with Chow results	122
4.2 Model operating conditions	124
4.3 Water surface profiles for 3 operating heads	125
4.4 Measured non-dimensional bottom pressure on the WES spillway	131
4.5 Measured hydraulic parameters over WES spillway for $H/H_d = 0.5$	133
4.6 Measured hydraulic parameters over WES spillway for $H/H_d = 1.0$	134
4.7 Measured hydraulic parameters over WES spillway for $H/H_d = 1.33$..	135
4.8 Fluid properties in experimental environment	135
5.1 Numerical prediction of non-dimensional bottom pressure	145
5.2 Numerical prediction of hydraulic parameters for $H/H_d = 0.5$	147

5.3	Numerical prediction of hydraulic parameters for $H/H_d = 1.0$148
5.4	Numerical prediction of hydraulic parameters for $H/H_d = 1.33$149

LIST OF PHOTOGRAPHS

Photo	Page
1.1 General view of three chutes of Karun I spillway in operation	10
1.2 View of damage in Karun I spillway (1977)	11
1.3 Cavitation damage on second convex curve	12
1.4 Damage initiated by convex curve in Karun I spillway	13
1.5 View of spillway showing the joints of slabs.....	25
1.6 Deterioration of the surface resulting in cracks and abrupt edges	26
1.7 Stating the cavitation in badly joined concrete	26
1.8 Removing the matrix above aggregate particle	27
1.9 Starting to remove the particles of concrete	27
1.10 Complete deterioration and removal of concrete particles	28
4.1 Crest geometry of WES spillway model built from plexiglass.....	111
4.2 Monitoring board and velocity & depth probe set of a spillway model ...	114
4.3 Overall view at model spillway, grid points, and recording probe set	123

NOTATIONS

The following list contains the symbols used in this thesis. These are also defined more clearly in the thesis where they first appear.

A_i	Pressure tap name in row A ($i = 1, \dots$)
\bar{A}	$\frac{gH_d}{2V_a^2 \cos^2 \varphi}$
b	Lateral width of spillway
B	Wide of the computational domain
\bar{B}	$(-\tan \varphi)$
B_i	Boundaries of domain D for ($i = 1-4$)
B_i^*	Boundaries of domain D^* for ($i = 1-4$)
B_j	Pressure tap name in row B ($j = 1, \dots$)
c	Centrifugal correction
C	Spillway coefficient
\bar{C}	$\frac{l}{H_d}$
C_0	Correction factor for units in Manning formula
\dot{C}	V-notch discharge coefficient
\ddot{C}	Corrected V-notch coefficient
C_d	Spillway discharge coefficient

C_j	η -lines with constant value ($j = 1-N$)
C_k	Pressure tap name in row C ($k = 1, \dots$)
C_p	Pressure coefficient
d	Spillway crest or V-notch weir apex height above approach channel bed
d_n	Normal depth to the flow surface
dy_s	Change in y_s to satisfy the constant pressure condition
D	Physical domain
\bar{D}	$\frac{e}{H_d}$
D^*	Computational domain
E	Total energy above horizontal datum, defined by upstream condition
\mathcal{E}	Defined vector in St. Venant equations
$E(x)$	Energy at free surface location x
e	Vertical thickness of the nappe
f	$f(\xi, \eta)$ -a twice continuously differentiable function of ξ and η
f_x	Sufficiently differentiable function of x
f_y	Sufficiently differentiable function of y
$\hat{f}_n(\eta)$	Normal vector component to line of constant η
$\hat{f}_n(\xi)$	Normal vector component to line of constant ξ

$\dot{f}_t(\eta)$	Tangent vector component to line of constant η
$\dot{f}_t(\xi)$	Tangent vector component to line of constant ξ
F	Froude number
\mathcal{F}	Defined vector in St. Venant equations
g	Gravity acceleration (9.80665 m/s^2)
h	Depth B_1 (and B_4) with respect to bottom at any point of liquid boundary
h_1	Upstream depth
h_2	Downstream depth
h'	Adjusted head of a triangular notch weir
\bar{h}	Piezometric head
h_c	Head related to centrifugal force
h_p	Pressure head
h_s	Static head pressure
h_T	Surface tension height (capillary rise) in tube
h_y	Height of column of flowing fluid producing the flow over a V-notch weir
H	Operating head
H_0	Total head over spillway
H_a	Approach velocity head

H_d	Design head (characteristic length)
H_s	Total head above sharp weir crest
i_{max}	Largest section number in x -direction
J	Jacobian
j_{max}	Largest section number in y -direction
K_i	ξ -lines with constant value ($i = 1-M$)
l	Vertical distance between weir crest and lower nappe crest
L	Length
L_m	Model length parameter
L_p	Prototype length parameter
L_r	Scale ($=\frac{L_m}{L_p}$; "model:prototype" ratio length)
n	Normal coordinate to surface
n	Manning roughness coefficient
N	Number of grid points in y direction
M	Number of grid points in x direction
P	Grid control function
P_0	Pressure at x location
P_{atm}	Atmospheric pressure

P_b	Bottom pressure
P_v	Vapor pressure
q	Discharge per unit width
\vec{q}	Velocity vector
Q	Volume flow rate over crest
Q	Grid control function
r	Radius of curvature
\bar{r}	Tube radius
R	Reynolds number [$(gH_d^3)^{1/2} v^{-1}$]
R_i	Upstream quadrant curve radius ($i = 1-3$)
S_{fx}	Friction slope in x -direction
S_{fy}	Friction slope in y -direction
S_{0x}	Channel bottom slope in the x -direction ($\sin\theta_x$)
S_{0y}	Channel bottom slope in the y -direction ($\sin\theta_y$)
S	Distance of global origin system from crest-top of spillway
S	Defined vector in St. Venant equations
t	Time
T	Temperature

T_h	Top width of V-notch weir respect to the head over it
T_s	Surface tension
u	Horizontal component of V
\mathcal{U}	Defined vector in St. Venant equations
u_s	Component velocity of free surface in x-direction
v	Vertical component of V
V	Velocity along streamline
V_0	Average velocity at location x
V_a	Approach velocity
V_A	Actual velocity
V_{max}	Maximum velocity at Z fall
V_s	Velocity along free surface
V_T	Theoretical velocity
V_y	Velocity at small distance y from the real bottom
W	Weber number [$W = H_a (\rho g / T_s)^{1/2}$]
b	Bottom width of approach channel upstream of V-notch weir
x	x-coordinate of physical plane (horizontal direction)
$\frac{H}{H_d}$	Relative head

$\frac{x}{H_d}$	Relative horizontal distance from crest of spillway
\bar{X}	Body force
y	y-coordinate of physical plane (vertical direction)
y_i	Flow depth at $i = 0, 1, \dots$ in global coordinate system
y_1	Tail water elevation
$\frac{y}{H_d}$	Relative vertical distance from crest of spillway
y_s	Water surface depth
z	Transverse coordinate with respect to $(x - y)$ coordinates
Z	Vertical distance from the upstream reservoir level to the floor at the toe

Subscripts

b	Bottom
c	Centrifugal force
d	Design
h	Head
i	Section number in x -direction
i	Incipient
j	Section number in y -direction

p	Pressure
P	Prototype
v	Vapor
max	Maximum
M	Model
n	Normal
r	Ratio
s	Water surface
S	Static
t	Tangent
T	Theoretical
η	Partial derivative with respect to η
ξ	Partial derivative with respect to ξ
y	Vertical direction in y -coordinate

Greek

α	$x_{\eta}^2 + y_{\eta}^2$
β	$x_{\xi}x_{\eta} + y_{\xi}y_{\eta}$

γ	$x_{\xi}^2 + y_{\xi}^2$
σ	$[y_{\xi}(\alpha x_{\xi\xi} - 2\beta x_{\xi\eta} + \gamma x_{\eta\eta}) - x_{\xi}(\alpha y_{\xi\xi} - 2\beta y_{\xi\eta} + \gamma y_{\eta\eta})] / J$
τ	$[x_{\eta}(\alpha y_{\xi\xi} - 2\beta y_{\xi\eta} + \gamma y_{\eta\eta}) - y_{\eta}(\alpha x_{\xi\xi} - 2\beta x_{\xi\eta} + \gamma x_{\eta\eta})] / J$
ρ	Density
μ	Dynamic viscosity
ζ	Vorticity
ψ	Stream function
ω	Relaxation factor
Ω	Kinematic viscosity
φ	The angle of inclination of the velocity v_0 with the horizontal
$\dot{\varphi}$	Velocity function
σ	Cavitation index
σ_A	Allowable cavitation index
σ_G	Gal'prin cavitation index
σ_i	Incipient cavitation index
γ_0	Specific weight of water
ξ	ξ -coordinate of transformed plane
η	η -coordinate of transformed plane

Φ	Angle included between sides of a triangular-notch weir
θ	Spillway bottom slope
$\hat{\theta}$	Liquid-air-Polyethylen interface ($\hat{\theta} = 0$ for water-air-Polyethylen)
Δ	Adjustment to be added to observed head of a triangular- notch weir
$\Delta\xi$	ξ -lines successive differential
$\Delta\eta$	η -lines successive differential
δ	Boundary layer thickness
ϕ	Dissipation energy

Chapter 1.0

INTRODUCTION

1.1 General

All storage dams must be protected by a spillway. The spillway is intended to discharge the excess river flow during times of flood, in such a manner as to ensure the safety of the dam and appurtenant works at all times. Although storage dams are relatively high dams and impound a significant storage volume, it is never economically feasible to build the dam high enough to store the low frequency high discharge floods in the reservoir e.g. PMF¹. Some provision must be made to get the excess flow safely through, over or around the dam. A spillway is used for this purpose. This study includes a description of the common forms of open-channel spillway and of the behavior which may be expected. Many variations in the shape of both controlled and uncontrolled spillways are employed to meet the requirements of different dam and reservoir sites. It will be appreciated that because spillways are site specific, it is not possible to describe every combination of feature which may be encountered. The study considers numerical and other approaches to flow behavior in greater detail. The analysis of flow behavior requires consideration of widely differing conditions of motion. Where the state of rest or

1. Probable Maximum Flood.

uniform motion of any object is disturbed, forces must arise to create these changes. In the context of spillway flows, these forces are generally manifested as changes of pressure or depth. These changes may occur either as flow approaches a spillway, or they may be the result of various factors, e.g., width, shape alignment, gradient of the spillway channel below the crest, or environmental conditions. Variation of channel roughness will also prompt changes of flow state, as will the tailwater conditions at the downstream end of the spillway.

In a natural watercourse, flow loses energy at a rate more or less proportional to the channel gradient. The construction of a dam obviously creates a substantial increase in depth and back water for considerable distances upstream of the dam. As flow enters the impounding reservoir, the rate of energy loss diminishes markedly as a consequence of both the increase in depth and the reduction in velocity. Thus, a condition is achieved in which the water within the reservoir, as it nears the dam and overflow, possesses a much higher energy level than was the case with the previously undammed river at that point. Flood waters discharged from the reservoir through the spillway works possess considerably more energy than in the natural watercourses a relatively short distance downstream. Thus, spillway channel gradients tend to be relatively steep, where kinematic energy is a substantial component of the head. This high velocity flow must be returned to the natural watercourse in such a way that no seriously detrimental effects are created in the river channel. It is necessary to have a tool to provide a basis for preliminary designs, adequate data for spillway modelling.

In research on hydraulic structures, model testing of the pressure distribution on crests of overflow spillways has become a routine procedure met with quite frequently, because of the rather common occurrence of this type of reservoir control. While the designs of such standard shape can be based to a large extent on previous experiences, every individual case is however, at present, required to be subjected to a model study.

This domain has been looking for new contributions such as the systematization of pressure computation for design purposes. The two-dimensional model seems to be an adequate assumption. This mathematical model is a sufficient approximation to the field of flow in the actual model, when the viscous effects do not have an appreciable influence on the overall flow.

The general agreement between model results and prototype in cases where Froude modelling is satisfied is usually good. The differences occur in either of the two cases, *viz.*, when viscous effect is meaning, and when there is a possible separation flow. The former is the case, for example, when the model scale is not large enough, and the experimenter is required to extrapolate the results from the observations of different geometrically similar models. The latter is likely to occur if a substantial subatmospheric pressure exists for a short while under any flow condition; as, for example, in the case of a weir profile designed to obtain a high coefficient of discharge.

For a given design head of free overfall past a sharp crest, the spillway crest is usually standardized using the lower of free surfaces, so that the pressures for this head are atmospheric both on the upper free surface as well as the lower. With the spillway crest formed using the lower free surface, the pressure on the spillway crest is ensured to be nearly atmospheric for the design head¹ and above atmospheric for lower heads. With higher heads, the pressures on the crest would be subatmospheric, and the coefficient of the discharge would be larger. For sufficiently higher heads, therefore, the same spillway crest profile would act as a weir profile with high coefficient.

It is important to find as an adequate solution of the field of flow for a standard profile used for any design head given followed by the derivation of a method for avoiding much of the computations for the case of other heads.

1. Design head is the head used for the design of crest shape. The operating head, however, could be lower or higher than the design head.

Some solution for free-boundary problems by relaxation methods have already been done. The application of the hydraulic problem related to spillway can be based on the physical principal that “small causes have small effects,” which as a fundamental concept is only approximately true. In reducing the equations for the mean motion to that of irrotational potential flow, the terms neglected in the equations of motion are those due to viscosity. The main basis on which the truth of assumption rests is that boundary layer development is significantly reduced in high acceleration flows, which is usual in the cases of high Reynold flow, so that viscous terms are negligible.

1.2 Physics of the problem

Experience in spillway operation shows that, under conditions of high velocity flows, cavitation damage can be expected just downstream from spillway elements, such as gate slots and any irregularities in the spillway surface. Cavitation occurs in the low pressure zone created by the deflection of flow away from the boundary (flow separation). If the pressure in this zone falls below the vapor pressure of water, the equilibrium of small undissolved amounts of air in the water becomes unbalanced. These unstable nuclei grow rapidly to form large cavities in the water, which are then carried downstream. When the cavities move into zones of sufficiently higher pressure, the growth ceases, the vapor condenses, and a sudden collapse of the cavity occurs. Extremely high, short-duration pressures develop. If the cavities collapse near or on the boundary, damage to the boundary material results. This can lead to a complete failure of the structure. Thus, cavitation corrosion (pitting) and its often accompanying vibration is a phenomenon that must taken into account in the design of hydraulic structures.

The importance of the subject is emphasized by the fact that cavitation has been researched extensively for the past years, but despite this knowledge, is still far from

complete in certain areas.

In order to investigate the development of air entrainment down the spillway by observation, these regions of the flow are defined (Fig. 1.1):

- ① Non-aerated flow from the spillway gate to the point of inception of air entrainment.
- ② The final uniform region in which the air concentration and the velocity profile do not change with distance down the spillway, and
- ③ The gradually varied flow region which connects regions 1 and 2. This region consists of:
 - A partially aerated flow region where the air does not reach the spillway surface, and
 - The fully aerated but gradually varied flow region where the air concentration and velocity profile slowly change to the equilibrium profiles in region 2.

For spillway design, the extent of region 3 is important, as it determines the greatest velocity and the maximum cavitation parameter next to the spillway in the pure non-aerated water. Region 2 is also important for a long spillway, as the uniform conditions determine the input condition into the flip bucket.

1.3 World experience of cavitation occurrence

The first major cavitation damage was experienced in 1941 when the Arizona spillway tunnel at the Hoover dam developed a large hole in the concrete lining. Since then, several cases of cavitation-related damage have been reported in the world's high dams. A selected list of these reported cases follows:

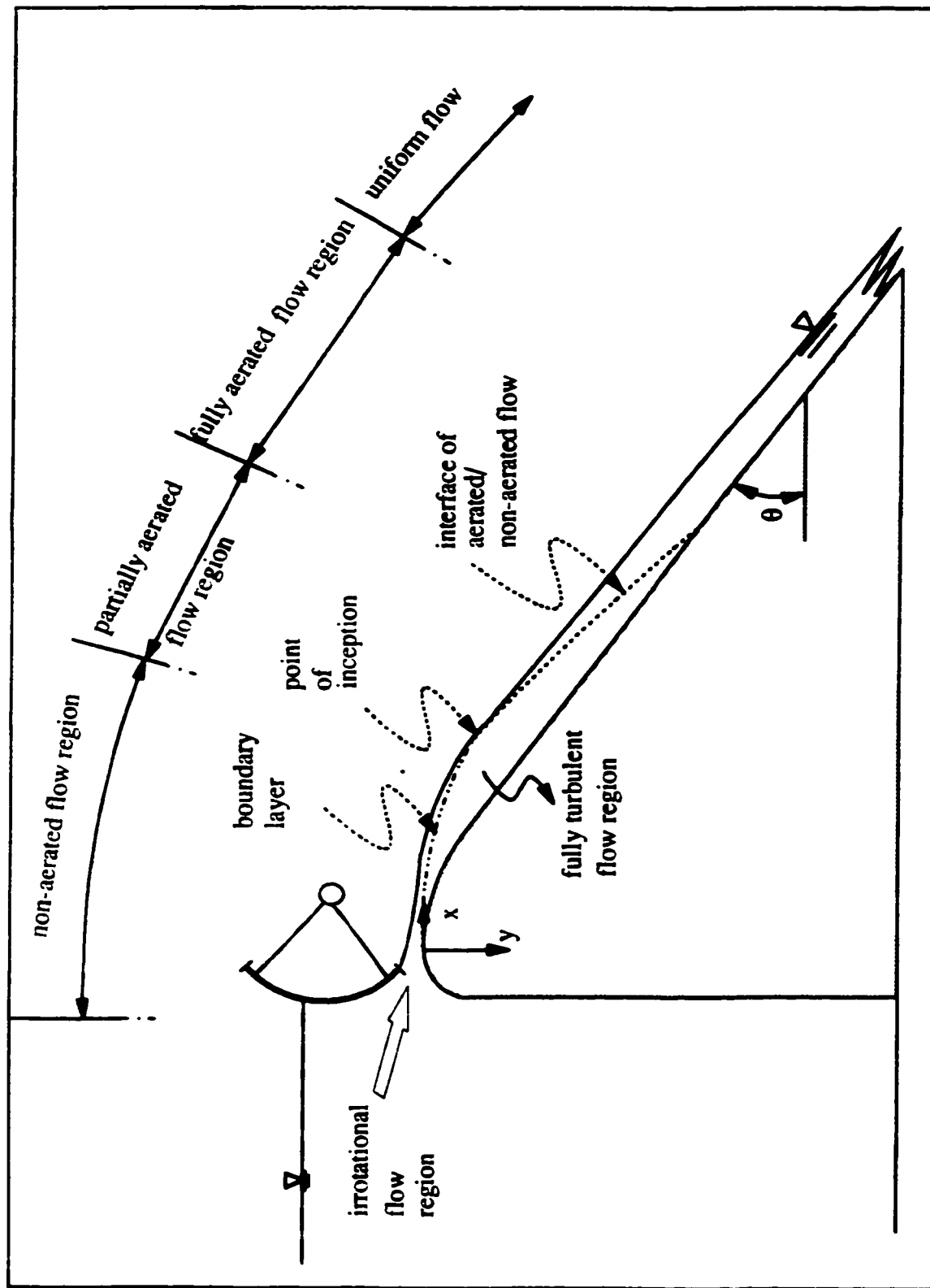


Fig. 1.1 Development of flow on a chute spillway (Cain & Wood).

Table 1.1: High velocity spillways damaged during operation

Dam	Location	Max. discharge m^3/s	Unit width discharge $m^3/s/m$	Max. velocity m/s	Fall to Max. velocity m	Dam height m
Bhakra	India	8,220	104	48	173	226
Dworshak	Idaho	1,130	33	47	204	219
Hoover	Arizona/Nevada	5,670	46	46	183	221
Aubrn	California	2,610	268	43	149	210
Yellowtail	Montana	2,610	268	43	148	203
Trinity	California	680		43	142	165
Anderson Ranch	Idaho	570	19	43	112	139
Karun I	Iran	16,500	297	42	145	200
Fontena	N. Carolina	4,480	105	42	134	146
Aleadavila	Spain	10,000	89	40	125	140
Detroit	Oregon	4,990	56	40	122	164
Libby	Montana	116	40	40	118	136
Navajo	New Mexico	1,190		38	116	
San esteban	Spain	4,500	90	38	109	115
Pine flat	California	11,080	249	38	107	136
Tarbela	Pakistan	18,410	173	38	101	148
Guri	Venezuela	34,990	288	37	96	107
Luckv peak	Idaho			37		104
Simikit	Thailand	1,900	138	36	88	
Lookout Point	Oregon	7,650	101	36	88	
Pit 7	California	2,270	72	31	66	70

The more recent instances of cavitation problems in spillway structures are Mica, Tarbela, and Karun I. Significant engineering and research efforts have been directed toward the understanding and analysis of the cavitation phenomenon and the development of measures to prevent damages to structures due to cavitation. From the author's experience with Karun I, the phenomena is described as follows.

The construction of Karun I dam, a double curvature arch dam with maximum height of 200 *m* and a crest length of 380 *m* was finished in 1977. The chute spillway consists of three 18 *m* bays, each equipped with a 15 *m* × 20 *m* (*W* × *H*) radial gate. The dam crest width is 6 *m* at an elevation of 542 *m.a.s.l*¹, (see Photo 1.1). The other features of the dam are as follows:

Height	200 <i>m</i>
Reservoir volume	2900 million <i>m</i> ³
Length of dam	380 <i>m</i>
Crest elevation	540 <i>m.s.l</i>
Max. water level	530 <i>m</i>
Max. discharge	16500 <i>m</i> ³ / <i>s</i>
End chute level	398.05 <i>m.a.l</i>
Spillway capacity	16500 <i>m</i> ³ / <i>s</i>

The first cavitation happened in 1977 for a value of 45 *m*³/*s/m*. The severest damage occurred in 1993 during an estimated flood of 92 *m*³/*s/m* (see Photo 1.2).

1. Mean average sea level

Close inspection of the chute revealed that cavitation was the primary cause of damage which was extended to continued water release through the spillway. As can be noted in Photo 1.3, several cavitation erosions occurred at the entrance of the chute to the flip-bucket (second convex curve) where the water velocity is 35 m/s . But most cavitation damage happened on the first convex curve (Photo 1.4).

The spillway contains 3 bays each with a width of 18 m which are controlled by radial gates $20 \times 15 \text{ m}$. These bays are designed for a PMF of $16500 \text{ m}^3/\text{s}$ for a discharge of $297 \text{ m}^3/\text{s}/\text{m}$. The shape of the spillway is not a WES shape. The hydraulic model for redesign of Karun I spillway was built based on some discrete points on the spillway because the spillway shape is unknown.



Photo 1.1 General view of three chutes at Karun I spillway in operation .

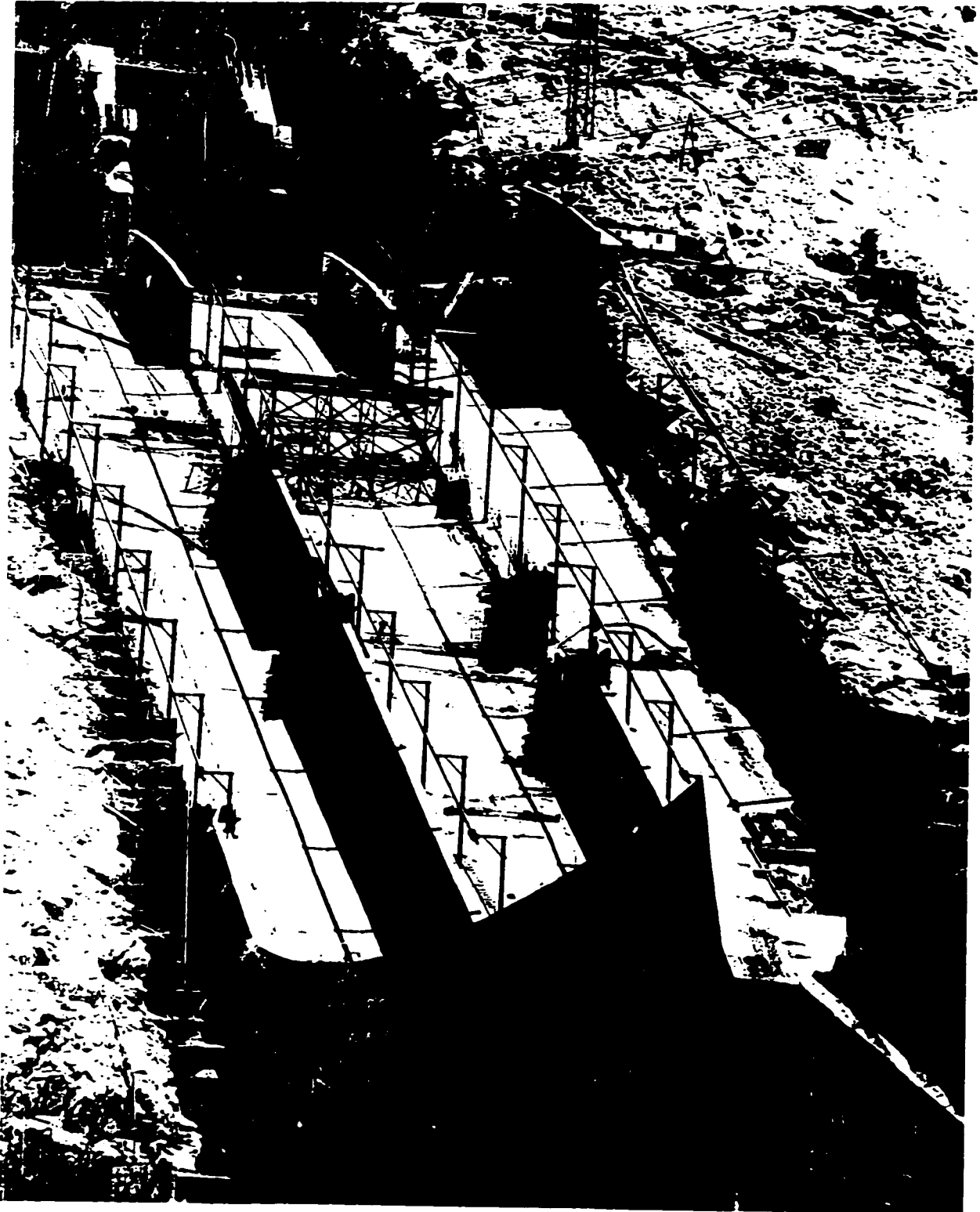


Photo 1.2 View of damage in Karun I spillway (1977).

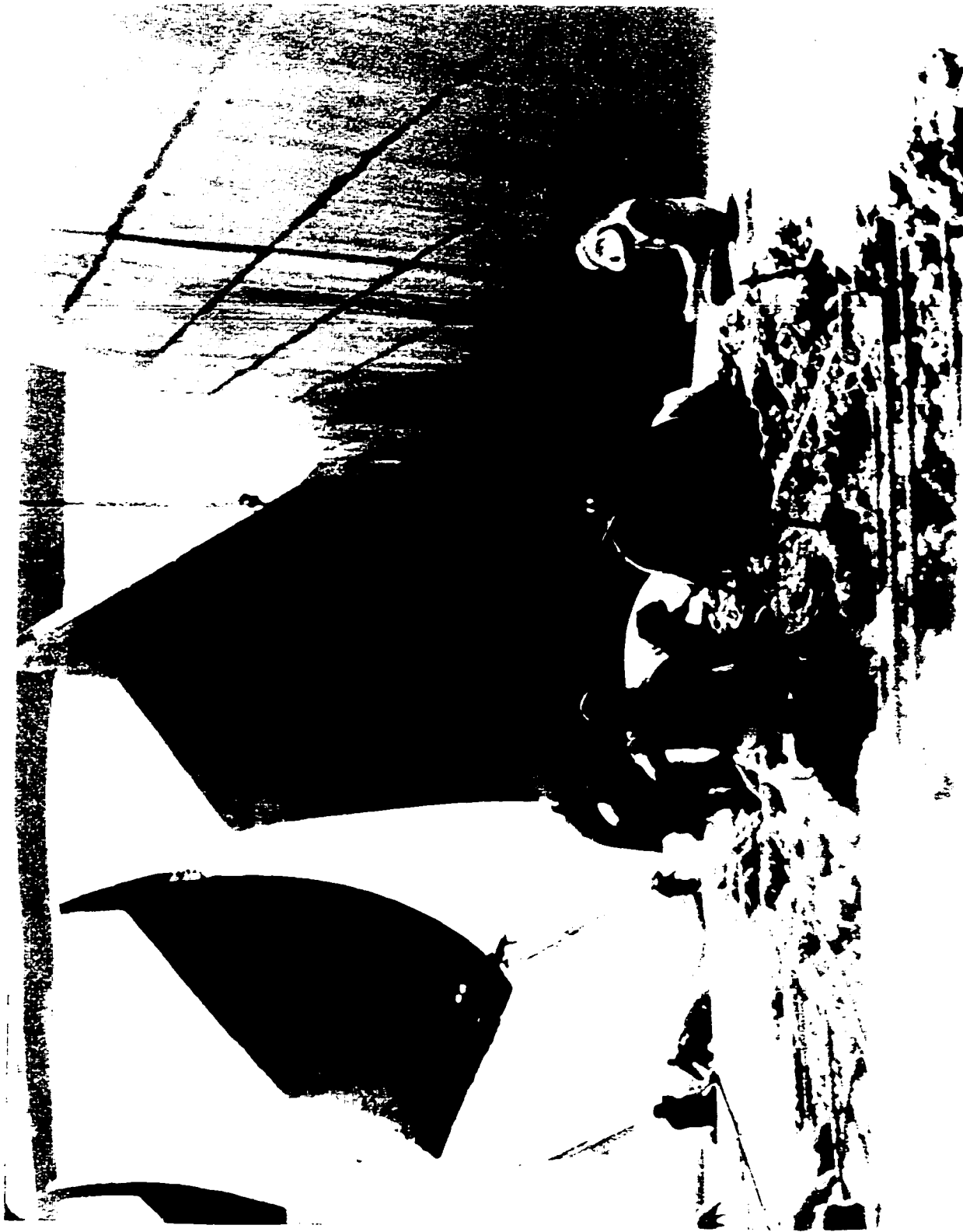


Photo 1.3 Cavitation damage on second convex curve.



Photo 1.4 Damage initiated by convex curve in Karun I spillway.

1.4 Literature review

A few studies on the dynamic pressure over spillways have been performed to date. These studies contain preliminary verification of hydraulic models employed. Theoretical and numerical analyses of previous studies have proven that the subject of cavitation is not the main reason for investigators to regard the design spillway structures and their shortcomings in dealing with the complex subject of cavitation. The spillway has been used as a special problem for calculating the velocity and water profile. Since the cavitation phenomena is related to high spillways with high velocities, therefore, vertical and curvilinear flows have more effect on these structures. By reviewing the previous investigations, it is clear their attention is focused on the spillway as a small structure and the assumed hydrostatic pressure over it; the greatest weakness of these studies is to extend hydrostatic pressure to high spillways. Because of the wide difference between hydrostatic and dynamic pressures, it is impossible to predict the cavitation in these models. During the course of this investigation, the most important works have been reviewed in two groups. The first group is concerned with a conceptual model of pressure distribution and numerical methods for solutions of the governing equations that are used at the present time. The second group includes physical modelling governing subjects such as velocity measuring, water surface profile, and pressure in model studies. Consequently, the lecture review is related to both groups of concern.

1.4.1 Numerical models

The first attempts of modeling spillways of finite height were made by Cassidy (1964, 1965). By means of the relaxation technique, he found discharge coefficients, pressure distributions, and free-surface profiles for a finite-height spillway of specified shape. The free-surface profile with assumed values of the discharge coefficient could

converge only for a limited range of the discharge coefficient. This range is limited to the first few iterations. Because the location of the points of minimum pressure (produced by flow over a spillway at particular head) depends on the boundary configuration, Cassidy's results can not be compared with a WES case; this is because of the unknown shape of the spillway.

Lenau and Cassidy (1969) developed analytical means of predicting free-surface profiles and floor pressures for spillways. They assumed that the flow is inviscid and irrotational. They solved the problem by using the potential flow theory in a complex plane.

Ikegawa and Washizu (1973), Dierch *et al.* (1977), Varoglu *et al.* (1978), Betts (1979), O'Carroll (1980), Hsu (1980), Bettess and Bettess (1983), O'Carroll and Toro (1984), and Sreetharan (1990) employed finite element methods to calculate the velocity field and water surface profile. The methodology is the same, but the shape of the weir under study is different for each one: rectangular, triangular, trapezoid, and Creager profile, in longitude view. These studies include a complex tunnel and open channel. Better convergence was obtained by finite element analysis on the free surface than with Cassidy's approach.

Villegas (1976) used a characteristic method without the influence of the normal acceleration, which may be significant in the case of steeply curved water surface profiles. Therefore, the pressure distribution is assumed to be hydrostatic, and the governing equations are shallow-water equations. In his investigation, Villegas (1976) found discontinuities in flow similar to hydraulic jumps. The result of his study was a calculation of water surface profile and velocity. Because he saw the discontinuities (such as jump) in the spillway flow, the Euler equations are not sufficient to define the solution of mixed continuous-discontinuous flow.

Sivakumaran, Hosking and Tingsanchali (1981) derived analytical and simple

shallow-water equations with bed curvature for steady flow over a high-overflow-spillway crest based on the Dressler's¹ approach. They calculated the bed pressure and free surface on a curved bed-like spillway. For large specific discharges, the theoretical free surface is slightly below the experimental points in the subcritical region, and this indicates inadequacy of the shallow water approximation for flow over the spillway.

Cheng, *et al.* (1981) used the boundary integral equation method (BIEM) for spillway flow. They found that for less than the design discharge over a standard WES spillway, the pressure on the spillway is everywhere positive, but at $x = 1.07 \text{ m}$ it has a low value for the design discharge. For the design head the pressure should be everywhere positive. They mentioned the BIEM is not the final answer to the problem, but it presents a further step toward the solution of flow over spillways and the replacement of physical models with numerical calculation.

Ransford (1983) employed an analytical study for pressure on a spillway apron downstream from a partly raised gate, by developing an equation for pressure on a trajectory type spillway. Because of rapid curvature of a Creager spillway profile, it needs a correction factor for pressure based on the slope of the spillway. The numerical scheme has oscillations that could lead to errors.

Ellis (1982, 1985) developed a model based on the steady Navier-Stokes equations for nearly horizontal flow in two-dimensions, both with and without frictional effects. After this simplification, he used the characteristics method which takes into consideration the nearly horizontal channel with assumed hydrostatic pressure in two-dimensions. The model chooses x and y as a rectangular coordinate system on the bottom. The x is the downstream direction and y is perpendicular to x in the bottom plane; the value of u and v are the velocity components in the x and y directions, respectively. Many assumptions were used

1. Dressler, R. F (1978) who first developed new nonlinear shallow-flow equations with curvature.

in this approach. The study neglected, for instance: concave curve, convex curve, and large spillway slopes that have a significant component of velocity in vertical direction that must be considered.

Mahab Ghodss (1987), by using gradually varied flow over the Karun chute spillway, found the critical cavitation index where the cavitation actually happened on joint offsets over spillways.

Slisskii and Kalandarov (1987) solved the equations of motion of a fluid in a cylindrical coordinate system flowing through the bend of a tunnel lying in plane p at angle α to the horizon by choosing axis z as normal to plane p . It is assumed that the velocity vectors along any normal to p lie in the same plane tangent to the streamlines however, terms containing velocity components V_r , V_z , and accelerations corresponding to them are omitted in the equations. The specific energy of flow for each streamline is assumed to be constant. The result performed is a hydrostatic pressure equation of flow in cylindrical coordinates.

Bongmin (1989) studied the turbulent boundary layer on the spillway curved surface and solved the problem with the finite element in the boundary fitted-coordinate system for studying the velocity distribution and the boundary layer thickness on the spillway. He calculated the velocity distribution and the boundary layer thickness on the spillway.

Xu and Sun (1990) studied the tangency points over spillways. Because of the abrupt change in curvature at tangency points, a considerable drop in pressure may occur, which causes damage. They gave two kinds of curves with gradually varied curvatures for connecting straight boundaries to the bucket (circular, elliptic and parabolic). Then, by using a finite element scheme and the stream function for these curves, they calculated pressure distribution and free-surface on the bucket of spillways. They mentioned with

these curves that it is possible to improve pressure at these points.

Henderson, Kok, and De Konning (1991) used the boundary element method and non-linear programming (in order to optimize the discharge coefficient) for the two dimensional flow over a fixed spillway. They used their model to solve the free surface and the discharge problem for the flow over a weir. They did not test the model for the spillway.

Berger and Carey (1991) used a perturbation analysis and a finite element approximate model for free surface flow over curved beds. They employed the approach of Dressler by means of a perturbation analysis. This led to a new formulation of the problems, and a generalized set of shallow water equations of the curvature effects. Their numerical method demonstrates a hydraulic jump in the downstream regime. By using an artificial dissipation technique¹, they got a better free surface than Sivakumaran.

Zaitsev (1991) calculated the velocity coefficient for various sections of the spillway face of a dam or chute based on a numerical solution of 2-D turbulent boundary layer equations. By using Lisa-Dorodnitsin type transformation of variables, he got the mean velocity in the different sections. For this method, he recommended a graph to find the velocity coefficient based on the head above the section and critical depth. He compared his model with published methods based on integral relations of the boundary layer. In this study, the shape of the chute and pressure results over the chute are unknown.

Robinson and Mc Ghee (1993) used the gradually varied flow equation in declining-flow regimes where it does not require boundary conditions of the declining-flow segment to be defined. His program, based on available energy and control in a reservoir, defined the maximum discharge. Then using this flow, the critical slope is found and is compared to the actual slope for the determination of supercritical or subcritical flow. By this method,

1. Because of the discontinuities in free surface at the hydraulic jump, it is common practice to include an artificial dissipation in the governing equation or a numerical arising from the discretization method.

they determined depth and flow over the weir.

Berger and Stockstill (1993) applied a finite element method to shallow water equations. The numerical model is a depth averaged, two-dimensional numerical flow model designed specially for flow fields containing supercritical and subcritical regimes, as well as the transitions between the regimes. Using this model they determined the super-elevation water surface in channel bends with high velocity. They tested the model for a curved-wall contraction with a Froude number, F , of 4.0.

1.4.2 Physical models

Some case study reviews on hydraulic models are as follows:

Johnson (1963) has shown that at a velocity of 30 m/s , cavitation will take place downstream of an offset away from the flow with only 3 mm . Now the velocity 30 m/s is accepted as a limited velocity for the spillways.

Foerster and Anderson (1969) made a hydraulic model of the existing Karun I spillway to study cavitation damage: the scale of the model was 1:80. Foerster and Anderson (1969) never saw negative pressure, but in some parts of the spillway, they saw low pressures coincident with the location of cavitation in the prototype. They noted low pressure could be the reason for cavitation for a velocity of more than 40 m/s .

Ball (1976), through investigation of the Karun I spillway prototype, stated that cavitation could happen in high velocity flow over surface irregularities on a spillway. Therefore, two factors to reduce cavitation damage are surface smoothness, and velocity reduction. Figure 1.2 shows his research for flow over offsets into flow.

Falvey (1982) investigated cavitation for irregularities over tunnel spillways. He

used data collected by Colgate (1977) and by Jin *et al.* (1980) to estimate the required chamfer to eliminate cavitation (Fig. 1.3).

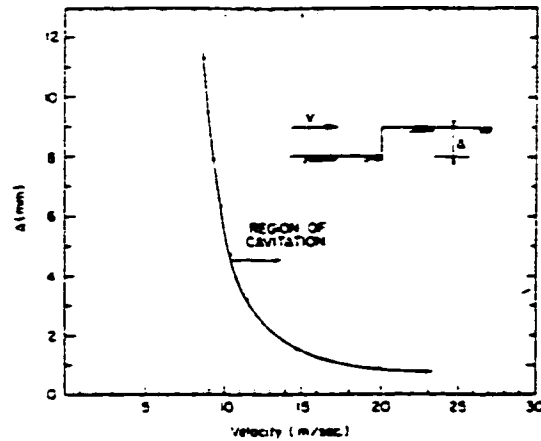


Fig. 1.2 Incipient cavitation for flow over offsets into flow (from data by Ball).

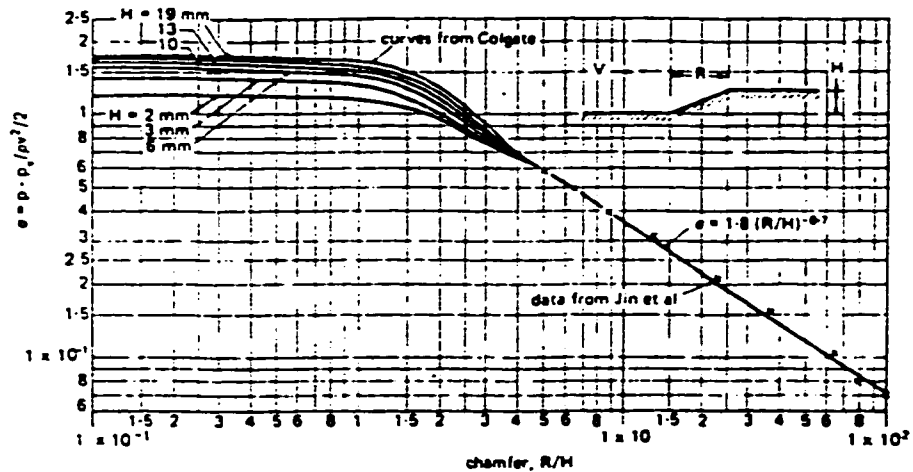


Fig. 1.3 Incipient cavitation with into-the-flow chamfers (from Falvey, 1982).

Mahab Ghodss (1984) developed a hydraulic model of the existing Karun I spillway. Although they followed the same method as Foerster and Anderson did on a different scale, the purpose of the model was to investigate flows over spillways that have been damaged by cavitation and to test the aerators. Ramps and deflectors were installed to investigate the effect of these aerators for discharges of 300-1500 m^3/s . The prototype spillway specifications for model with scale $L_r = 1/62.5$ are as follows:

3 Bays:	18.5 <i>m</i> wide
Side walls height:	15.5 <i>m</i>
Middle walls:	6.5 <i>m</i>
Total length:	324 <i>m</i> with slope 5°
Chute length:	128 <i>m</i> with slope 35°
Max. flood design:	16500 m^3/s
Spillway output in case of cavitation:	1160 m^3/s
Crest elevation:	510 <i>m.a.s.l</i>

This model includes the dam body close to the inputs of chute, spillway, radial gates. 250 meters upstream of the dam and an 800 meter length of river downstream. Chute of spillway and radial gates are built from plexiglass, other parts of the spillway are built from wood, and the dam body is made of masonry.

Discharge for this model comes from 2 motor pumps from 2 canals. The output discharge from the model is done by a rectangular weir. For measuring pressure in different points of the spillway a number of piezometers are installed.

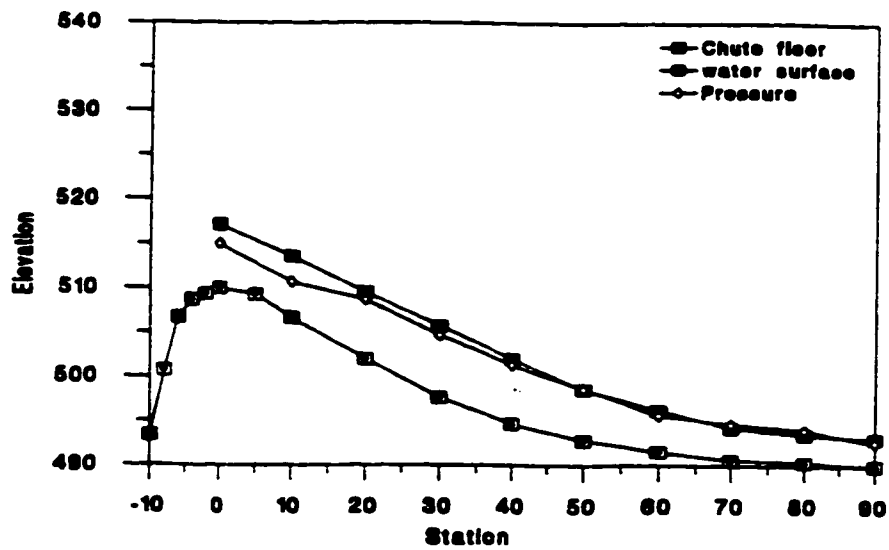
The similitude ratio in both model and prototype for open channel which consider

Froude law for length, discharge, and pressure are:

$$L_r=1:62.5, Q_r=1:30881.6, P_r=1:62.5$$

Figure 1.4 shows the pressure, water surface and chute profiles of the Karun I spillway. From data gathered in the experimental test, it can be seen that the Karun I spillway operating conditions are probably one of the most critical with regard to cavitation erosion because of the high water flow velocity developed, combined with a high discharge. This is of course due to the geometry of the structure which presents very steep slopes and rather sharp curvatures, which also induces low or negative dynamic pressures.

This author has done research on the high Karun dam spillway in Iran for 2 years. The dam is 200 meters high, about 500 meters long and has $16500 \text{ m}^3/\text{s}$ design discharge. It has seen subatmospheric phenomena that damaged some parts of the spillway. After each flooding, we might expect to repair the spillway. The interesting point is when a the bucket of concrete was transported by helicopter to the damaged place for repairing, the concrete that leaked on the surface of the spillway caused new cavitation. It was created when water passing over a local ground surface at high velocity suddenly changed from one condition to another and back again. This causes a sandblasting effect and a worse texture of concrete downstream with a potential for cavitation. Also, during the life of the structure, deterioration of the concrete surface occurred, resulting in cracks and abrupt edges which promote subsequent cavitation damage. This can be seen in the joint of the concrete slab that was observed by this author in Photos 1.5, 1.6 and 1.7. Another symptom of the damage of subatmospheric pressure is removing the matrix above aggregate particles (Photo 1.8). This tends to hold them in place, thereby making them susceptible to plucking and being removed even more easily (Photos 1.9, and 1.10). By using Ball's findings, after each repair with fibrous concrete, grinding and epoxy paint was used to smooth the spillway surface, and to make high resistance against cavitation erosion. Still, because of bad designing of the shape of spillway with a steep vertical



Note: $Q = 4000m^3/s$

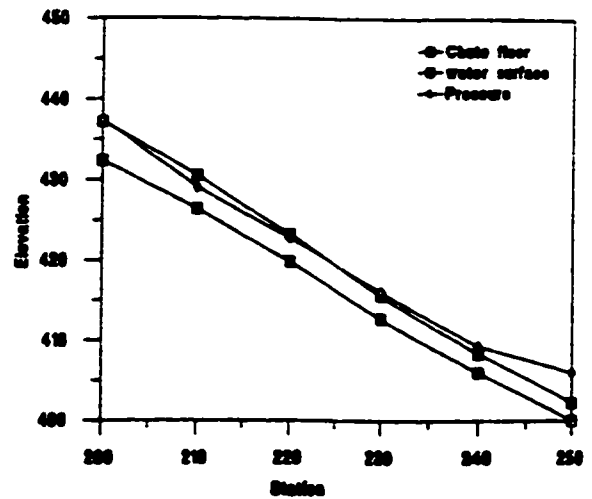
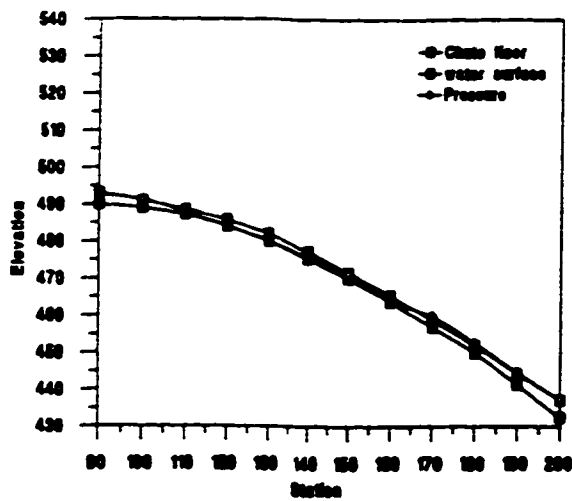


Fig. 1.4 Water surface, pressure, and chute floor profiles in Karun model.

curvature, for any discharge less than design head, there is subatmospheric damage to the spillway. The remedy for this kind of dam is designing a short spillway instead of a long one. The result is a reduction in velocity, $V_{max} = \sqrt{2gZ}$. Another problem is waste water, because water is sprayed in the air as fog and makes the environment hard to work in.

There are potential difficulties in interpreting results obtained from reviewed physical and numerical models for prototype conditions as:

1. The weakness in the state-of-the-art of small scale hydraulic models
2. Incompleteness of equations of numerical models, especially from the view point of hydrostatic pressure

This necessitates the development of a comprehensive numerical model for cavitation prediction.

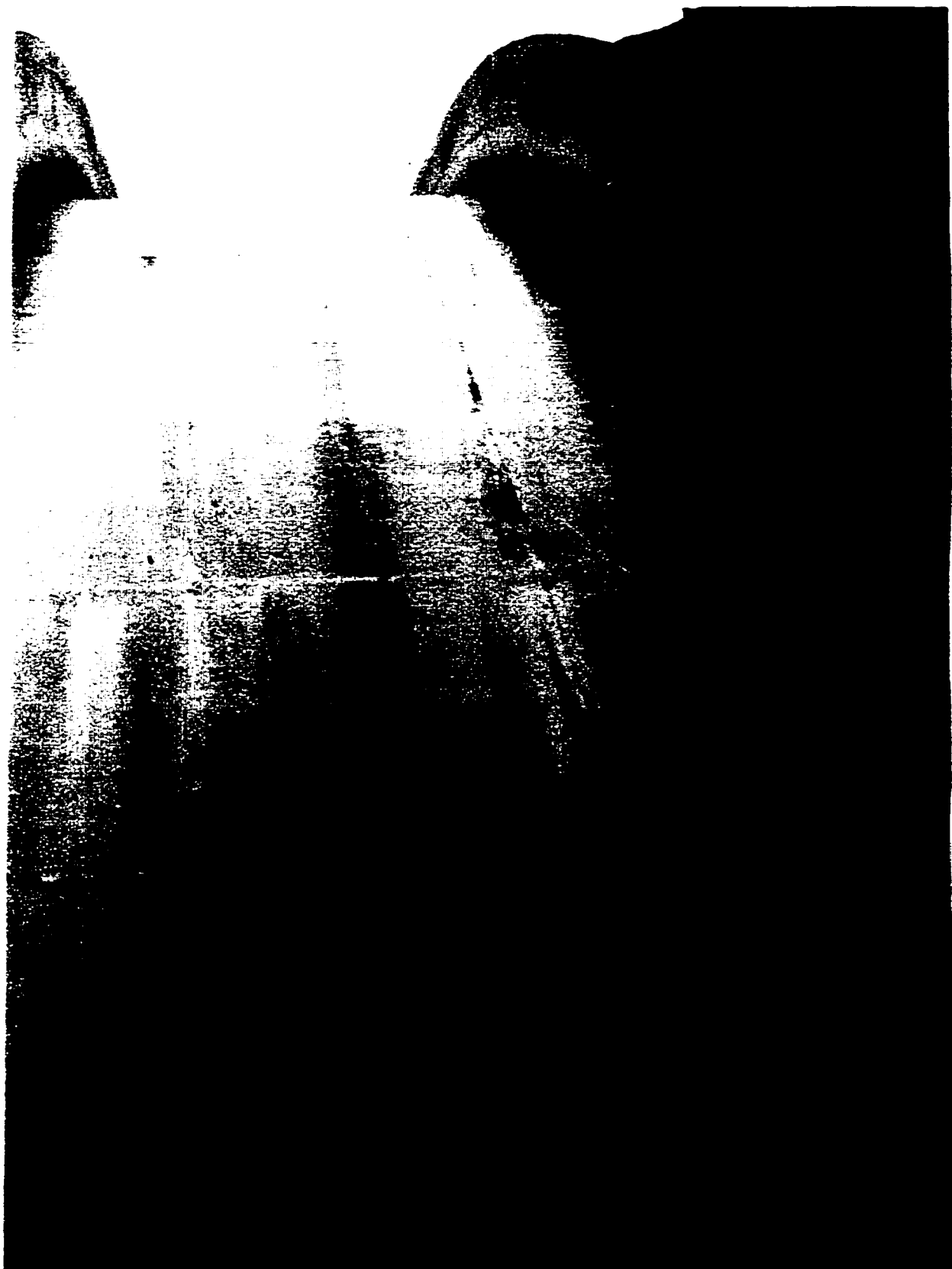


Photo 1.5 View of spillway showing the joints of slabs



Photo 1.6 Deterioration of the surface resulting in cracks and abrupt edges.



Photo 1.7 Stating the cavitation in badly joined concrete.



Photo 1.8 Removing the matrix above aggregate particle.



Photo 1.9 Starting to remove the particles of concrete.

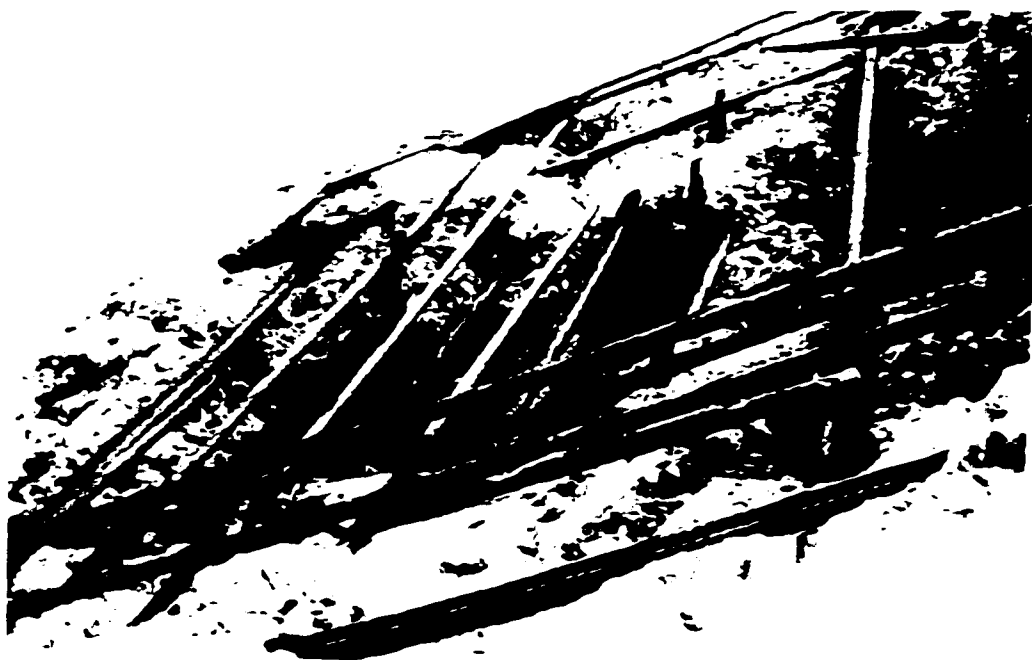


Photo 1.10 Complete deterioration and removal of concrete particles.

1.5 Scope of the study

This project is primarily concerned with high velocity flows on spillways. such flows will generally be supercritical. At higher velocities, inertial effects become increasingly important, leading to an increased complexity of analysis with considerable variations of flow conditions developing across a channel section. In order to model flow over spillways in the present study, a two-dimensional finite difference numerical model is developed. Up to the present, the finite difference method (FD) is the most often used numerical technique applied in the fluid field. Further development of FD techniques in computational hydraulics has been limited, due to the poor approximation of boundary conditions by use of interpolation between grid points, to using a rectangular discretization to represent a curved boundary.

At the present stage of development, there is no doubt that FD's are more powerful, readily applicable and economically feasible for problems with regular domains. This has led many investigators to map analytically, physical domains of arbitrary geometry into regular ones, where computations may be carried out efficiently. With this idea, the so-called Boundary-Fitted Curvilinear Coordinate technique (BFCC) has been developed in the last ten years, originally in aerodynamics.

The basic idea of the BFCC is to numerically transform the physical domain into a regular one, and thus eliminate the shape of the boundary as a complicating factor. This allows the flow bounded by arbitrary boundaries to be treated essentially as easily as in simple boundaries.

The ultimate goal of this project is to create a model that will simplify the prediction of subatmospheric pressure on high spillways. To meet this goal, the model must exhibit the following objectives:

- Develop a method of analysis to pre-design spillways by a direct mathematical approach instead of physical modelling;
- Develop the methodology of spillway design which meets the elimination of subatmospheric pressure, and
- Propose a model to calculate pressure and velocity on spillways that have been damaged by cavitation.

It is intended to develop a model to predict flow behavior on open channel spillways which can assist engineers. This is done as follows:

1. To permit a preliminary assessment of flow behavior to be obtained, as well as a qualitative description of flow patterns on spillways.
2. To bridge the gap between what can be achieved by hand calculation and by physical modelling. In some circumstances it is intended that the numerical model will remove the requirement for physical modelling by providing a more expedient alternative.

The model can be used in circumstances where changes in state of flow occur, with attendant variations in depth and velocity over a cross-section. The engineer will thus be in a better position to analyze the flow and to take appropriate steps to improve spillway performance.

A numerical model will help the dam engineer determine the necessary spillway wall heights required to contain extreme flood events. At the end of spillways, the numerical model will simulate the conditions of approach to a downstream channel or stilling pool, providing the distribution of depth and velocity both in magnitude and direction across the channel at the inlet to the tailwater.

To achieve the goals herein described, the project is subdivided into the following chapters:

In Chapter 1, a detailed evaluation based on lecture reviews and author experience is made in order to outline in detail the nature of problem under consideration.

In Chapter 2, the mathematical model of the flow over spillways is developed, based on the two-dimensional incompressible Navier-Stokes, continuity, and free-surface equations. Such an analysis allows us to extrapolate the computational results to the class of spillways based on variation of the size and shape. Also, the assumptions of the developed mathematical spillway model are discussed in this Chapter.

In Chapter 3, the computer model of the spillway is formulated. This includes the discretization of the governing equations in potential flow mesh carried out by central differences in space. The boundary conditions on the flow variables are derived for free-and non-slip velocity conditions at a rigid wall and for the free-slip condition at the free surface. Finally, the computer code to solve the formulated spillway flow is developed and some aspects of the numerical procedure are discussed.

In Chapter 4, the small scale model of a standard spillway is tested on a specially created test set-up. Where more validation was necessary, we used the data gathered from the actual big scale models that was damaged with cavitation.

In Chapter 5, a comparison of numerical and experimental studies was done. This comparison included the WES spillway and numerical model. A good agreement between the experiment and model is found.

In Chapter 6, a discussion of the results obtained in this investigation, conclusions and recommendations for future work are presented.

Chapter 2.0

MATHEMATICAL MODELLING OF FLOW OVER SPILLWAYS

2.1 General

Since the shape of the free surface will be determined as part of the solution, it will generally not coincide with one of the coordinate lines in any predetermined and fixed coordinate system. Thus, the traditional finite difference discretization in a predetermined frame of reference turns out to be quite cumbersome in solving free- surface problems.

The potential flow method, based on the Boundary-Fitted Curvilinear Coordinate (BFCC) system, will be described and applied to the solution of flow profiles, velocities and pressures for flow on a spillway.

The difficulty in determining the free surface will be resolved using the BFCC system. In such a scheme, the shape of the free surface will be made to fit with one of the coordinate lines. The coordinate lines in the entire flow domain will not be fixed prior to solving the free surface but will be determined during the course of the iterative solution procedure. A comprehensive review on BFCC is describe by Thompson and Warsi (1982).

2.2 Methods of spillway design

2.2.1 Spillway layout

The spillway layout must be determined before any detailed design is made. The layout study frequently involves the investigation of several alternatives. Important considerations in selecting the layout are the foundation conditions, the amount and type of excavation, the alignment of the approach and discharge channels, as well as the location of the spillway with respect to the dam and other structures. The foundation conditions alone often require detailed study, with consideration given to such items as faults, seepage, swelling, rebound, settlement, weathering, frost heaving allowable bearing pressures, and a particular allowable shear stress.

2.2.2 Hydraulic and structural design

The detailed hydraulic design to establish the dimensions of the structure can be made once the design discharge tailwater rating curve and layout have been determined. This part of the design is concerned with the lengths, widths, wall height elevations, shapes, and positions of the various components of the structure. Actually, some of the dimensions are usually established approximately in a preliminary hydraulic design, since studies on the outflow hygrograph and layout must be closely related to the hydraulic design.

The structural design is the final phase of the complete spillway design. This involves assessment of the magnitude and distribution of the ice, earth, water pressures, calculation of loads, solution of permissible steel and concrete stresses, and hence calculation of the concrete thickness and steel design. This phase also includes the design of a number of very important details, such as the drainage system, joints, cutoffs,

anchors, hoists, and bridges.

2.2.3 Crest design

It is common practice to design a pressure-free profile for the crest shape of large high head spillways. A pressure free profile is where the pressure at the design flow is neither positive nor negative, but essentially at atmospheric pressure. This is achieved by shaping the crest to fit the underside of the nappe as it would occur when discharging freely from a sharp crested weir at the design head (Fig. 2.1). If the spillway profile is designed exactly in the shape of the lower nappe of a free overflow, the pressure on the spillway crest under the design head should theoretically be nil. For practical reasons, however, such an ideal profile is designed so that low pressures will develop on the surface of the spillway. The x and y coordinates for the spillway shape are given in Table 2.1.

These coordinates give the nappe shape for a high spillway such that reservoir conditions exist upstream and the total energy line coincides with the reservoir surface. The total head measured above the sharp crest is defined as H_s , and H_d is the distance between the crest of under nappe profile and water surface level at reservoir, as shown in Fig. 2.1. The empirical shape of the flow nappe over a sharp-crested weir can be interpreted by the parabolic trajectory of a projectile (Chow, 1959). The lower surface of the nappe in the trajectory profile is:

$$\frac{y}{H_d} = \bar{A} \left(\frac{x}{H_d} \right)^2 + \bar{B} \frac{x}{H_d} + \bar{C} \quad (2.1)$$

and the similarly upper surface of the nappe is:

$$\frac{y}{H_d} = \bar{A} \left(\frac{x}{H_d} \right)^2 + \bar{B} \frac{x}{H_d} + \bar{C} + \bar{D} \quad (2.2)$$

Table 2.1: Vertical weir lower nappe coordinates^a

x/H_s	y/H_s	x/H_s	y/H_s	x/H_s	y/H_s
0.00	0.0000	0.35	0.1060	0.90	-0.140
0.05	0.0575	0.40	0.0970	1.00	-0.215
0.10	0.0860	0.45	0.0845	1.20	-0.393
0.15	0.1025	0.50	0.070	1.40	-0.606
0.20	0.1105	0.60	0.032	1.60	-0.850
0.25	0.1120	0.70	-0.016	1.80	-1.132
0.30	0.1105	0.80	-0.074	2.00	-1.451

a. Negligible velocity of approach V_a (Fig. 2.1).

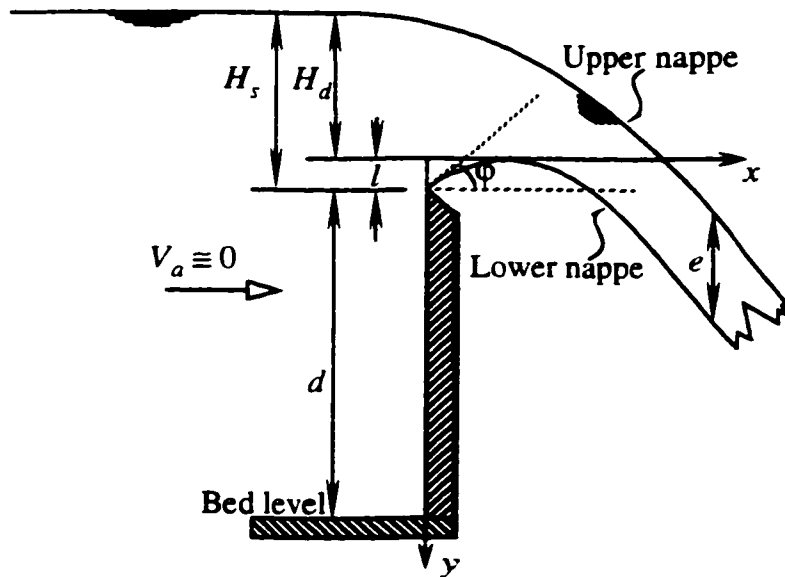


Fig. 2.1 Crest shape for a spillway

where $\bar{A} = (gH_d/2V_a^2) \cos^2 \phi$, V_a is the approach velocity, ϕ is the angle of inclination of the velocity V_a with the horizontal, $\bar{B} = -\tan \phi$, $\bar{C} = l/H_d$, l is equal to the vertical distance between the highest point of the lower surface of the nappe and the elevation of the crest, $\bar{D} = e/H_d$, e is the vertical thickness of the nappe, that is constant because V_a is constant. If the approach flow is subcritical, the above equations apply. For supercritical flow ($F > 1$) the nappe profile becomes essentially a function of the Froude number rather than a function of the boundary geometry. The discharge for this weir is given by the well-known equation for a sharp crested weir.

$$Q = C_d 2/3 \sqrt{2g} b H_s^{3/2} \quad (2.3)$$

In which Q is the discharge in m^3/s , b is the net crest length in meters and C_d is the coefficient of the discharge. The standard value of C_d for a sharp crested weir, as originally determined by Francis (1850), is 0.622, and hence the discharge equation becomes:

$$Q = 1.837 b H_s^{3/2} \quad (2.4)$$

The value 1.837 is called the weir coefficient, and has the units of \sqrt{g} . When the area under the nappe is filled in with solid material, the crest of the weir is effectively $0.112H_s$ above the origin of the coordinates for the nappe curve. This point is H_d below the reservoir surface, and not H_s . If H_d is used in the discharge equation, the corresponding weir coefficient will be greater than 1.837 and can be computed by equating $1.837 b H_s^{3/2}$ to $C L H_d^{3/2}$, where C is the weir coefficient corresponding to head H_d . Noting that $H_d = (1 - 0.112) H_s$, then $C = 1.837 / (1 - 0.112)^{3/2}$ and the discharge is

$$Q = 2.195 b H_d^{3/2} \quad (2.5)$$

The actual coefficient may be reduced slightly due to the additional frictional

resistance which results when a solid boundary is substituted for the space under the nappe. This correction may amount to 1 or 2% in the usual case, the smaller value being applicable to larger spillways where crest friction is relatively small.

Now it becomes evident that if the space under the nappe is filled in with solid material, then it will only fit the nappe for the one head for which it was designed. At a lower head, the nappe will be supported, positive pressure will develop on the crest, and the coefficient will decrease. At a head greater than the design head, negative pressures will develop and the coefficient will increase. The effect on the coefficient in terms of the ratio H/H_d is given in Table 2.2, in which H_d is the head used for the design of the crest shape and H is the head on the crest at any time.

Table 2.2: Experimentally determined coefficient C (from Blevins, 1984)

H/H_d	0.1	0.2	0.4	0.6	0.8	1.0	1.2	1.4	1.6
C (SI units)	1.78	1.84	1.97	2.07	2.15	2.22	2.29	2.34	2.40

Owing to the energy loss involved in the flow over spillways, the actual velocity is always less than the theoretical value. The magnitude of the actual velocity depends mainly on the head on the spillway crest, the fall, the slope of the spillway surface, and the spillway surface roughness. Experiments by Bauer (1954) indicate that the frictional losses in accelerating the flow down the face of a spillway may be considerably less than the normal friction loss in fully well-developed turbulence. Therefore, the friction loss is not significant on steep slopes, but it would become important if the slope were small. Where the downstream face of the overflow is formed in a manner which produces streamlined flow, the experimental work of Bradley and Peterka (1957) may be employed to determine conditions where flow enters the downstream channel. This work is applicable in cases where the WES profile is applied (Fig. 2.2). Data for computing depths

and velocities of flow down steep slopes is still inconclusive. The research presented may make it possible to get data for depths and velocities at any points over spillways. Theoretical velocity, neglecting losses, is given by:

$$V_T = \sqrt{2g(Z + H_a - y_1)} \quad (2.6)$$

where Z is the vertical distance from the upstream reservoir level to the floor at the toe, H_a and y_1 are upstream approach velocity head, and the tailwater elevation where the velocity is calculated. A reasonable estimate for the actual velocity, V_A , may be determined from graph (U.S. Bureau of Reclamation) for the various head H on the spillway crest and drop heights (Fig. 2.2).

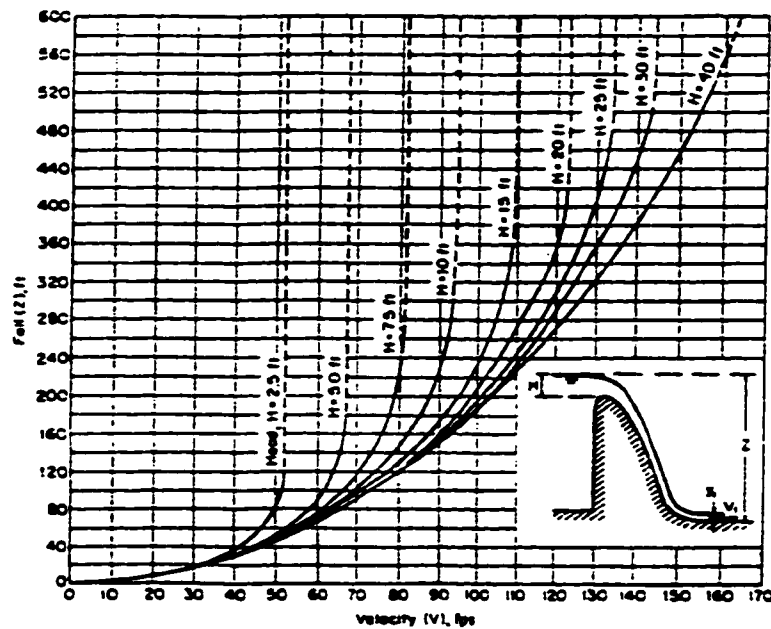


Fig. 2.2 Curves for determination of velocity at the toe of spillway.

2.2.4 Point of tangency

The slope function graph of a tangent to the downstream quadrant is shown in Fig. 2.3 to facilitate the location of point tangency. Although it is realized that the tangent point will often be determined analytically for the final design, this graph should be useful in the preliminary layouts in connection with stability analyses and cost estimates.

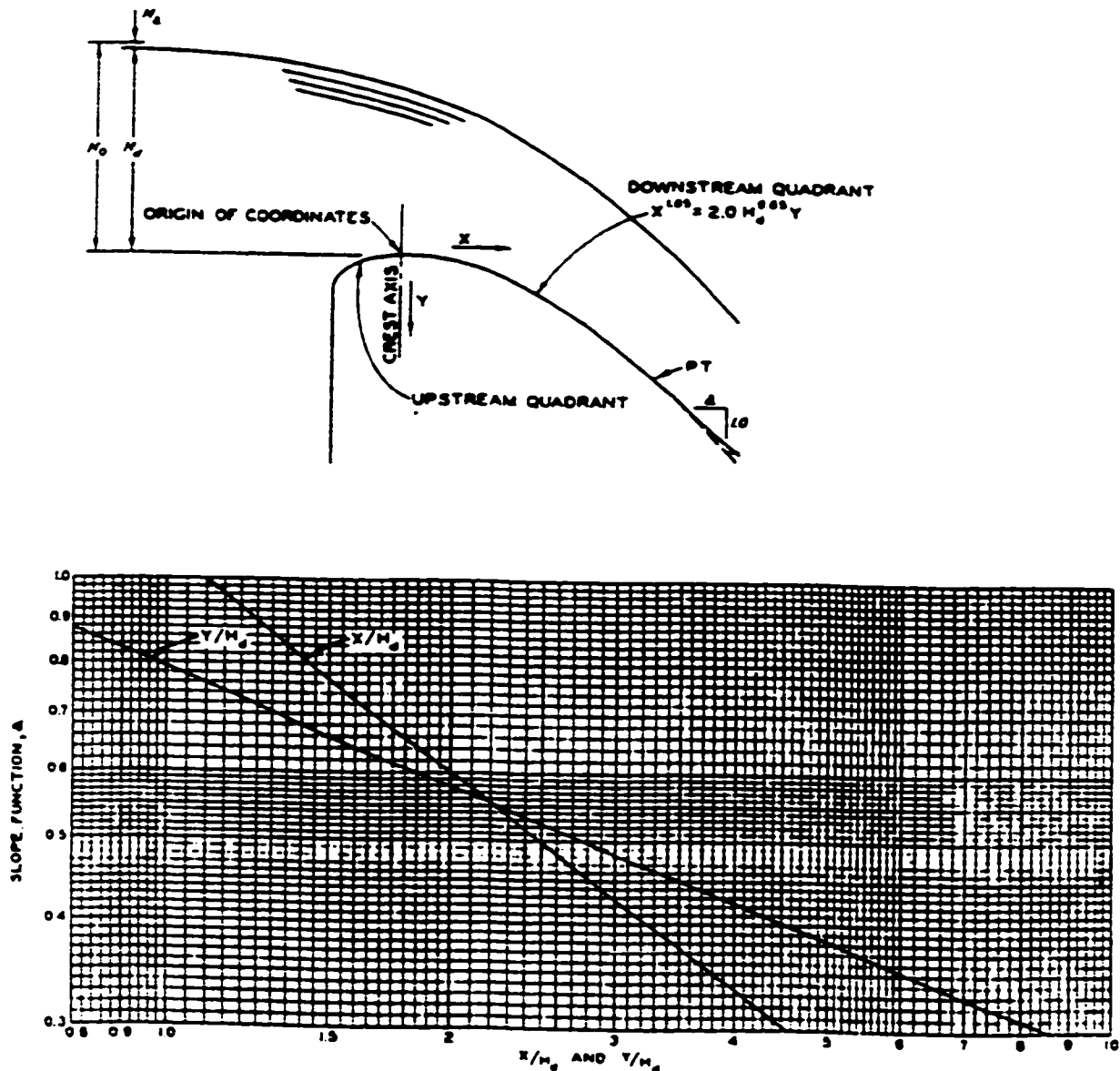


Fig. 2.3 Spillway crest tangent ordinates.

2.2.5 Numerical methods

In this section, some numerical methods in the area of free surface solvers are reviewed. To compute supercritical flow in channels including the effects of bottom slope and friction, the shallow-water equations are commonly used. Liggett and Vasudev (1965) used these equations in two-dimensional flow.

Ellis and Pender (1982) used an implicit method of characteristics to compute high-velocity flows in channels of arbitrary alignment and slope.

The well-known equations in this area are the St. Venant equations, in which two-dimensional flows may be written in vector forms as:

$$\frac{\partial \mathcal{U}}{\partial t} + \frac{\partial \mathcal{E}}{\partial x} + \frac{\partial \mathcal{F}}{\partial y} + \mathcal{S} = 0 \quad (2.7)$$

where \mathcal{U} , \mathcal{E} , \mathcal{F} , and \mathcal{S} are vectors given by:

$$\mathcal{U} = \begin{bmatrix} h \\ uh \\ vh \end{bmatrix} \quad \mathcal{E} = \begin{bmatrix} uh \\ u^2h + \frac{1}{2}gh^2 \\ uvh \end{bmatrix}$$

$$\mathcal{F} = \begin{bmatrix} vh \\ uvh \\ v^2h + \frac{1}{2}gh^2 \end{bmatrix} \quad \mathcal{S} = \begin{bmatrix} 0 \\ -gh(S_{0x} - S_{fx}) \\ -gh(S_{0y} - S_{fy}) \end{bmatrix}$$

In which t = time, u = depth-averaged flow velocity in x-direction, v = depth averaged flow velocity in y-direction, h = water depth measured vertically, g = acceleration due to gravity, $S_{0(x,y)} = \sin\theta_{(x,y)}$ = channel bottom slope in the (x, y) direction, $\theta_{(x,y)}$ = angle between the bottom of the channel and the (x, y) directions,

$S_{f(x,y)}$ = frictions in the (x, y) directions, the friction slope S_f is calculated from following steady-state formulas:

$$S_{fx} = \frac{n^2 u \sqrt{u^2 + v^2}}{C_o^2 h^{1.33}} \quad (2.8)$$

$$S_{fy} = \frac{n^2 v \sqrt{u^2 + v^2}}{C_o^2 h^{1.33}} \quad (2.9)$$

In which n = Manning roughness coefficient and C_o = correction factor for units ($C_o = 1$ in SI units and $C_o = 1.49$ in customary units).

Of all the simplifying assumptions made to derive the St. Venant equations, the hydrostatic pressure distribution is the weakest one for the present application.

2.3 Mathematical modelling the spillway

2.3.1 Background

A large channel slope has a longitudinal vertical profile of appreciable curvature. Also, as mentioned in Chapter 1, the effect of the curvature in high spillway channels is to produce appreciable acceleration components or centrifugal forces normal to the direction of flow. Thus, the pressure distribution over the section deviates from hydrostatic if curvilinear flow occurs in the vertical plane. Such curvilinear flow may be either convex or concave (Fig. 2.4). The computation of flowfields in and around complex shapes such as airfoil or spillways, etc., involve computational boundaries that do not coincide with coordinate lines in physical space.

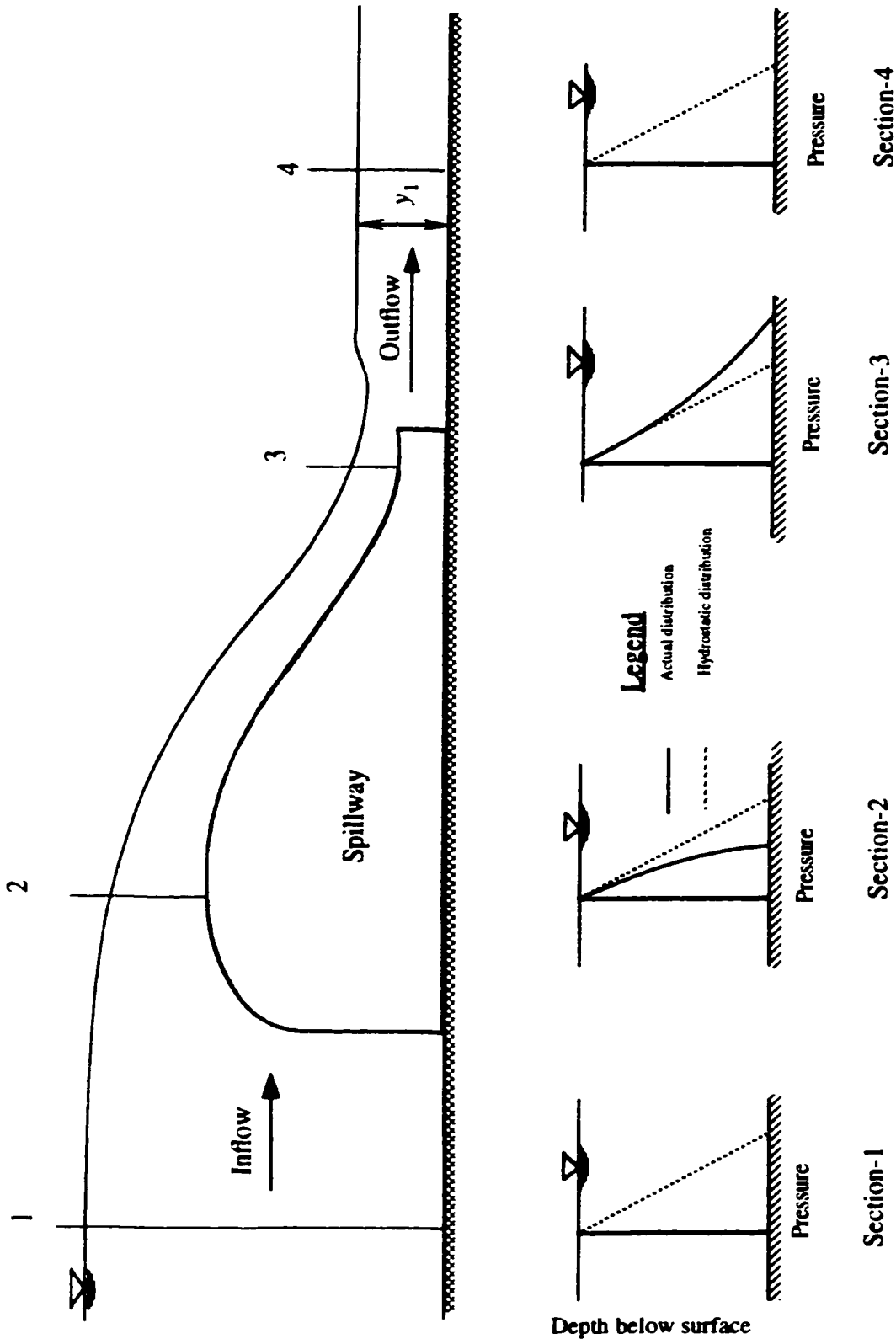


Fig. 2.4 Pressure variation in straight and curved flows.

For finite difference methods, the imposition of boundary conditions for such problems has required a complicated interpolation of data on local grid lines and, typically, a local loss of accuracy in the computational solution. Such difficulties motivate the introduction of a mapping or transformation from physical (x, y) space to a generalised curvilinear coordinate (ξ, η) space. The generation of a boundary conforming coordinate system is accomplished by the determination of the values of curvilinear coordinates in the interior of the physical region from specified values on the boundary of the region. The generalised coordinate domain is constructed so that a computational boundary in physical space coincides with a coordinate line in generalised coordinate space (BFCC).

The use of generalised coordinates implies that a distorted region in physical space is mapped into a rectangular region in the generalised coordinate space. The governing equations are expressed in terms of the generalised coordinates as independent variables, and the discretization is undertaken in the generalised coordinate space. Thus, the computation is performed in the generalised coordinate space, effectively. The use of generalised coordinates introduce some specific complications; e.g., it is necessary to consider what form the governing equations take in generalised coordinates.

The equivalent problem in the transformed region is the determination of values of physical (Cartesian or other) coordinates in the interior of the transformed region from boundary of this region (Fig. 2.5).

This is a more amenable problem for computation, since the boundary of the transformed region is comprised of horizontal and vertical segments, so that this region is composed of rectangular blocks which are contiguous, at least in the sense of being joined flow nets (branch cuts).

The generation of field values of a function from boundary values can be done in

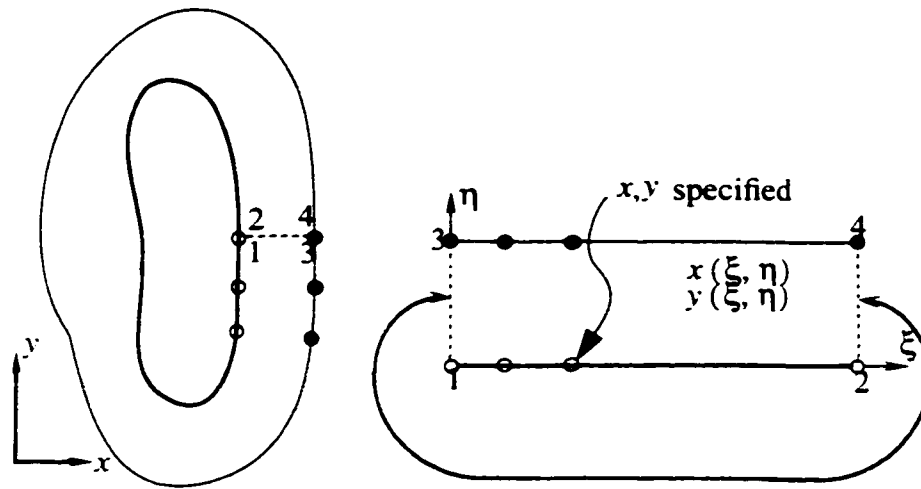


Fig. 2.5 Determination of the transformed domain from the physical domain.

various ways. The solution of such a boundary-value problem, however, is a classic problem of partial differential equations, so that it is logical to take the coordinates to be solutions of a system of practical differential equations (as will be discussed in section 2.8). If the coordinate points are specified on the entire closed boundary of the physical region, the equations must be elliptic.

Mathematically, the free surface problem is a typical initial-boundary value problem. The main difficulty in solving the free surface problem in spillways comes from the uncertainty of the boundaries of the solution domain. Therefore, the free surface position and the shape must be treated as unknowns and obtained as part of the solution. The numerical method seems to be the only way to treat free surface problems. Numerous investigations have been conducted to solve free surface problems restricted by the free surface boundary difficulty. Various simplifications have been made in numerical work. By using Boundary Fitted Coordinate systems generated by numerical methods, the difficulty of treating the free surface can be lessened, since all the calculations will be performed on uniform rectangular grid lines. The elliptic type partial differential equation

encountered in the fluid flow problem is also a natural scheme for the boundary fitted coordinate. since many of the interpolation calculations using the elliptic equation can be much simplified on the rectangular grid. All the computations can be done on a rectangular transformed field with a square mesh, regardless of the shape or configuration of the boundaries in the physical field. Finally, any numerical algorithm in FD can thus be applied.

Before discussing the governing equations, the numerical generation of the BFCC technique dealing with the subject of curvilinear flow is described in the following section.

2.3.2 Numerical generation of Body-Fitted Curvilinear Coordinate systems.

This section presents a detailed development of a method for generating natural coordinate systems for general two-dimensional regions. The numerical technique is used to implement the method. Consider transforming a two-dimensional, single-connected region, e.g: D as shown in Fig. 2.6 bounded by four simple, closed, arbitrary contours onto a rectangular region, D^* . It is required B_1 to map onto B_1^* , B_2 to map onto B_2^* , B_3 onto B_3^* , and B_4 onto B_4^* . For identification purposes region D will be referred to as the physical plane D^* as the transformed plane. Note that the transformed boundaries (B_1^* , and B_2^*) are made constant coordinate lines (η -lines) in the transformed plane.

The general transformation from the physical plane (x, y) to the transformed plane (ξ, η) is given by the vector valued function:

$$\xi = \xi(x, y) \quad (2.10a)$$

$$\eta = \eta(x, y) \quad (2.10b)$$

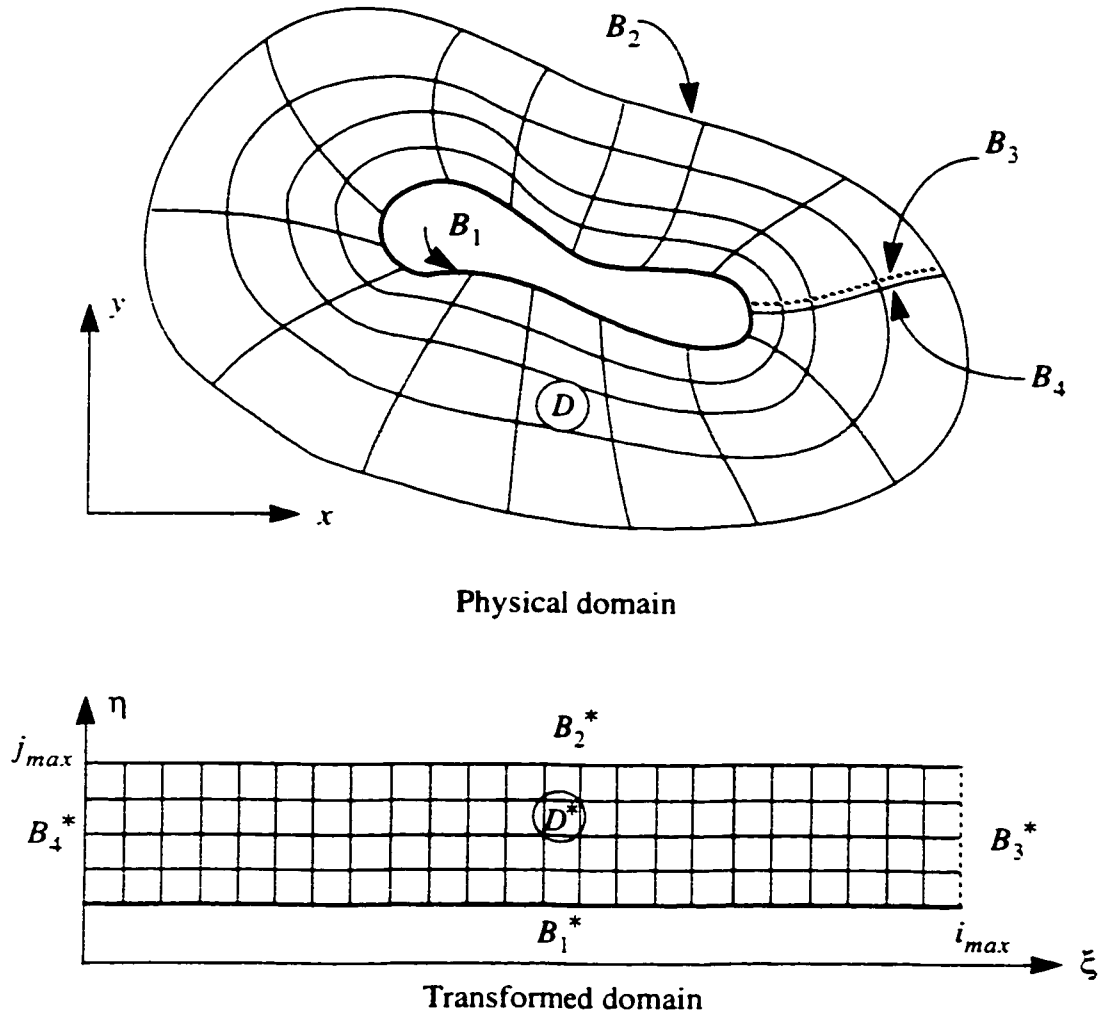


Fig. 2.6 Field transformation-Single body

$$\begin{bmatrix} \xi \\ \eta \end{bmatrix} = \begin{bmatrix} \xi(x, y) \\ \eta(x, y) \end{bmatrix} \quad (2.11)$$

The following differential expressions are obtained:

$$d\xi = \xi_x dx + \xi_y dy \quad (2.12a)$$

$$d\eta = \eta_x dx + \eta_y dy \quad (2.12b)$$

Which are written in a compact form as:

$$\begin{bmatrix} d\xi \\ d\eta \end{bmatrix} = \begin{bmatrix} \xi_x & \xi_y \\ \eta_x & \eta_y \end{bmatrix} \begin{bmatrix} dx \\ dy \end{bmatrix} \quad (2.13)$$

The Jacobian matrix for this transformation is:

$$J_1 = \begin{bmatrix} \xi_x & \xi_y \\ \eta_x & \eta_y \end{bmatrix} \quad (2.14)$$

Reversing the role of independent variables:

$$x = x(\xi, \eta) \quad (2.10a)$$

$$y = y(\xi, \eta) \quad (2.10b)$$

or in vector form:

$$\begin{bmatrix} x \\ y \end{bmatrix} = \begin{bmatrix} x(\xi, \eta) \\ y(\xi, \eta) \end{bmatrix} \quad (2.15)$$

The following may be written as:

$$dx = x_\xi d\xi + x_\eta d\eta \quad (2.16a)$$

$$dy = y_\xi d\xi + y_\eta d\eta \quad (2.16b)$$

In a compact form they are written as:

$$\begin{bmatrix} dx \\ dy \end{bmatrix} = \begin{bmatrix} x_\xi & x_\eta \\ y_\xi & y_\eta \end{bmatrix} \begin{bmatrix} d\xi \\ d\eta \end{bmatrix} \quad (2.17)$$

The Jacobian matrix of Eq. (2.17) will be denoted by J_2 and given by:

$$J_2 = \begin{bmatrix} x_\xi & x_\eta \\ y_\xi & y_\eta \end{bmatrix} \quad (2.18)$$

Comparing equations (2.14) and (2.18), it can be concluded that:

$$\begin{bmatrix} \xi_x & \xi_y \\ \eta_x & \eta_y \end{bmatrix} = \begin{bmatrix} x_\xi & x_\eta \\ y_\xi & y_\eta \end{bmatrix}^{-1} \quad (2.19)$$

$$J = \det [J_2] = x_\xi y_\eta - x_\eta y_\xi \quad (2.20)$$

and is defined as the Jacobian of the transformation which implies the relations:

$$\xi_x = y_\eta / J \quad (2.21a)$$

$$\xi_y = -x_\eta / J \quad (2.21b)$$

$$\eta_x = -y_\xi / J \quad (2.21c)$$

$$\eta_y = x_\xi / J \quad (2.21d)$$

Terms such as x_ξ , y_ξ , x_η , and y_η appearing in transformation derivatives are defined as the metrics of transformation or simply as the metrics. The computation of the metrics is considered as equations (2.21a)-(2.21d). The interpretation of the metrics is obvious considering the following approximation:

$$x_\xi = \frac{\partial x}{\partial \xi} \equiv \frac{\Delta x}{\Delta \xi} \quad (2.22)$$

This expression indicates that metrics represent the ratio of arc lengths in the physical space to that of the computational space.

For grid generation, metrics can be determined numerically by the use of finite difference expressions where the subscripts denote partial differentiation in the usual manner.

2.3.3 Governing Equations

The mathematical basis of the proposed numerical model for the simulation of flow over a spillway for the determination of the cavitation parameter is presented. The two-dimensional viscous incompressible flow about any number of bodies may be described by the Navier-Stokes equations in the vorticity-stream function formulation. Therefore, the full Navier-Stokes equations are:

$$\nabla \cdot \vec{q} = 0 \quad (2.23)$$

$$\rho \vec{q} \cdot \nabla \vec{q} = \rho \vec{X} - \nabla P + \mu \nabla^2 \vec{q} \quad (2.24)$$

where \vec{X} and \vec{q} are body force, and velocity vectors respectively. For flows not involving body forces, the non-dimensionalisation of Eqs. (2.23) and (2.24) produce the following equations in two-dimensional Cartesian coordinates:

$$\frac{\partial u}{\partial x} + \frac{\partial v}{\partial y} = 0 \quad (2.25)$$

$$u \frac{\partial u}{\partial x} + v \frac{\partial u}{\partial y} + \frac{\partial P}{\partial x} = \frac{1}{R} \left(\frac{\partial^2 u}{\partial x^2} + \frac{\partial^2 u}{\partial y^2} \right) \quad (2.26)$$

$$u \frac{\partial v}{\partial x} + v \frac{\partial v}{\partial y} + \frac{\partial P}{\partial y} = \frac{1}{R} \left(\frac{\partial^2 v}{\partial x^2} + \frac{\partial^2 v}{\partial y^2} \right) \quad (2.27)$$

By differentiating Eq. (2.24) with respect to x , y , and by subtracting the resulting equations, the following equation is constructed:

$$u \frac{\partial \zeta}{\partial x} + v \frac{\partial \zeta}{\partial y} = \frac{1}{R} \left(\frac{\partial^2 \zeta}{\partial x^2} + \frac{\partial^2 \zeta}{\partial y^2} \right) \quad (2.28)$$

$$\zeta = \frac{\partial u}{\partial y} - \frac{\partial v}{\partial x} \quad (2.29)$$

where x , y , ζ , u , v , and R are respectively: horizontal direction, vertical direction, vorticity, velocity in x direction, velocity in y direction, and Reynold's number. Eq. (2.29) is a two-dimensional vorticity transport flow in the x - y plane, that indicates the rate of dissipation of vorticity through friction. Fig. 2.7 is showing the piecewise spatial view of spillway channel geometry in (x, y, z) coordinates.

For irrotational flow ζ equals zero. In case of flow with very large Reynolds numbers, the effects of viscosity are confined to a very thin layer in the immediate vicinity of a solid boundary. The boundary layer turbulence effect is small and can usually be neglected at the high velocities that are normally encountered in hydraulic structures where cavitation is suspected (Johnson, 1963). In the region outside this thin boundary layer, viscous forces can be completely neglected in comparison with inertial forces; hence only potential flow exists. Investigations in hydrodynamics of irrotational flow stating that the minimum pressure in the flow field always occurs at the boundary. If the boundary layer is not separated the minimum pressure occurs at the body wall. The minimum pressure may not occur on the wall (for large body curvatures) but slightly away from it in the center of the eddies inside the boundary layer, because the flow in the boundary layer is rotational. Thus, cavitation actually begins at values of $\sigma(x)$ that are slightly greater than $\sigma_i(x)$ ¹ because of the additional pressure reduction caused by turbulence. Cavitation is a phenomenon depending on the absolute pressure and is closely associated with the momentum pressure relation of the main flow outside the boundary layer. Whereas separation depends on the momentum pressure relation within the boundary layer. Basically separation occurs at a position along a guiding boundary surface

1. Inception index of cavitation is defined as $\sigma(x) = 2(P_0 - P_v) / \rho V_0^2(x)$. Where $P_0(x)$ and $V_0(x)$ are the pressure and mean velocity, and P_v is vapor pressure.

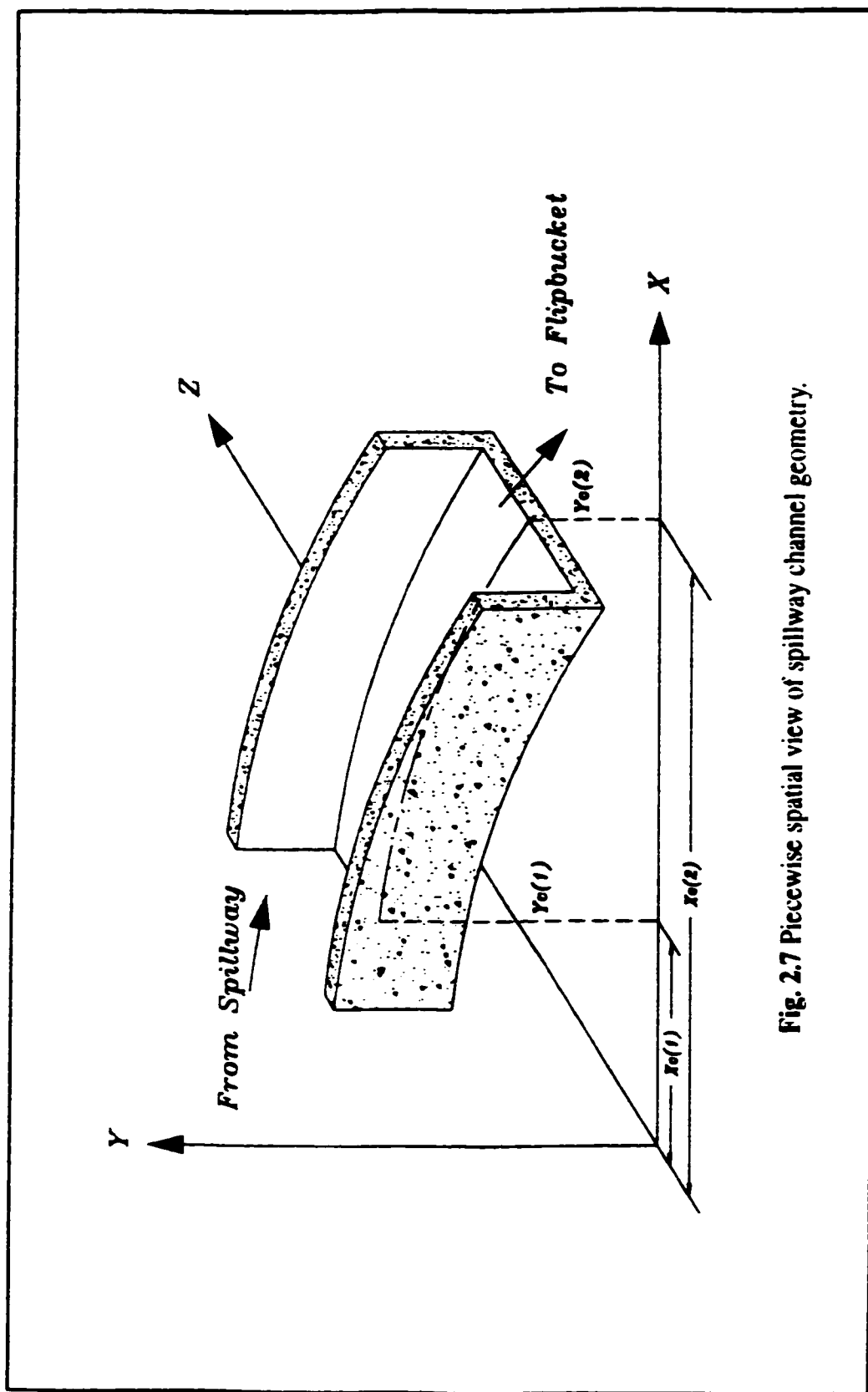


Fig. 2.7 Piecewise spatial view of spillway channel geometry.

where the flow-direction increase in pressure must be obtained by a decrease in the momentum of the fluid. The fluid in the boundary layer moves at a lower velocity than that in the main fluid domain because part of its energy is dissipated by boundary friction. When the assumptions that are made are justified, the flow must be a good approximation to potential flow with no boundary-layer separation and, if the flow is separated, $\sigma(x)$ has little significance as to the location or magnitude of the true minimum pressure in the flow. The above discussion implies the assumption that the flow is irrotational. This assumption is a reasonable one, since losses must be small over a short length of spillway involved, and the highly turbulent approaching flow must have a transverse velocity distribution very close to the uniform distribution which is characteristic of irrotational flow of a perfect fluid. Also, there is little risk of separation when a solid boundary is continually curving into the flow, as in this case, pressure distributions should therefore be close to those in the irrotational flow of a perfect fluid. This conclusion is confirmed by the good agreement between theory and experiment. However incipient cavitation index, $\sigma_i(x)$, is the negative of the minimum pressure coefficient in the flow field. The minimum pressure in flow field will exist at the core of the rotational vortex in the boundary layer. Therefore, for the present model, the assumptions are:

- 1) High Reynold's number
- 2) Uniform flow at inflow and outflow boundaries
- 3) Smooth surface, therefore no irregularities
- 4) Separation does not occur during the operation at design head or for operating heads less than three times the design head $H/H_d < 3$ (Rouse *et al.* 1935). If the spillway profile is smoothly curved according to a given nappe profile, the absence of abrupt changes in curvature at any point would permit an increase in head without danger of separation. Indeed, model studies of Rouse, and Reid (1935) and of Dillman (1933) for

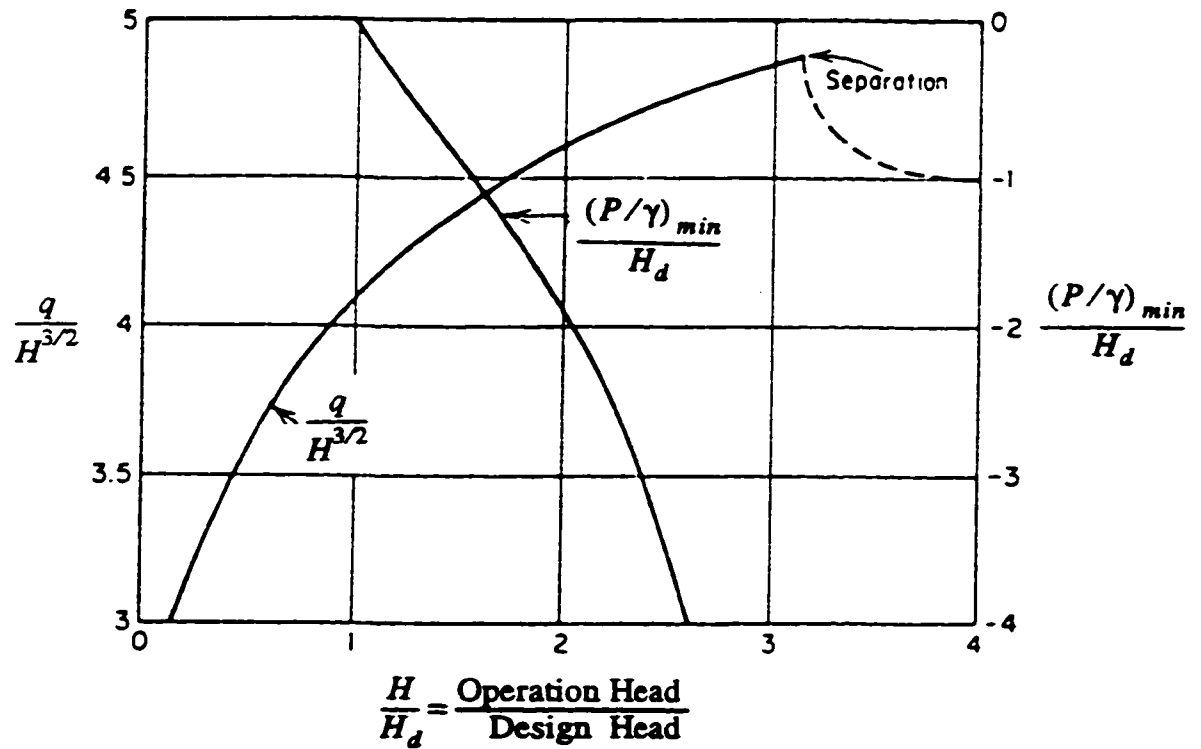


Fig. 2.8 Spillway crest characteristic (after H. Rouse and L. Reid, 1935 and O. Dillman, 1933).

pressure plotted in Figure 2.8, show that the actual head H may safely exceed the design head by at least 50 percent, with a 10 percent increase in the discharge coefficient. Separation could happen if $H/H_d > 3$, this does not occur in the life of spillway (Rouse, and Reid, 1935, and Dillman, 1933).

What is known is that boundary layers separate in adverse pressure gradients, so that the magnitude and extent of such pressure gradients should be minimized. This means that bodies should be streamlined rather than bluff and should be oriented at small angles of attack. Also, it is known that sharp corners which bend away from the fluid become separation point, so that such corners should be avoided if separation is to be delayed as far as possible (Currie, 1974).

5) Flow is irrotational, so potential flow and the Bernoulli equation are satisfied.

There are several reasons for this assumption:

5.1 Experiments by Bauer (1954) indicate that friction losses related to accelerated flow over a spillway may be considerably less than the normal friction loss in flow with well-developed turbulence in channel. Therefore, the friction loss is not significant on steep slopes, but it would become important if the slope were small.

5.2 Based on energy dissipation ϕ by Lamb (1932) formula:

$$\phi = \mu \iiint_V (\vec{\nabla} \times \vec{q}^2) dv + \mu \iint_S \frac{\partial}{\partial n} q^2 ds - 2\mu \iint_S (\vec{q} \times \vec{\nabla} \times \vec{q}) \cdot \vec{n} ds \quad (2.30)$$

When a liquid passes over an obstacle having the form of a lamina of thickness h placed between two plates, the kinematical conditions are accordingly identical, for the most part, to those relating to the two-dimensional flow of frictionless fluid past an obstacle whose section has the shape of the lamina.

By Bauer's statement $\phi = 0$ for spillway and for inviscid flow, from Lamb's equation, it is clear that $\vec{\nabla} \times \vec{q} = 0$, meaning that, flow could be assumed irrotational. Also irrotational potential flow can be determined by the velocity vector as follows:

$$\vec{V} = \vec{\nabla} \phi \quad (2.31)$$

where ϕ is the velocity function and vorticity is defined as:

$$\zeta = \vec{\nabla} \times \vec{V} \quad (2.32)$$

But, mathematically:

$$\zeta = \vec{\nabla} \times \vec{\nabla} \phi = 0 \quad (2.33)$$

It says potential flow could be irrotational.

5.3 U.S. Bureau of Reclamation:

Considerable experimental work has been done on this problem at the U.S. Bureau of Reclamation which presents that when the head H and the discharge are small, the depth of flow will be small, and the effect of resistance will be marked.

Introducing a stream function ψ such that:

$$u = \frac{\partial \psi}{\partial y} \quad (2.34)$$

$$v = -\frac{\partial \psi}{\partial x} \quad (2.35)$$

Substitution of Eq. (2.34) and Eq. (2.35) into Eq. (2.25) gives:

$$\nabla^2 \psi = 0 \quad (2.36)$$

This is an elliptic function in space. It is known as the Laplace's equation and can be written as:

$$\psi_{xx} + \psi_{yy} = 0 \quad (2.37)$$

2.4 Application to potential flow

As an initial application of the Cartesian coordinate system, the Laplace equation for the stream function potential flow is solved numerically using the curvilinear coordinate system. There were several reasons for this choice. First, the solution was of interest in itself as simply another potential flow method for spillway. Secondly, it provided an

excellent starting solution (i.e., an impulsive start) for the viscous flows (Thames, 1976). Roache (1982) says that potential flow can provide an excellent solution close to the analytical solution. Thirdly, it is easy to formulate the boundary conditions of the free surface. Finally, since Laplace's equation arises in many areas of physical science, a demonstrated proficiency in solving this equation for arbitrary regions would imply that the Cartesian coordinate method would be of general interest. Montes (1992) in his paper on step overfall says:

"A complete solution of free overfall, requires an integration of the turbulent Reynolds equations using an adequate turbulence model to present the shear stresses. Finnie and Jeppson (1991) have attempted this type of calculation for related problems of flow under a sluice gate using the $K - \epsilon$ method. With the success of the previous potential flow calculation, notably that which Markland (1965) showed within the limitation of free overfalls preceded by horizontal or adverse slopes, it is not necessary to resort to such complexity to obtain a very detailed account of all flow features, namely water surface profile, velocity, pressure and angle of inclination characteristics."

Because the spillway is an alternative for overfall, it can be said that potential flow must also be applicable in this problem.

2.5 Transformation of the Governing partial differential equations

The equations of fluid motion include the continuity and the momentum equations. For the present 2-D problem the transformation of a PDE¹ to the BFCC and the complexity of the resultant equation is proposed. It should be mentioned that the form and type of the transformed equations remains the same as the original PDE, i.e., if the original equation is elliptic, then the transformed equation is also elliptic. Now, we define the

1. Partial differential equation

following relations between the physical and computational spaces.

$$x = x(\xi, \eta) \quad (2.38a)$$

$$y = y(\xi, \eta) \quad (2.38b)$$

The chain rule for partial differentiation yields the following expression:

$$\frac{\partial}{\partial \xi} = \frac{\partial x}{\partial \xi} \times \frac{\partial}{\partial x} + \frac{\partial y}{\partial \xi} \times \frac{\partial}{\partial y} \quad (2.39)$$

The partial derivatives will be denoted using the subscripts notation, i.e. $\frac{\partial x}{\partial \xi} = x_\xi$. Hence,

$$\frac{\partial}{\partial \xi} = x_\xi \frac{\partial}{\partial x} + y_\xi \frac{\partial}{\partial y} \quad (2.40a)$$

and similarly:

$$\frac{\partial}{\partial \eta} = x_\eta \frac{\partial}{\partial x} + y_\eta \frac{\partial}{\partial y} \quad (2.40b)$$

Partial derivatives are transformed using the relations (2.40a) and (2.40b) as follows:

$$f_x = (y_\eta f_\xi - y_\xi f_\eta) / J \quad (2.41a)$$

$$f_y = (-x_\eta f_\xi + x_\xi f_\eta) / J \quad (2.41b)$$

where f is some sufficiently differentiable function of x and y .

The first step is to express Laplace's equation in the transformed plane. Utilizing Eqs. (2.40a) and (2.40b), we obtain:

$$\alpha \psi_{\xi\xi} - 2\beta \psi_{\xi\eta} + \gamma \psi_{\eta\eta} + (Dx) (y_\xi \psi_\eta - y_\eta \psi_\xi) / J + (Dy) (x_\eta \psi_\xi - x_\xi \psi_\eta) / J = 0 \quad (2.42)$$

where:

$$Dx = \alpha x_{\xi\xi} - 2\beta x_{\xi\eta} + \gamma x_{\eta\eta} \quad (2.43a)$$

$$Dy = \alpha y_{\xi\xi} - 2\beta y_{\xi\eta} + \gamma y_{\eta\eta} \quad (2.43b)$$

Introducing the definitions:

$$\sigma \equiv [y_{\xi}(Dx) - x_{\xi}(Dy)] / J \quad (2.43c)$$

$$\tau \equiv [x_{\eta}(Dy) - y_{\eta}(Dx)] / J \quad (2.43d)$$

equation (2.42) reduces to:

$$\alpha \psi_{\xi\xi} - 2\beta \psi_{\xi\eta} + \gamma \psi_{\eta\eta} + \sigma \psi_{\eta} + \tau \psi_{\xi} = 0 \quad (2.44)$$

where transformation parameters are:

$$\alpha = x_{\eta}^2 + y_{\eta}^2 \quad (2.45a)$$

$$\beta = x_{\xi}x_{\eta} + y_{\xi}y_{\eta} \quad (2.45b)$$

$$\gamma = x_{\xi}^2 + y_{\xi}^2 \quad (2.45c)$$

$$J = x_{\xi}y_{\eta} - x_{\eta}y_{\xi} \quad (2.45d)$$

$$\sigma = [y_{\xi}(\alpha x_{\xi\xi} - 2\beta x_{\xi\eta} + \gamma x_{\eta\eta}) - x_{\xi}(\alpha y_{\xi\xi} - 2\beta y_{\xi\eta} + \gamma y_{\eta\eta})] / J \quad (2.45e)$$

$$\tau = [x_{\eta}(\alpha y_{\xi\xi} - 2\beta y_{\xi\eta} + \gamma y_{\eta\eta}) - y_{\eta}(\alpha x_{\xi\xi} - 2\beta x_{\xi\eta} + \gamma x_{\eta\eta})] / J \quad (2.45f)$$

If a non-contracting natural coordinate system is employed, Dx and Dy vanish by equations:

$$\alpha x_{\xi\xi} - 2\beta x_{\xi\eta} + \gamma x_{\eta\eta} = 0 \quad (2.46a)$$

$$\alpha y_{\xi\xi} - 2\beta y_{\xi\eta} + \gamma y_{\eta\eta} = 0 \quad (2.46b)$$

The quantities σ and τ also vanish which reduces Eq. (2.42) to:

$$\alpha \psi_{\xi\xi} - 2\beta \psi_{\xi\eta} + \gamma \psi_{\eta\eta} = 0 \quad (2.47)$$

2.6 Boundary conditions

The boundary conditions for the single body solution Fig. 2.9 have the general form:

$$\psi|_{B_4} = 0 \quad (2.48a)$$

$$\psi|_{B_3} = q \quad (2.48b)$$

$$\psi|_{B_1} = q \frac{h}{h_1} \quad (2.48c)$$

$$\psi|_{B_2} = q \frac{h}{h_2} \quad (3.48d)$$

where:

h = the depth B_1 (and B_4) with respect to solid boundary at any studied point on the liquid boundary

h_1 = upstream depth

h_2 = downstream depth

q = discharge per unit width



60

The actual boundary conditions and the equivalent versions for numerical implementation are summarized in Table 2.3.

Table 2.3: Boundary conditions and numerical equivalent in physical domain D .

Boundary region	Conditions	Numerical implementation
Solid surface	$\psi = 0$	$\psi = 0$
Inlet	$\frac{\partial \psi}{\partial n} = 0$	$\psi _{B_1} = q \frac{h}{h_1}$
Free surface	$\frac{\partial \psi}{\partial n} = V_s = \sqrt{2g(E-y_s)}$	$\psi = q$
Outlet	$\frac{\partial \psi}{\partial n} = 0$	$\psi _{B_2} = q \frac{h}{h_2}$

2.6.1 Transformation of boundary conditions in Boundary Fitted Curvilinear Coordinate

$$\psi|_{B_1^*} = 0 \quad (2.49a)$$

$$\psi|_{B_2^*} = q \quad (2.49b)$$

$$\frac{\psi}{h} \Big|_{B_1^*} = \frac{q}{B} \quad (2.49c)$$

$$\frac{\psi}{h} \Big|_{B_2^*} = \frac{q}{B} \quad (2.49d)$$

where:

D^* = New flow Domain in ξ, η direction

B_1^*, B_2^*, B_3^* and B_4^* are boundaries of domain D^* , B is wide of this domain.

Finally, the transformed potential flow and velocities Eqs. (2.37), (2.34) and (2.35) with stream function in BFCC ($\zeta \equiv 0$) are:

$$\alpha\psi_{\xi\xi} - 2\beta\psi_{\xi\eta} + \gamma\psi_{\eta\eta} + \sigma\psi_{\eta} + \tau\psi_{\xi} = 0 \quad (2.44)$$

$$u = (\psi_{\eta}x_{\xi} - \psi_{\xi}x_{\eta})/J \quad (2.50)$$

$$v = (\psi_{\eta}y_{\xi} - \psi_{\xi}y_{\eta})/J \quad (2.51)$$

2.7 Tangent and normal velocity vector components to lines of constant ξ and η

Tangent and normal unit vectors are shown in Fig. 2.10. Where C_j (for $j = 1 \dots N$) is a η -line with constant value, and K_i is a ξ -line with constant value. The tangent and normal vector components to lines of constant ξ and η are given by:

$$\dot{f}_n(\eta) = (-y_{\xi}f_x + x_{\xi}f_y)/\sqrt{\gamma} \quad (2.52a)$$

$$\dot{f}_t(\eta) = (-x_{\xi}f_x + y_{\xi}f_y)/\sqrt{\gamma} \quad (2.52b)$$

$$\dot{f}_n(\xi) = (y_{\eta}f_x - x_{\eta}f_y)/\sqrt{\alpha} \quad (2.52c)$$

$$\dot{f}_t(\xi) = -(x_{\eta}f_x - y_{\eta}f_y)/\sqrt{\alpha} \quad (2.52d)$$

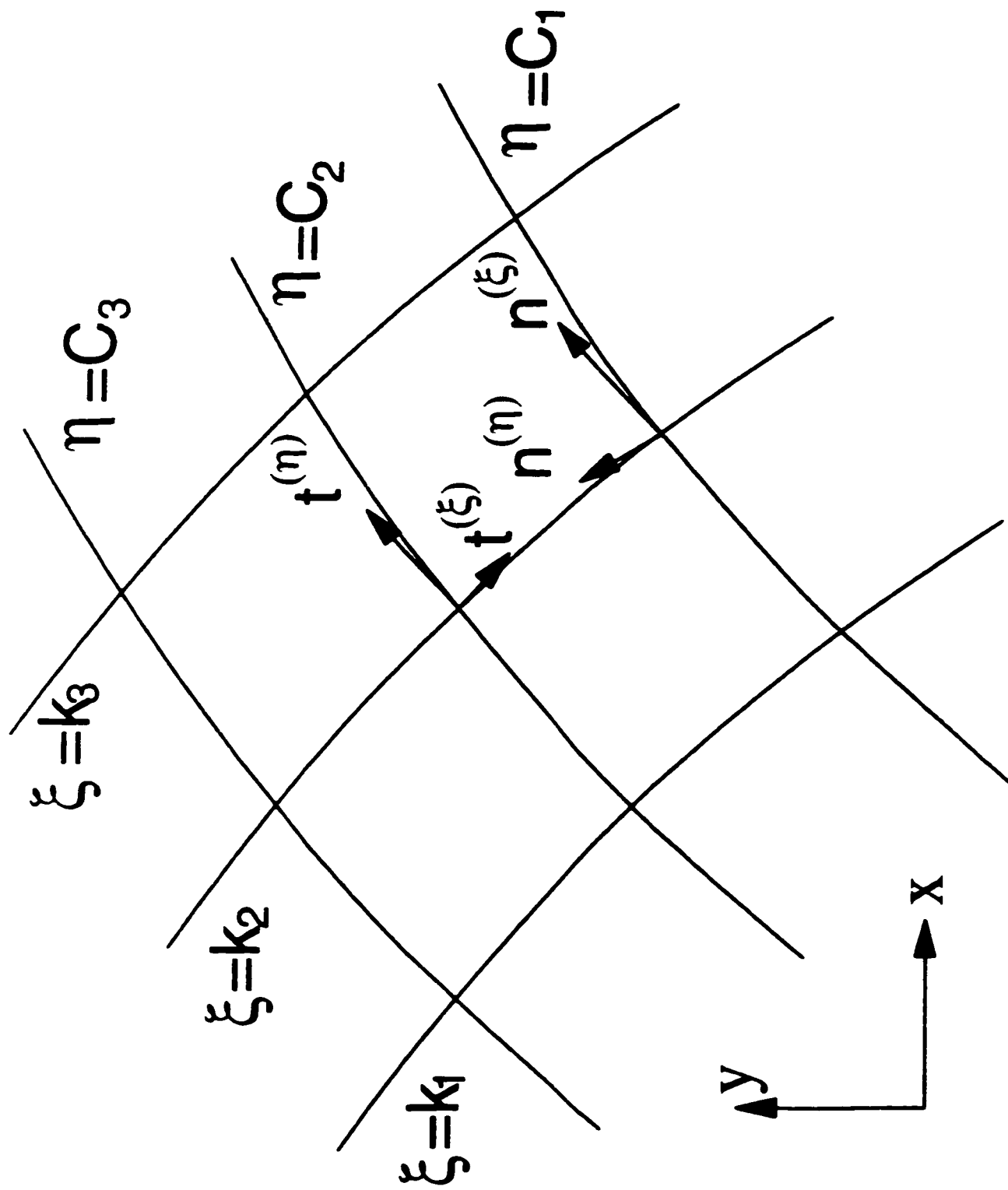


Fig. 2.10 Tangent and normal unit vectors.

where $\dot{f}_n(\eta)$, $\dot{f}_n(\xi)$ are normal vector components to line of constant η , ξ , and $\dot{f}_t(\eta)$, $\dot{f}_t(\xi)$ are tangent vector components to line of constant η , ξ .

By substituting vectors $f_x = u$ and $f_y = v$ from Eqs. (2.50) and (2.51) in Eqs. (2.52a-d) we have:

$$V_n(\eta) = -\frac{\psi_\xi}{\sqrt{\gamma}} \quad (2.53a)$$

$$V_t(\eta) = \frac{\gamma\psi_\eta - \psi_\xi\beta}{J\sqrt{\gamma}} \quad (2.53b)$$

$$V_n(\xi) = \frac{\psi_\eta}{\sqrt{\alpha}} \quad (2.53c)$$

$$V_t(\xi) = \frac{\alpha\psi_\xi - \beta\psi_\eta}{J\sqrt{\alpha}} \quad (2.53d)$$

2.8 Coordinate transformation

The grid can be done by an algebraic or an elliptic partial differential method. In this study, the algebraic method or a mixture of both can be used. First, for the mixed method, the domain of flow is covered by the algebraic grid, and second, the elliptic partial differential is used for more accuracy. The elliptic grid generator is the most extensively developed method. It is commonly used for 2-D problems but the procedure has been extended to 3-D problems. For domains where all the physical boundaries are specified, elliptic grid generators work very well (Hoffmann, 1985). A system of elliptic equations in the form of Laplace's equation is introduced. Elliptic systems have

advantages as:

1. Inherent smoothness that prevails in the solutions of elliptic systems,
2. Boundary slope discontinuities are not propagated into the field, and
3. Smoothing tendencies of elliptic operators allow grids to be generated for any configurations without overlap of grid lines.

For this problem, because of the discontinuity at the upstream face of the spillway, the elliptic partial differential method works well.

Thompson (1980) proposed Poisson equations as the coordinate generation system for the boundary-fitted coordinates (ξ, η) as follows:

$$\xi_{xx} + \xi_{yy} = P(\xi, \eta) \quad (2.54a)$$

$$\eta_{xx} + \eta_{yy} = Q(\xi, \eta) \quad (2.54b)$$

where P and Q are the grid control functions, and for this study, P and Q are set equal to zero.

Since it is desired to perform all numerical computations in the uniform rectangular transformed plane, the dependent and independent variables must be interchanged in (2.54a)-(2.54b). Using the equations (2.40a) and (2.40b) yields the coupled system in the computational (ξ, η) domain:

$$\alpha x \xi \xi - 2\beta x \xi \eta + \gamma x \eta \eta = -J^2 (P x \xi + Q x \eta) \quad (2.55a)$$

$$\alpha y \xi \xi - 2\beta y \xi \eta + \gamma y \eta \eta = -J^2 (P y \xi + Q y \eta) \quad (2.55b)$$

Eq. (2.55a) and Eq. (2.55b) can be solved in (ξ, η) plane, which is hence called the

computational plane, in rectangular shape with a rectangular mesh. Once the natural coordinates are generated for a given physical domain, the set of partial differential equations and their associated boundary conditions are transformed utilizing the relations mentioned. This technique not only broadens the applicability of finite differences to general domains but also initiates a new topic in numerical grid generation, including solids and curved surfaces by partial differential equations.

It is of primary importance that the equations do not change elliptic type under transformation. The transformed equations are then approximated using finite difference expressions and are solved numerically in the transformed plane. Thus, regardless of the shape of the original physical plane (region D in Fig. 2.9) and regardless of the spacing of the finite grid in that plane, the numerical solution of the partial differential system is carried out on a rectangular field with a square mesh (region D^* in Fig. 2.9) with no interpolation required on the boundaries.

2.9 Determination of pressure on the solid boundary

The pressure intensity at any point in a static body of liquid is equal to the product of the depth of the point from the free surface, the gravitational acceleration and the mass density of the liquid. This type of pressure distribution is known as the hydrostatic distribution. Strictly speaking, the hydrostatic distribution prevails in flowing fluid only when the normal acceleration is zero. This condition occurs when the streamlines are straight. When the streamlines are curved, the pressure distribution is different from that of the hydrostatic due to centrifugal forces. In flows with concave curvature these forces cause the pressure to be greater than the corresponding hydrostatic value, the increase being directly proportional to the square of the velocity and inversely proportional to the radius of curvature. The centrifugal force causes the pressure to be less than hydrostatic in

the case of flows with convex curvature (Fig. 2.4). The section near the crest has a convex curvature of streamlines, whereas the streamlines have a concave curvature in a bucket. Downstream of the spillway, the streamlines are straight and parallel. In general, the empirical equation for pressure is:

$$P = C_p \rho g h_y \quad (2.56)$$

h_y = being the depth of flow above the point under consideration (vertical distance).

C_p = is called the pressure coefficient

= 1 for parallel flows.

< 1 for flows with convex curvature of streamlines.

> 1 for flows with concave curvature of streamlines.

Reduction in pressure difference will cause undesirable effects, such as the following: (1) increase in pressure difference on the spillway. (2) change in shape of the nappe for which the spillway crest is generally designed, (3) increase in discharge, sometimes accompanied by fluctuation or pulsation of the nappe, which may be very objectionable if spillway is used for measuring purposes, and (4) unstable performance of the hydraulic model (Chow, 1959). The accompanying increase in discharge coefficient is often desirable in that a given flow can be discharged with less head. However, there is a limit to how far the pressures on the crest may be allowed to go. Although the subatmospheric limit may be near -10 m of water (depending on the atmospheric pressure and the water temperature), it is not desirable to approach this limit in a hydraulic structure. The actual boundary pressures continually fluctuate above and below the average value and the range of fluctuation increases as the flow velocity increases. If the concrete surfaces are unusually true, smooth, and dense, a design pressure of -5 m may be acceptable (Smith.

1992). In general, however, the minimum pressure should be limited to about -2m. The spillway crest may be controlled or uncontrolled. The uncontrolled crest is set at the reservoir full supply level (FSL) and discharges freely whenever the reservoir rises above it. The controlled crest is gated, and is set with the reservoir FSL near the top of the gates. The uncontrolled crest has the advantage of automatic discharge. However, if the permissible pool rise or crest length is limited for any reason, it may be necessary to use the gated crest in order to develop sufficient head on the spillway crest to pass the required discharge. Discharge, head, width, and nappe shape are related by an appropriate weir equation ($Q = CbH_d^{3/2}$). For the velocity vector, that is tangential to the streamline at the free surface points, Bernoulli's equation should be satisfied (Brebbia, 1983). By taking this into consideration, the pressure on the solid boundary, can be given by:

$$\left(\frac{P}{\gamma_0} + \frac{(v + u)^2}{2g} + y \right) = E \quad (2.57)$$

where v and u are vertical and horizontal velocities respectively. The transformed form of Eq. (2.57) in BFCC is:

$$\frac{1}{2g\gamma J^2} (\gamma\psi_\eta - \beta\psi_\xi)^2 + \frac{P}{\gamma_0} + y(\xi, \eta) = E \quad (2.58)$$

where γ_0 is specific weight of water.

2.10 Spillway configuration

One of the boundaries is either the solid part or the spillway profile that must be known for a solution. Before going to the fixed equation, the effect of this boundary on the flow should be defined.

2.10.1 Influence of spillway profile and crest alignment

As the flow passes over the crest into the downstream channel, energy losses which are dependant on the form of the spillway profile and on the flow conditions in the downstream channel are incurred. For the simple case of a crest normal to the downstream channel axis and having a smooth, streamlined downstream face merging with the channel invert, relatively little energy dissipation can occur. In this case, the velocity vector over the crest is aligned largely with the downstream direction of the flow. In cases where the downstream face of the overflow is not streamlined, or where flow separates to form a free overfall, the degree of energy dissipation will be higher, leading to a supercritical flow in the downstream channel. This flow has a lower Froude number and a lower energy level than when it is not streamlined. The flow below the crest is influenced both by the shape of the crest and by the conditions of the flow over the crest. The surface form and, in particular the profile of the spillway below the crest, can exert an appreciable influence upon flow conditions downstream. For instance, a smooth streamlined slope to the downstream face of the overflow will permit flow to enter the downstream channel with a higher energy level. The amount of energy, and the Froude number of the flow may have an appreciable influence upon the depth of flow in the downstream channel and also on the possibility of the spillway crest becoming submerged by tailwater conditions.

Where flow passes over the spillway with noticeably non-uniform conditions along the crest, supercritical flow in the spillway channel downstream will have a variable depth and discharge across the channel. These effects can persist for appreciable distances

downstream. It is desirable that any non-uniformity of flow entering the channel be taken into account in any determination of downstream super-elevation effects.

Supercritical flow is characterized by the fact that small changes of channel geometry can not influence the flow upstream to the section of channel at which the change occurs.

Every spillway has three components: a crest section, a conveyance section, and a discharge section. The crest section is the inlet to the spillway, situated at or near the reservoir level. From the crest, flow must be conveyed in a chute to a level near the natural river level on the downstream side of the dam. The spillway terminates in the discharge section, from which the flow re-enters the channel. It is evident that a high coefficient spillway gives a more economical design, in this regard it has been common practice to use an ogee spillway (Smith, 1992). The initial part of the curve fits the underside of the free nappe and is tangent to the reverse curve comprised of the spillway's bucket. Crest shape is based on a simple parabola designed to fit the trajectory of the falling nappe over the weir. The spillway geometry more common used was proposed in 1971 by the Waterway Experiment Station (WES), including the three-arc curve upstream quadrant, and a power function in the downstream quadrant.

Upstream includes the three-arc curve as shown in Fig. 2.11 or the equation (Blevins, 1984) as follows:

$$y = 0.724 \frac{(x + 0.270H_d)^{1.85}}{H_d^{0.85}} + 0.126H_d - 0.4315H_d^{0.375} (x + 0.270H_d)^{0.625} \quad (2.59)$$

The standard shape of the downstream quadrant (Fig. 2.12) on the basis of Bureau of Reclamation data (Corps of engineers, 1952) is:

$$x^{1.85} = 2.0H_d^{0.85}y \quad (2.60)$$

A non-dimensional curve for upstream and downstream coordinates for standard spillway is shown in Fig. 2.13.

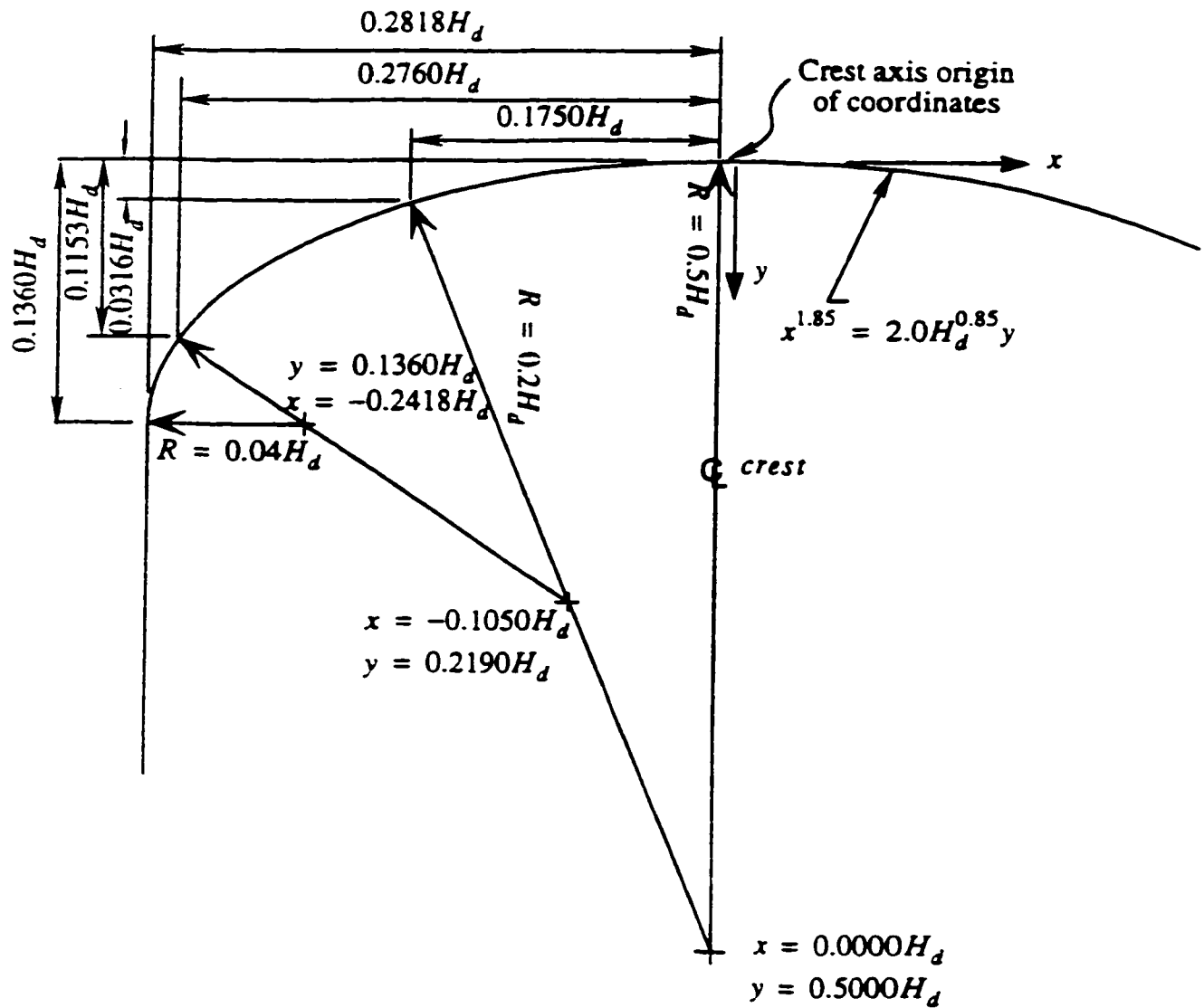


Fig. 2.11 WES spillway upstream quadrant (Corps of Engineers, 1952).

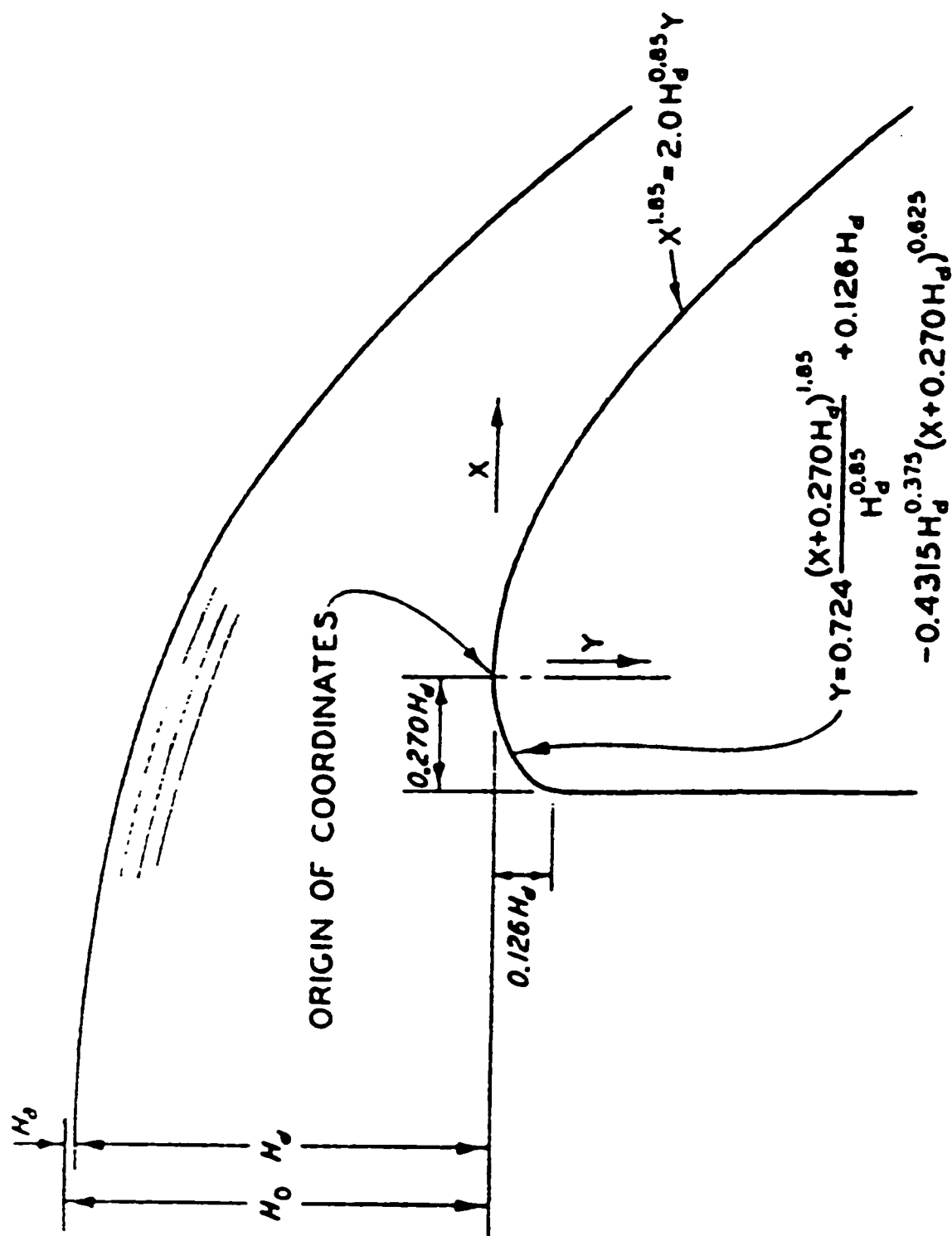


Fig. 2. 12 WES spillway crest downstream quadrant (Corps of engineers, 1952)

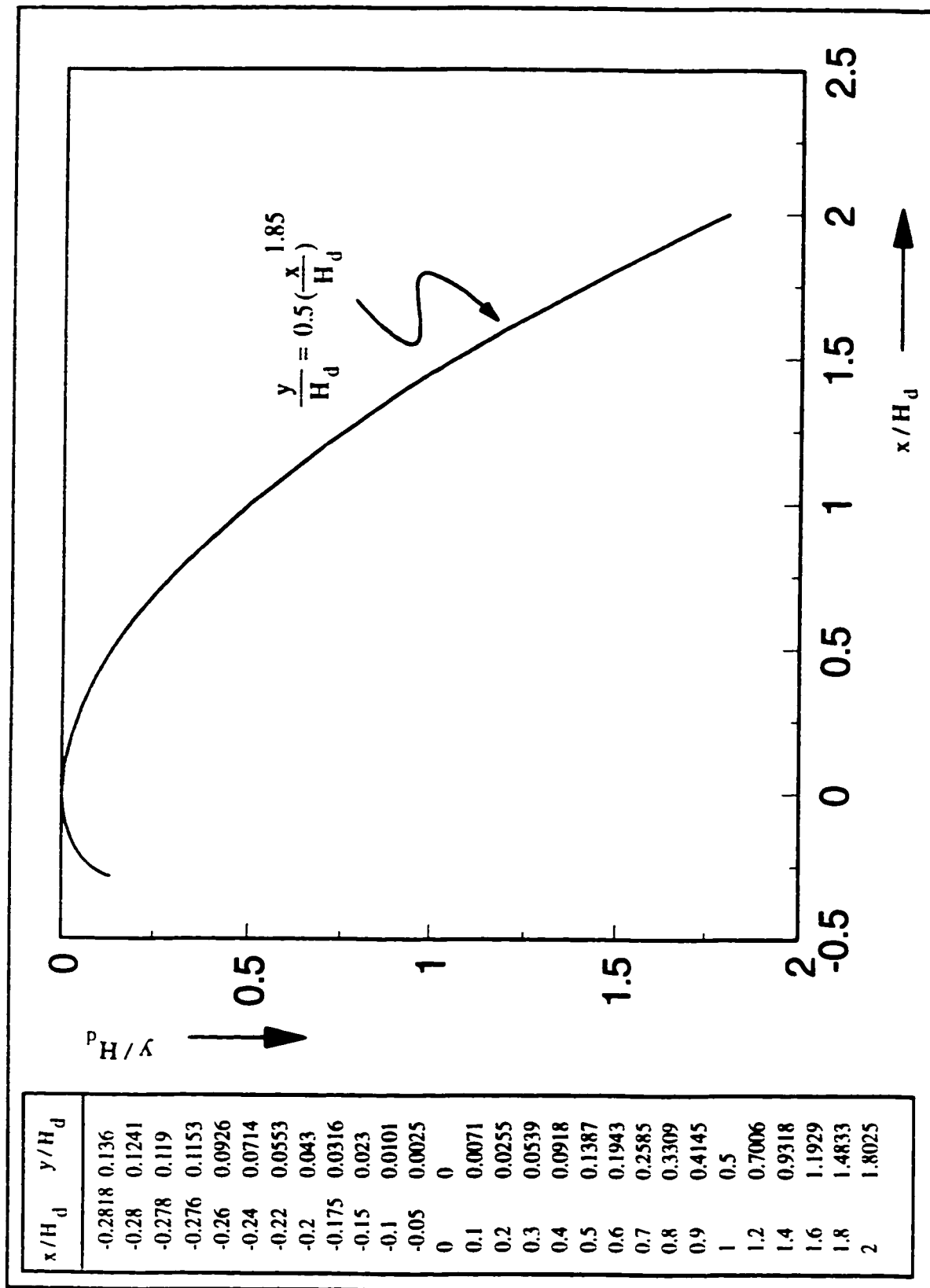


Fig. 2.13 Non-dimensional crest of WES spillway.

2.10.2 Approach conditions at the spillway crest

As flow approaches the spillway crest, velocities are usually relatively low, with Froude numbers much less than one. To obtain good spillway discharge characteristics, it is important to ensure that the approach conditions are satisfactory. Separation of flow can occur at high operating head, and the effective length of the overflow will be correspondingly reduced. The flow will also be non-uniformly distributed as it enters the downstream channel. Computations of flow over the crest usually assume that uniform conditions are obtained along the effective length of the crest. However, appreciable differences in flow can arise, which depicts the observed variation in depth along a model spillway crest. In addition to considering approach conditions from the point of view of discharge capacity of the overflow crest, energy losses in the forebay area may require consideration and super-elevation effects if the approach to the crest is curvilinear.

2.10.3 Spillway toe

When the flow reaches the end of the spillway's inclined face, it is deflected through a vertical curve into the horizontal or into an upward direction.

2.11 Cavitation phenomenon

2.11.1 Inception and initial growth

The nuclei theory describes the inception of cavitation. The stability of an air volume surrounded by water is determined by the forces acting on the inside and outside of the bubble. The inside forces constitute the air pressure and the water vapour pressure. At the interface is the surface tension and outside the bubble is the ambient water pressure. An

analysis of these forces shows that a minimum or critical ambient water pressure exists at which the bubble becomes unstable, continually growing without a further decrease in pressure. This nucleus instability occurs for water pressure below the vapour pressure to an extent depending on the original nucleus size. The generally accepted assumption is that the vapour pressure is the critical pressure for cavitation. The presence of the air nuclei in the water, therefore, is a basic condition for the occurrence of cavitation and their presence can be traced back to:

- The free undissolved bubble.
- The nuclei that exit through the crevices of foreign particles entering the flow, and
- The nuclei that exit via the crevices of the boundary material.

2.11.2 Continued growth and collapse

Bubble growth continues even after the ambient fluid pressure starts to exceed the vapour pressure because of the inertia of the water mass. When the pressure which tends to retard the bubble expansion is applied long enough to overcome the water inertia, the expansion ceases and collapse begins. Thus, during their inception and initial growth, the bubbles travel a certain distance downstream before collapsing. This is confirmed by observations of cavitation occurrence and damage observed for prototype conditions. The principal features that influence the growth and collapse rate of cavitation bubbles, with the nature of their effects, are shown in Table 2.4. A high rate of collapse increases the intensity of the high-pressure zone produced by an extreme change in momentum when the water moving toward the centre of the bubble is finally brought to zero velocity. It is intense pressure which produces noise and boundary material damage associated with cavitation.

Table 2.4: Effective factors for the rate of collapse

Factors	Rate of collapse
Surrounding fluid pressure (P_0)	high
Surface tension (T_s)	high
Initial content of air in the bubble	low
The water vapour pressure (P_v)	high
The diffusion of gas into and out of the bubble	low
Heat transfer through the bubble walls (T)	high

2.11.3 Factors contributing to cavitation

Experience in spillway operation in combination with investigations carried out over the last 20 years (including model and prototype testing) shows that the occurrence and extent of cavitation damage are subject to a variety of conditions and causes. A single condition has some problems, but a combination of geometric, hydrodynamic and interrelated factors may result in cavitation damage. The following factors are of importance:

2.11.3.1 Geometric factors

- ☐ Spillway surface roughness, particularly local humps and recesses.
- ☐ The presence of cavitation-prone structural elements in the spillway such as:
 - Slide slots or slots and sills of tainter gates,
 - Piers,

- Construction joints.
- Flow splitters and deflectors.
- Ports of ducts and pipes.
- Change of water passage shape.

2.11.3.2 Hydrodynamic factors

- ☐ Specific discharge (discharge per unit width of the spillway)
- ☐ Flow velocity
- ☐ Gate operation
- ☐ Boundary layer development

2.12.3.3 Other factors

- ☐ Heat transfer during collapse
- ☐ Water temperatures
- ☐ Number and size of air bubbles in the water
- ☐ Air diffusion

The amount of cavitation damage at a certain location on the spillway results from a combination of the above factors and, in general, can be identified prior to construction of the spillway.

Since some cavitation prone elements, such as gate slots, are necessary for proper functioning of the spillway, a method to prevent cavitation at those elements may therefore be required on an otherwise cavitation-free spillway.

2.12 Prediction of cavitation

Experience has shown that high velocities over the concrete surfaces of spillways can produce damaging cavitation. Determining whether or not cavitation will occur at a particular velocity may be necessary during design or after construction when grinding or repair of surface deviations may be necessary to prevent damage.

Local bulges in forms of irregularities or improper finishing of concrete can result in local surface deviations which create local zones of subatmospheric pressure. In spite of using the high strength concrete in areas subjected to high velocity will aid in preventing damage. cavitation takes place and damage will occur. The degree of potential cavitation at a surface in contact with high velocity flow is measured by the value of $\sigma(x)$, the cavitation coefficient. However, if the solid boundary over which the high velocity flow traverses is very smooth and conforms to the flow line at the boundaries, there should be no cavitation irrespective of the $\sigma(x)$ value. The critical $\sigma(x)$ value becomes significant only when there is a change in the flow contact boundary or when surface irregularities are present.

It is essential to eliminate abrupt irregularities from surfaces traversed by high velocity flows. This essential requirement is emphasized and explained in the introductory paragraphs of the paper "Cavitation From Surface Irregularities in High Velocity" by Ball (1976). Surface irregularities cause local pressure reductions which reach the vapor pressure of the fluid to form vapor cavities or bubbles that move downstream into a higher pressure regime. At this point, bubbles condense or collapse to produce high forces which inflict damage when cavitation occurs at or near the flow boundary.

Cavitation is a phenomenon which depends on the absolute pressure and is closely associated with the momentum pressure relation of the main flow outside the boundary layer. Whereas separation depends on the momentum pressure relation within the

boundary layer. Basically, separation occurs at a position along a guiding boundary surface where the flow-direction increase in pressure must be obtained by a decrease in momentum of the fluid. The fluid in the boundary layer moves at a lower velocity than that in the main flow domain because part of its energy has been removed through boundary friction.

Assume the pressure distribution on the spillway as obtained from the potential flow theory and is in agreement with experimental measurements, then the boundary layer thickness would be thin. This condition is usually met if the Reynolds number is sufficiently high to produce a fully developed turbulent boundary layer. Cavitation occurs whenever the pressure in the flow of water drops to the value of the pressure of the saturated water vapor, P_v (at prevailing temperature); in other words the cavities are filled by vapor and partly by gases excluded from the water due to the low pressure. By looking at Table 2-4 and Figure 2.14 there are two factors, pressure P_0 and velocity V_0 , which influence the cavitation. It is noted that viscosity effects and surface tension can be expressed by Reynold number $[R = (gH_d^3)^{1/2} v^{-1}]$ and Weber number $[W = H_d (\rho g / T_s)^{1/2}]$. For an ordinary water temperature, both W and R have an effect on H_d and H limited values, Matthew (1963), Maxwell and Weggel (1969). Both factors are combined with density ρ in the cavitation number, $\sigma(x)$, which is a form of the Euler number:

$$\sigma(x) = \frac{(P_0(x) - P_v)}{\frac{1}{2} \rho V_0^2(x)} \quad (2.61)$$

where $P_0(x)$ and $V_0(x)$ are the pressure and mean velocity of potential flow, respectively, at arbitrarily chosen reference points and P_v is the vapor pressure (Novak, 1984). The mean velocity at each mesh point can be derived from the known discharge.

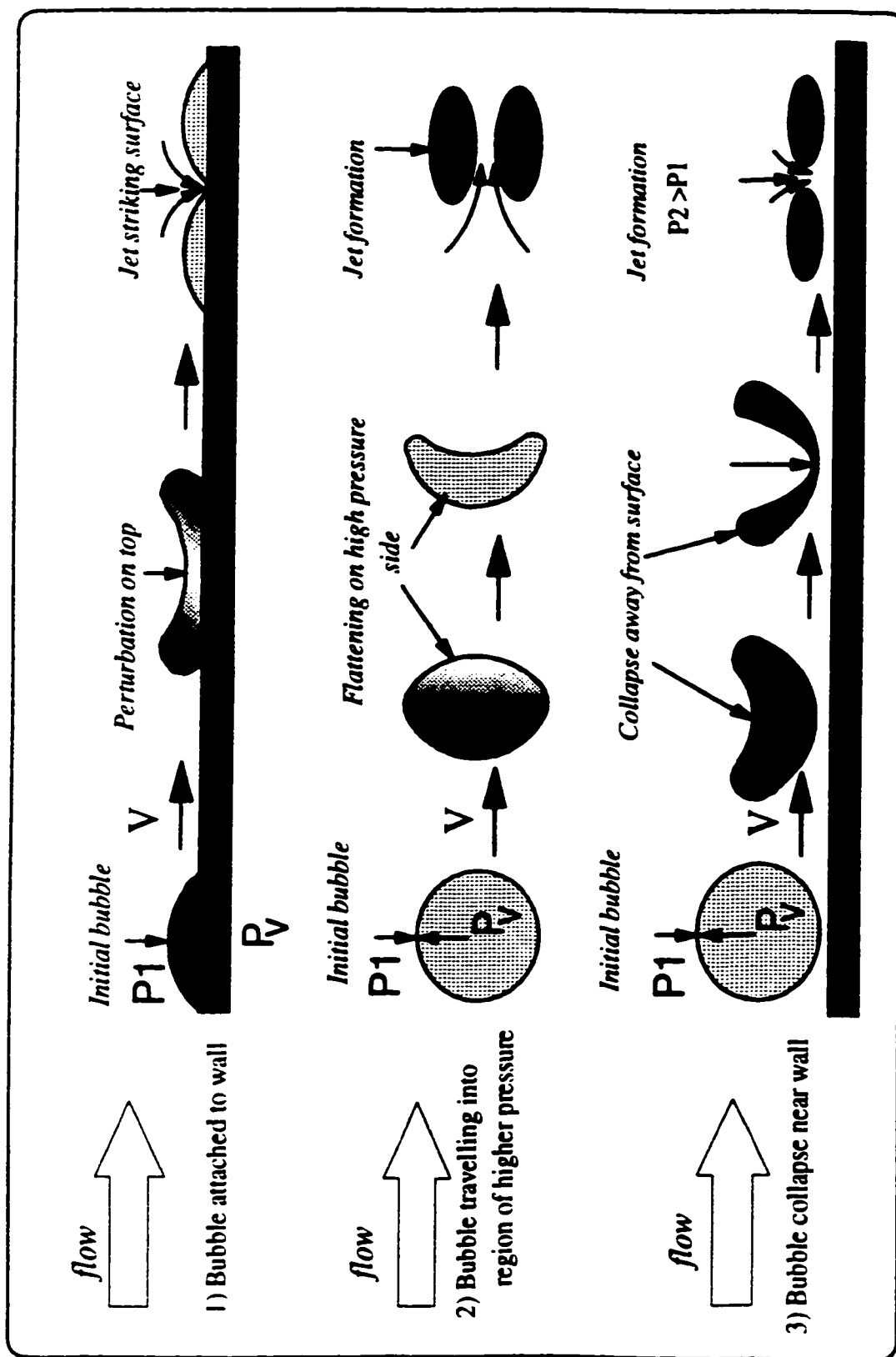


Fig. 2.14 Important factors effecting bubble collapse models.

the mesh angle and the height of the domain above the mesh point. The $P_0(x)$ is found by each element point from the solution of the potential flow. When cavitation begins (incipient cavitation), $\sigma(x)$ has the $\sigma_i(x)$. When the reference point coincides with the point where the bubble explosions are initiated, $\sigma_i(x)$ is found to be zero. The reference velocity and pressure can be measured at a number of different points. For example, with sudden into-the flow offsets, the reference point may be located:

- ☐ Upstream from an offset outside the boundary layer
- ☐ Immediately upstream from an offset and at its maximum height
- ☐ Outside of the boundary layer in the plane of an offset

In each of these cases, the reference pressures would be greater than the vapor pressure. Thus, the value of $\sigma_i(x)$ would be positive when cavitation begins (Acres, 1982). The cavitation number is now universally used for correlating the characteristics of cavitating flows (Novak, 1990). The second form of Eq. (2.61) in terms of heads h instead of pressure is:

$$\sigma(x) = \frac{(h_s(x) + h_c(x) - h_v)}{\frac{V_0^2(x)}{2g}} \quad (2.62)$$

$h_s(x)$ = static head due to water

h_v = vapor pressure head

g = acceleration due to gravity

$$h_c(x) = \frac{V_0^2(x)}{gr} \quad (2.63)$$

where:

r = the vertical radius of curvature for the spillway surface. An algebra sign must be included with h_c , since a negative pressure arises as a result of a convex surface.

Thus, if the value of $\sigma(x)$ for a given structure and operating condition is such that $\sigma(x) > \sigma_z(x)$ the structure should operate cavitation free. However, if $\sigma(x) < \sigma_z(x)$ cavitation should be expected and the degree of cavitation will depend on the magnitude of $[\sigma_z(x) - \sigma(x)]$.

Ball (1976) suggests that a 3 mm offset perpendicular to the flow can cause cavitation at velocities as low as 11 m/s. The critical velocity is about 32 m/s in spillway design. A cavitation problem could be serious at velocities exceeding 35 m/s, even if the spillway surface is smooth and well constructed. The velocity at a small distance y (i.e. $y = 0.01$) from the real bottom can be defined (Henderson, 1966) as:

$$V_y(x) = \left(\frac{y}{\delta(x)} \right)^{0.2} V_0(x) \quad (2.64)$$

The thickness of the boundary layer is found from (Falvey, 1980 and Henderson, 1966):

$$\frac{\delta(x)}{x} = 0.38 \left(\frac{x V_0(x)}{\Omega} \right)^{-0.2} \quad (2.65)$$

The definition of Gal'Perin value $\sigma_G(x)$ is:

$$\sigma_G(x) = 1.76 \left(\frac{V_y(x)}{V_0(x)} \right)^2 \quad (2.66)$$

where $\delta(x)$ is the boundary layer thickness (Fig. 2.15), x is the distance from a global coordinate origin (for $x > 3H_d$) and ν is the kinetic viscosity of water. With a solution of the potential model, we can calculate Eq. (2.61) and Eq. (2.66) at every mesh point on the shape.

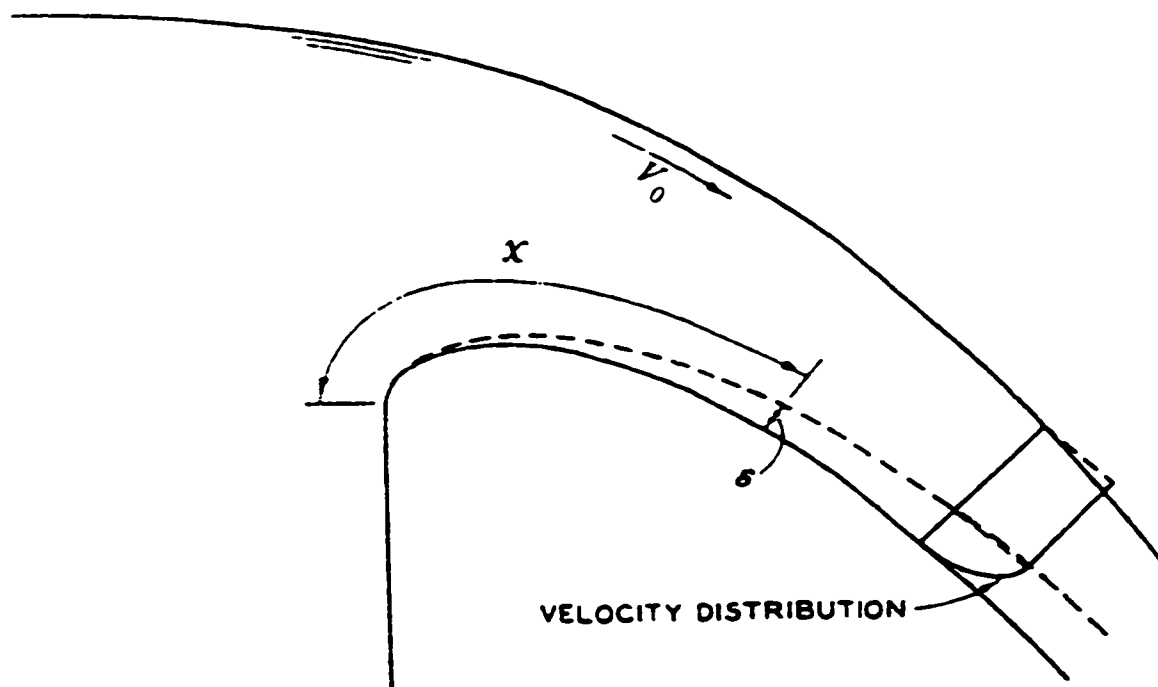


Fig. 2.15 Boundary layer development on a spillway crest.

From a discrete model the distance x to a mesh can be derived from the size of the meshes on the shape of the spillway. By detection of cavitation on the spillway, the point on the shape of the spillway where cavitation starts can be controlled by changing the shape.

The method for determining the cavitation potential for the experimental test by Eq. (2.62) is to calculate flow profiles for the range of operating discharges. Then, from each profile, piezometric pressures at various locations on the spillway are calculated. Correction to these pressures must be made to account for slopes, as well as any boundary curvature present. Some theoretical work on self-aerated uniform flow is available. It is considered difficult to adjust these analyses to the case of aerated flows in spillways. In general, bottom slope and curvature of the chute influence the spacing of aerators in addition to flow velocity. At this time, a purely analytical approach to the design of an adequate spillway aeration system does not exist. The design of an aerator is based on an

experimental formula that cannot cover air surface required for the spillway. Due to advantages and disadvantages of different aerators, use of them is limited. Finally, by comparing the cavitation index of the flow $\sigma_i(x)$, under different conditions to the allowable cavitation index $\sigma_A(x)$, for all flow conditions and locations on the spillway where $\sigma_i(x) < \sigma_A(x)$, a potential for cavitation exists.

The cavitation index was determined experimentally for different discharges. A number of circumstances where high-velocity flow is encountered with a free surface are considered.

Chapter 3.0

POTENTIAL FLOW SOLVER

3.1 General

As an initial application of the natural coordinate systems, the Laplace equation for the stream function for potential flow is solved numerically, using the Curvilinear Coordinate Systems. This chapter contains a compilation of the second order finite difference expressions used to approximate partial derivatives in the transformed plane. Computational molecules for the derivative approximations appear to the right of each expression. Combined difference forms for the transformation parameters α , β , γ , τ , σ , and J are also included here. The discretization scheme chosen is in line with the essential simplicity of BFCC, which is the principal advantage claimed over this powerful and complex method.

3.2 Governing equations

The transformed Laplace equation as derived in chapter 2 is

$$\alpha\psi_{\xi\xi} - 2\beta\psi_{\xi\eta} + \gamma\psi_{\eta\eta} + (Dx)(y_{\xi}\psi_{\eta} - y_{\eta}\psi_{\xi})/J + (Dy)(x_{\eta}\psi_{\xi} - x_{\xi}\psi_{\eta})/J = 0 \quad (3.1)$$

where

$$Dx = \alpha x_{\xi\xi} - 2\beta x_{\xi\eta} + \gamma x_{\eta\eta} \quad (3.2)$$

$$Dy = \alpha y_{\xi\xi} - 2\beta y_{\xi\eta} + \gamma y_{\eta\eta}. \quad (3.3)$$

Introducing the definitions

$$\sigma \equiv [y_{\xi}(Dx) - x_{\xi}(Dy)]/J \quad (3.4)$$

and

$$\tau \equiv [x_{\eta}(Dy) - y_{\eta}(Dx)]/J. \quad (3.5)$$

then Eq. (3.1) can be reduced to:

$$\alpha\psi_{\xi\xi} - 2\beta\psi_{\xi\eta} + \gamma\psi_{\eta\eta} + \sigma\psi_{\eta} + \tau\psi_{\xi} = 0 \quad (3.6)$$

where

$$\alpha = x_{\eta}^2 + y_{\eta}^2 \quad (3.7)$$

$$\beta = x_{\xi}x_{\eta} + y_{\xi}y_{\eta} \quad (3.8)$$

$$\gamma = x_{\xi}^2 + y_{\xi}^2 \quad (3.9)$$

$$\sigma = [y_{\xi}(\alpha x_{\xi\xi} - 2\beta x_{\xi\eta} + \gamma x_{\eta\eta}) - x_{\xi}(\alpha y_{\xi\xi} - 2\beta y_{\xi\eta} + \gamma y_{\eta\eta})]/J \quad (3.10)$$

$$\tau = [x_{\eta}(\alpha y_{\xi\xi} - 2\beta y_{\xi\eta} + \gamma y_{\eta\eta}) - y_{\eta}(\alpha x_{\xi\xi} - 2\beta x_{\xi\eta} + \gamma x_{\eta\eta})]/J \quad (3.11)$$

$$J = x_{\xi}y_{\eta} - x_{\eta}y_{\xi} \quad (3.12)$$

For non-contracting grid, coordinate transformation Eqs. (2.46a), and (2.46b) reduce to:

$$(\alpha x_{\xi\xi} - 2\beta x_{\xi\eta} + \gamma x_{\eta\eta}) = 0 \quad (3.13a)$$

$$(\alpha y_{\xi\xi} - 2\beta y_{\xi\eta} + \gamma y_{\eta\eta}) = 0 \quad (3.13b)$$

Water surface profile can be defined as:

$$\frac{1}{2g\gamma J^2} (\gamma\psi_{\eta} - \beta\psi_{\xi})^2 + y(\xi, \eta) = E \quad \text{for} \quad 1 \leq i \leq i_m, \quad \text{and} \quad j = j_{max} \quad (3.14)$$

Velocities in x and y direction are:

$$u = (\psi_{\eta}x_{\xi} - \psi_{\xi}x_{\eta}) / J \quad (3.15)$$

$$v = (\psi_{\eta}y_{\xi} - \psi_{\xi}y_{\eta}) / J \quad (3.16)$$

Tangent and normal vector velocity components to the lines of constant ξ and η are:

$$V_t(\eta) = \frac{\gamma\psi_{\eta} - \psi_{\xi}\beta}{J\sqrt{\gamma}} \quad (3.17)$$

$$V_n(\eta) = -\frac{\psi_{\xi}}{\sqrt{\gamma}} \quad (3.18)$$

$$V_n(\xi) = \frac{\psi_{\eta}}{\sqrt{\alpha}} \quad (3.19)$$

$$V_t(\xi) = \frac{\alpha\psi_{\xi} - \beta\psi_{\eta}}{J\sqrt{\alpha}} \quad (3.20)$$

Pressure over a solid boundary could be calculated by:

$$\frac{1}{2g\gamma J^2} (\gamma\psi_\eta - \beta\psi_\xi)^2 + \frac{P}{\gamma_o} + y(\xi, \eta) = E \quad (3.21)$$

where γ_o is specific weight of water.

Dynamic similitude is guaranteed by duplicating the Froude and Reynold numbers of the equations and boundary conditions between prototype and model.

3.3 Finite difference approximations in the transformed plane

$\Delta\xi$ and $\Delta\eta$ in the (ξ, η) plane are taken as unity (but they have values in the program) for simplification of all partial differential approximations and do not appear explicitly. The following definitions are used throughout this section:

$f = f(\xi, \eta)$ - A twice continuously differentiable function of ξ and η .

$x = x(\xi, \eta)$ - Coordinate transformation function defined by Eq. (2.29a)

$y = y(\xi, \eta)$ - Coordinate transformation function defined by Eq. (2.29b)

α , β , γ , τ , σ , and τ -transformations of parameters defined by Eqs. (3.7), (3.8), (3.9), (3.10) and (3.11), respectively.

In addition, the following notation convention is utilized to indicate the position at which functions and derivatives are evaluated in the discrete (ξ, η) plane:

$$f_{i,j} \equiv f(\xi_i, \eta_j)$$

$$(f_\xi)_{i,j} \equiv f_\xi(\xi_i, \eta_j)$$

$$(f_\eta)_{i,j} \equiv f_\eta(\xi_i, \eta_j)$$

$$(f_{\xi\xi})_{i,j} \equiv f_{\xi\xi}(\xi_i, \eta_j)$$

$$(f_{\xi\eta})_{i,j} \equiv f_{\xi\eta}(\xi_i, \eta_j)$$

$$(f_{\eta\eta})_{i,j} \equiv f_{\eta\eta}(\xi_i, \eta_j)$$

3.4 Discretization

Approximating the derivatives in Eq. (3.6) with second-order central differences, we obtain the difference equation:

$$\psi_{i,j} = \frac{\alpha_{i,j}(\psi_{i+1,j} + \psi_{i-1,j}) - 2\beta_{i,j}(\psi_{\xi\eta})_{i,j} + \gamma_{i,j}(\psi_{i,j+1} + \psi_{i,j-1}) + \sigma_{i,j}(\psi_{\eta})_{i,j} + \tau_{i,j}(\psi_{\xi})_{i,j}}{2(\alpha_{i,j} + \gamma_{i,j})} \quad (3.22)$$

For all $2 \leq i \leq i_{max} - 1$ and $2 \leq j \leq j_{max} - 1$, the boundary conditions (2.49a)-(2.49d) are specified for each, along $j = 1$ by (2.49a) and the remote condition given by Eq. (2.49b) is required along $j = j_{max}$ for $1 \leq i \leq i_{max} - 1$. A complete form of these boundaries is given in section 3.5. The computational field appears in Fig. (3.1). The point SOR¹ method has been used to solve equations generated by Eq. (3.22). The method is unconditionally convergent and the convergence is quite rapid if the optimum SOR acceleration parameter is used. The optimum parameter was determined to be $\omega = 1.5$ by numerical experimentation and was found to be essentially independent of region shape.

1. Successive Over Relaxation technique

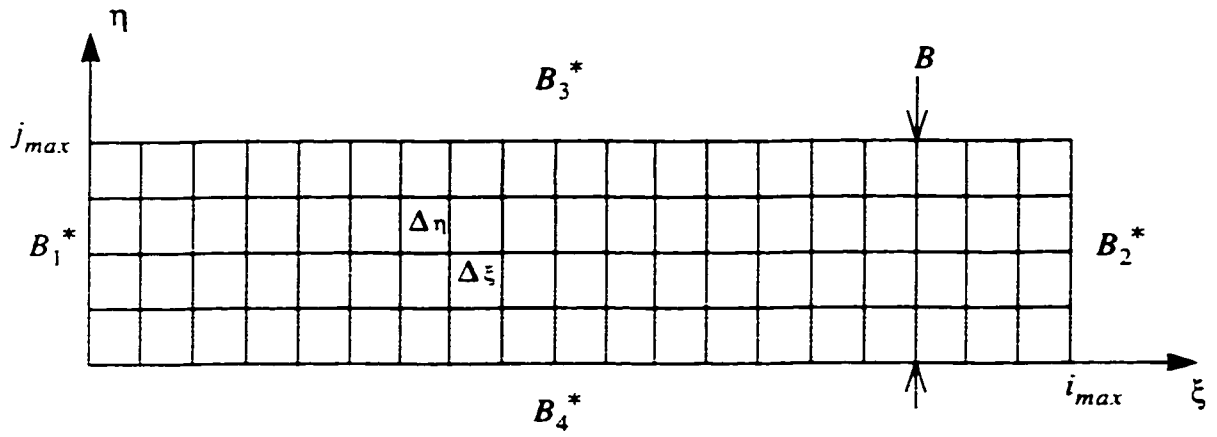


Fig. 3.1 Computational field of spillway flow in Domain D^* .

3.4.1 Derivative approximation

■ First derivative (central differences):

$$(f_{\xi})_{i,j} = \frac{f_{i+1,j} - f_{i-1,j}}{2}$$

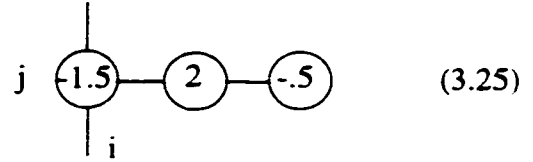
$$(3.23)$$

$$(f_{\eta})_{i,j} = \frac{f_{i,j+1} - f_{i,j-1}}{2}$$

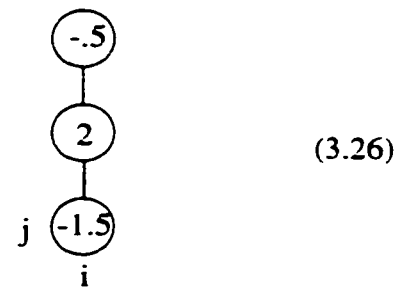
$$(3.24)$$

■ First derivative (forward differences):

$$(f_{\xi})_{i,j} = \frac{(-f_{i+2,j} + 4f_{i+1,j} - 3f_{i,j})}{2}$$

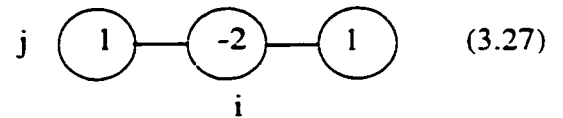


$$(f_{\eta})_{i,j} = \frac{(-f_{i,j+2} + 4f_{i,j+1} - 3f_{i,j})}{2}$$

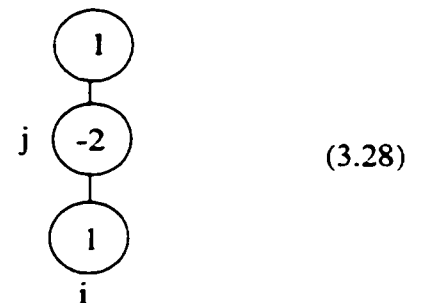


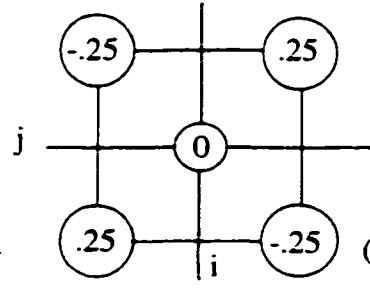
■ Second derivative (central differences):

$$(f_{\xi\xi})_{i,j} = f_{i+1,j} - 2f_{i,j} + f_{i-1,j}$$



$$(f_{\eta\eta})_{i,j} = f_{i,j+1} - 2f_{i,j} + f_{i,j-1}$$



$$(f_{\xi\eta})_{i,j} = \frac{(f_{i+1,j+1} - f_{i+1,j-1} + f_{i-1,j-1} - f_{i-1,j+1})}{4} \quad (3.29)$$


3.4.2 Transformation parameters

The following relationships exist:

$$\alpha_{i,j} = \alpha'_{i,j}/4 \quad (3.30)$$

$$\alpha'_{i,j} = (x'_{\eta})_{i,j}^2 + (y'_{\eta})_{i,j}^2 \quad (3.31)$$

$$\beta_{i,j} = \beta'_{i,j}/4 \quad (3.32)$$

$$\beta'_{i,j} = (x'_{\xi})_{i,j} (x'_{\eta})_{i,j} + (y'_{\xi})_{i,j} (y'_{\eta})_{i,j} \quad (3.33)$$

$$\gamma_{i,j} = \gamma'_{i,j}/4 \quad (3.34)$$

$$\gamma'_{i,j} = (x'_{\xi})_{i,j}^2 + (y'_{\xi})_{i,j}^2 \quad (3.35)$$

$$J_{i,j} = J'_{i,j}/4 \quad (3.36)$$

$$J'_{i,j} = (x'_{\xi})_{i,j} (y'_{\eta})_{i,j} - (x'_{\eta})_{i,j} (y'_{\xi})_{i,j} \quad (3.37)$$

$$\sigma_{i,j} = \sigma'_{i,j}/2 \quad (3.38)$$

$$\sigma'_{i,j} = \frac{[(y'_{\xi})_{i,j}(Dx')_{i,j} - (x'_{\xi})_{i,j}(Dy')_{i,j}]}{J'_{i,j}} \quad (3.39)$$

$$\tau_{i,j} = \tau'_{i,j}/2 \quad (3.40)$$

$$\tau'_{i,j} = \frac{[(x'_{\eta})_{i,j}(Dy')_{i,j} - (y'_{\eta})_{i,j}(Dx')_{i,j}]}{J'_{i,j}} \quad (3.41)$$

$$(Dx')_{i,j} = \alpha'_{i,j}(x'_{\xi\xi})_{i,j} - 2\beta'_{i,j}(x'_{\xi\eta})_{i,j} + \gamma'_{i,j}(x'_{\eta\eta})_{i,j} \quad (3.42)$$

$$(Dy')_{i,j} = \alpha'_{i,j}(y'_{\xi\xi})_{i,j} - 2\beta'_{i,j}(y'_{\xi\eta})_{i,j} + \gamma'_{i,j}(y'_{\eta\eta})_{i,j} \quad (3.43)$$

$$(x'_{\xi})_{i,j} = (x'_{\xi})_{i,j}/2 \quad (3.44)$$

$$(x'_{\xi})_{i,j} = x_{i+1,j} - x_{i-1,j} \quad (3.45)$$

$$(y_{\xi})_{i,j} = (y'_{\xi})_{i,j}/2 \quad (3.46)$$

$$(y'_{\xi})_{i,j} = y_{i+1,j} - y_{i-1,j} \quad (3.47)$$

$$(x_{\eta})_{i,j} = (x'_{\eta})_{i,j}/2 \quad (3.48)$$

$$(x'_{\eta})_{i,j} = x_{i,j+1} - x_{i,j-1} \quad (3.49)$$

$$(y_{\eta})_{i,j} = (y'_{\eta})_{i,j}/2 \quad (3.50)$$

$$(y'_{\eta})_{i,j} = y_{i,j+1} - y_{i,j-1} \quad (3.51)$$

$$(x_{\xi\xi})_{i,j} = x_{i+1,j} - 2x_{i,j} + x_{i-1,j} \quad (3.52)$$

$$(x_{\xi\xi})_{i,j} = (x'_{\xi\xi})_{i,j} \quad (3.53)$$

$$(y_{\xi\xi})_{i,j} = y_{i+1,j} - 2y_{i,j} + y_{i-1,j} \quad (3.54)$$

$$(y_{\xi\xi})_{i,j} = (y'_{\xi\xi})_{i,j} \quad (3.55)$$

$$(x_{\xi\eta})_{i,j} = (x'_{\xi\eta})_{i,j}/4 \quad (3.56)$$

$$(x'_{\xi\eta})_{i,j} = x_{i+1,j+1} - x_{i+1,j-1} + x_{i-1,j-1} - x_{i-1,j+1} \quad (3.57)$$

$$(x_{\eta\eta})_{i,j} = x_{i,j+1} - 2x_{i,j} + x_{i,j-1} \quad (3.58)$$

$$(x'_{\eta\eta})_{i,j} = (x_{\eta\eta})_{i,j} \quad (3.59)$$

$$(y_{\eta\eta})_{i,j} = y_{i,j+1} - 2y_{i,j} + y_{i,j-1} \quad (3.60)$$

$$(y'_{\eta\eta})_{i,j} = (y_{\eta\eta})_{i,j} \quad (3.61)$$

$$(y_{\xi\eta})_{i,j} = (y'_{\xi\eta})_{i,j}/4 \quad (3.62)$$

$$(y'_{\xi\eta})_{i,j} = y_{i+1,j+1} - y_{i+1,j-1} + y_{i-1,j-1} - y_{i-1,j+1} \quad (3.63)$$

3.5 Boundary discretization

3.5.1 General boundary conditions:

The equivalent versions of the transformation of boundary conditions in the Fitted Boundary Coordinate for numerical implementation are given as follows:

$$\Psi|_{B_1^*} = 0 \quad (3.64-a)$$

$$\Psi|_{B_3^*} = q \quad (3.64-b)$$

$$\frac{\Psi}{h}\bigg|_{B_1^*} = \frac{q}{B} \quad (3.64-c)$$

$$\frac{\Psi}{h}\bigg|_{B_3^*} = \frac{q}{B} \quad (3.64-d)$$

where

D^* = New flow domain in ξ , and η directions

B_1^* , B_2^* , B_3^* and B_4^* are boundaries of domain D^* , B is width of this domain.

For Fig. 3.1, the actual boundary conditions and the equivalent versions for numerical implementation are summarized in Table 3.1.

Table 3.1: Boundary conditions in computational domain D^* .

Boundary region	Conditions	Numerical implementation
Solid surface	$\psi = 0$	$\psi _{B_1^*} = 0$
Inlet	$\frac{\partial \psi}{\partial n} = 0$	$\psi _{B_2^*} = q \frac{h}{B}$
Free surface	$\frac{\partial \psi}{\partial n} = V_s = \sqrt{2g(E - y_s)}$	$\psi _{B_3^*} = q$
Outlet	$\frac{\partial \psi}{\partial n} = 0$	$\psi _{B_4^*} = q \frac{h}{B}$

3.5.2 Additional boundary condition on free surface

For this problem the free surface profile is unknown, therefore the problem becomes considerably difficult, since the streamlines at the border between the liquid and the atmosphere are prescribed by a fixed boundary. The identical construction of the flow net then follows. However, in checking the position of the streamlines, not only the Bernoulli equation at the free surface must be satisfied, but the pressure distribution curve must pass through zero (atmospheric) at every point lying on a free surface.

$$\frac{\psi_n^2(B_3)}{2g} + y(B_3) + P(B_3) = E \quad (3.65)$$

where E is total energy above the horizontal datum, defined by upstream conditions. The surface horizontal velocity can be approximated by the equation:

$$\frac{dy}{dx} = \frac{v}{u} \quad (3.66)$$

Along the free surface, the pressure is constant,

$$P|_{B_3} = 0 \quad (3.67)$$

thus the energy equation defines the surface elevation $y(B_3)$ as:

$$y(B_3) = E - \frac{v^2}{2g} = E - \frac{u_s^2(B_3)}{2g} \left[1 + \left(\frac{\partial y}{\partial x} \right)_s^2 \right] \quad (3.68)$$

where the kinematic surface condition has been used. Energy $E(x)$ at the free surface location x computed from Eq. (3.14) is differentiated thus:

$$dE = E - E(x) = dy_s + \frac{u_s}{g} du_s \left[1 + \left(\frac{dy}{dx} \right)_s^2 \right] + \frac{u_s^2}{g} \frac{d^2 y_s}{dx^2} dy_s \quad (3.69)$$

where y_s is free surface coordinate. So that the velocity change du_s is given by:

$$du_s = -\frac{q}{y_s^2} dy_s \quad (3.70)$$

and the change in $y_s(x)$ is given by:

$$dy_s = \frac{E - E(x)}{1 - \frac{q^2}{gy_s^3} \left[1 + \left(\frac{dy_s}{dx} \right)^2 - y_s \frac{d^2 y_s}{dx^2} \right]} \quad (3.71)$$

The derivatives in this equation can be approximated by the finite difference expressions scheme and converged successfully. In addition, its stability was improved considerably by applying it by means of an under-relaxation coefficient $\omega < 1$, so that the free surface

depth y_s at the node i, j_{max} is given by:

$$dy_s = \omega dy_s (new) + (1 - \omega) dy_s (old) \quad (3.72)$$

where $dy_s (new)$ is defined in Eq. (3.71) and $dy_s (old)$ refers to the final, under-relaxed, surface correction in the previous iteration. The choice of the under-relaxation coefficient was not critical and $\omega = 0.75$ was typical. The free surface computations converged after 30-50 iterations, to a maximum energy difference of $E/1000$.

If result is not obtained, not only the profile of the free surface, but the form of all other streamlines as well must be modified. Use of the energy equation written in terms of head is suited to such conditions of flow. In combination with the principle of continuity and Bernoulli theorem $\psi(i, j)$ affords a means of determining the pressure and velocity distribution in steady two-dimensional flows in which the total head is reasonably uniform at all points. There is only one arrangement of the chosen number of streamlines that will fulfill the mathematical statement of the equations of potential flow. Once the correct velocity is obtained, the pressure may be found through use of the energy equation, indeed, the pressure distribution $\frac{P}{\gamma_0}$ is computed in terms of head, could be equal to pressure head from manometer at specified point over the spillway surface.

3.6 Computer program for spillway design

Based on the governing equations, a computer program for calculating pressure, velocity, and the cavitation index was developed. Fig. 3.2 is a schematic diagram showing the main steps involved in the program. It shows the logical connection between the different stages of the program and of its development. Three different operation heads, $H/H_d = 0.5, 1.0, 1.33$, were chosen for numerical calculation. The computational

domain was discretized with 49×15 nodes for the calculation $H/H_d = 1.33$, 54×10 nodes for $H/H_d = 1.0$, and 54×5 nodes for $H/H_d = 0.5$.

The assumed free surface and boundary conditions can be directly fed into the computer program during data input. Geometrical data defining the channel are in terms of x , y co-ordinates with references to a set of orthogonal axes. Flow boundary conditions, i.e., the starting velocity components and the depth at and below the spillway crest should also be given.

Then, the remaining initial hydraulic values are calculated in connection with energy head E , which also has to be fed in. The next step is the calculation of the free surface corresponding to the respective input boundary conditions. At a later stage, the values for the water-surface profiles are obtained by iteratively rearranging the free surface in *SUR* subroutine (Fig. 3.3). Lastly, the actual flow calculation is carried out using the steps illustrated in Fig. 3.2.

The computer produces the results as an extensive list of quantities in the order corresponding to the steps in the calculation.

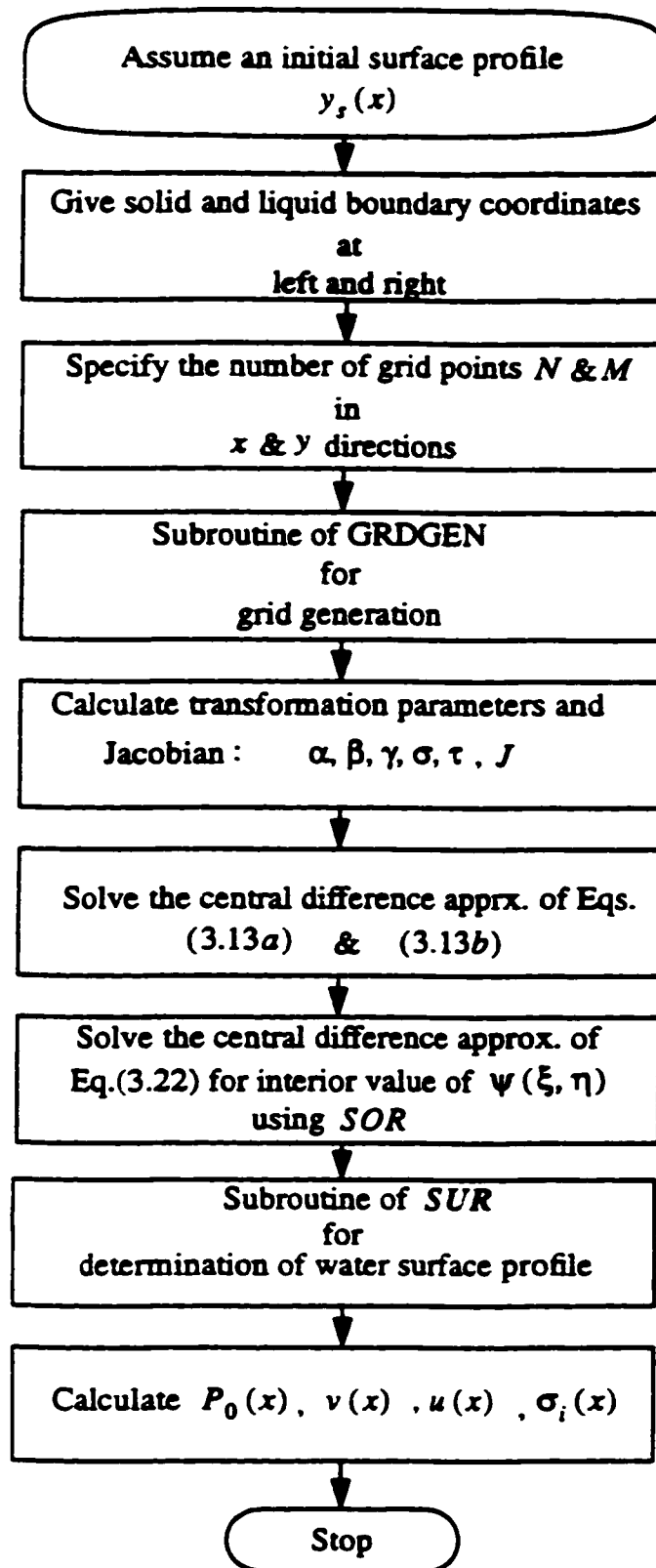


Fig. 3.2 Schematic diagram showing the steps in an iteration.

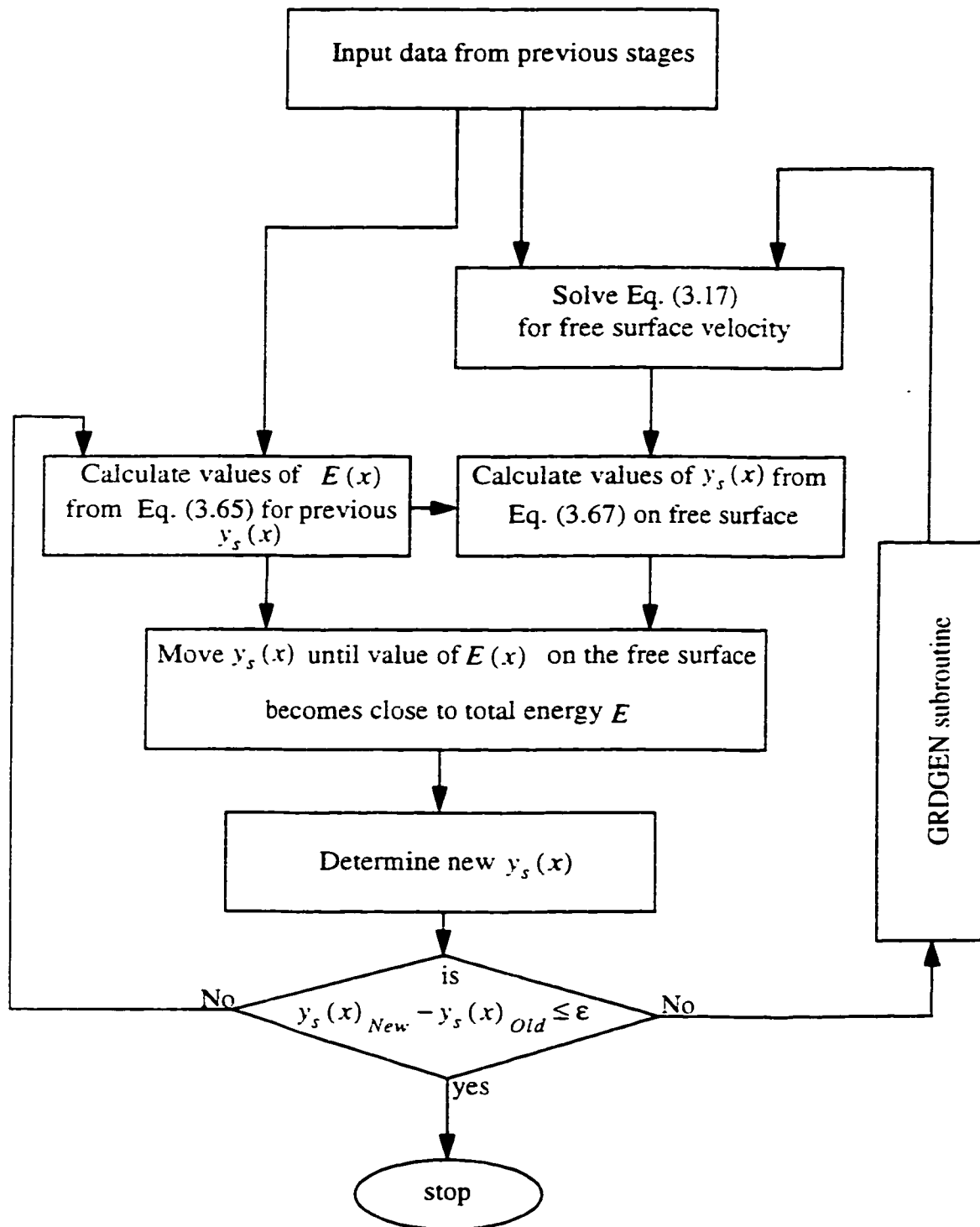


Fig. 3.3 Subroutine of **SUR** for determination of water surface profile.

Chapter 4.0

EXPERIMENTAL STUDY

4.1 General

Solutions for real problems usually involve a combination of analysis and experimental information. First, the real physical flow situation is approximated with a mathematical model that is simple enough to yield a solution. Then, experimental measurements in the analysis are made.

Of primary interest in this study was the nature of the flow through the spillway chute. The majority of the tests were related to this aspect. The requirements for dynamics similarity are that two flows must possess both geometric and kinematic similarity to be dynamically similar. In addition, spillway and crest pressures were measured. The spillway crest was calibrated for various operating conditions and some observations were made of the flow in the approach channel for different levels. The results of all these tests are described in the following sections.

4.2 Experimental methodology

4.2.1 Physical modelling

To avoid the damage due to cavitation, then either the design and/or the mode of operation of a particular structure must be changed. The widely accepted aid in determining the sensitivity of cavitation effects is the (incipient) cavitation index $\sigma_i(x)$. This index varies considerably according to local conditions. The optimization of these conditions can be performed by means of a numerical model. The accuracy of the numerical model was verified and a physical model developed which presents the small scale of prototype. The following factors are important aspects of physical modelling:

4.2.1.1 Reynold's number

The Reynold's number has a significant effect on the incipient cavitation index:

$$R = (gH_d^3)^{1/2} \Omega^{-1} \quad (4.1)$$

where ν is the kinematic viscosity.

It has been found that cavitation index, $\sigma_i(x)$ decreases with an increase in the Reynold's number for flow in the model (Acres. 1983).

4.2.1.2 Froude's number

The prototype and model spillways, which are geometrically similar, represent a hydraulic system in which gravity is the predominant force in producing motion. Fluid friction and surface tension effects are negligible in the model built at a relatively large

scale. In this type of hydraulic system, with gravity being the governing force, model prototype relationships are determined by the Froude law of similarity.

If the flow has a free surface gravitational force, it will give rise to Froude's number:

$$F = \frac{V}{\sqrt{gH_d}} \quad (4.2)$$

A model study can be interpreted only if F is given the same value in the model as in the prototype and is repeated several times. Herein lies the key to the interpretation of the model tests. For similarity, it is evident that model and prototype must be completely similar geometrically. The flow characteristics will then be similar if the fluid properties are such that the Froude, Reynold (or whichever of these have bearing upon the phenomenon) are respectively equal in both cases. Once this condition is established, the characteristics of flow may be varied at will without destroying the similarity between prototype and model. The “model : prototype” scale is a dimensionless ratio of dimensional units or of actual dimensional measurements in SI units.

All velocities and pressures must have the same “prototype: model” ratio using the subscripts m and p to indicate model and prototype respectively. Velocity at points a and b on model and prototype are:

$$\frac{(V_a)_p}{(V_a)_m} = \frac{(V_b)_p}{(V_b)_m} \quad (4.3)$$

Of course, $(V_a)_p$ and $(V_a)_m$ must be in the same direction. This is termed as kinematic similarity between model and prototype. The detailed interpretation of model measurements requires that the scale ratios be available for translating values of various

quantities, e.g. velocity, discharge, etc., into the corresponding prototype values.

It is convenient to introduce here the subscript r to indicate the ratio of "model : prototype" quantity. e.g.. if model lengths are one-tenth those of the prototype, then $L_m/L_p = L_r = 0.1$. In open channel flow, the presence of a free surface means that the Froude's number F is always significant.

The only perfect way of dealing with the effect of viscosity is to keep both F and R the same in the model and the prototype.

When two flows force distributions such that identical types of forces are parallel and are related in magnitude by a constant scale factor at all corresponding points, the flows are dynamically similar.

Therefore the prototype pressure, which is defined as the difference between atmospheric pressure and the pressure on solid surface, under nappe, may be estimated similarly:

$$\left(\frac{\Delta p}{\gamma_0}\right)_p = \left(\frac{\Delta p}{\gamma_0}\right)_m / L_r \quad (4.4)$$

ΔP = pressure below nappe

γ_0 = specific weight of water.

L_r = scale

4.3 Similitude-scale relationships for hydraulic similarity

Similarity theory is applied to variables such as the geometrical boundary dimensions, the characteristics of flow and the fluid properties may be grouped together in similarity. If complete similarity is to exist between flow components in the prototype and flow in the model, every dimensionless parameter referring to conditions in the model must have the same scale as the corresponding parameter referring to the prototype.

A list of flow characteristics used for spillway modelling includes: velocity, rate of discharge, and pressure. Designated by L_r , the numerical value of the selected length scale and the numerical values of the corresponding fluid property scales designated by ρ , μ or ν the following equations are the combination of these scales according to which the flow characteristics must vary to ensure complete similarity:

$$L_r = \frac{L_m}{L_p} \quad (4.5)$$

In curvilinear flows, the requirements of geometry similarity should be fulfilled. Transferring test results from the small spillway model to the prototype structures by means of Froude similarity often commonly neglects the effects of surface tension and viscosity (Matthew, 1964, and Maxwell, 1969).

$$F_m = \frac{V_m}{(gL_m)^{1/2}} = F_p = \frac{V_p}{(gL_p)^{1/2}} \quad (4.6)$$

Then:

$$V_r = \frac{V_m}{V_p} = (L_r)^{1/2} \quad (4.7)$$

For any model scale, match of the Froude numbers determines the velocity ratio. Only the kinematic viscosity can be varied to match Reynolds numbers. Therefore:

$$R_m = \frac{V_m L_m}{\Omega_m} = R_p = \frac{V_p L_p}{\Omega_p}$$

leads to the condition that

$$\frac{\Omega_m}{\Omega_p} = \frac{V_m L_m}{V_p L_p} \quad (4.8)$$

Using the velocity ratio obtained from matching Froude numbers Eq. (4.8) leads to a kinematic viscosity ratio:

$$\frac{\Omega_m}{\Omega_p} = \left(\frac{L_m}{L_p} \right)^{3/2} \quad (4.9)$$

If $L_m/L_p = 0.02$ (a small scale 1:50 for spillway model), then Ω_m/Ω_p must be 2.83×10^{-3} . By investigating the viscosity, water is a practical fluid for most model tests of free-surface flows. To obtain complete dynamic similarity then, a full-scale test would be required. However, model studies do provide useful information even though complete similarity cannot be obtained (Fox, 1992).

Because the Reynolds number cannot be matched for model tests of free surface, the boundary-layer behavior is not the same for model and prototype. The model viscosity is $(L_m/L_p)^{3/2}$ times of the prototype value, so the extent of the boundary-layer on the model is much more large by a corresponding scale factor. The numerical model just described assumes that boundary-layer behavior can be scaled. To make this possible, the model boundary layer is “stimulated” to become turbulent at a location that corresponds to the behavior on the full-scale test high Reynolds number (Fox, 1992). It is for this reason that a thin boundary-layer was assumed (the first assumption for developing the numerical model described in Chapter 2).

$$Q_r = \frac{Q_m}{Q_p} = (L_r)^{5/2} \quad (4.10)$$

$$P_r = \frac{P_m}{P_p} = L_r \quad (4.11)$$

in which L_r , Q_r , and P_r are the length, the discharge, and the pressure ratios, respectively.

Using Eq. (4.10), the model discharges can be determined. The model discharge and pressure readings recorded on the model can be translated into prototype values with an acceptable accuracy. Additional information from modelling scales can be transformed to prototype.

Since, in the majority of hydraulic engineering problems, the influence of fluid weight is greater than that of other force properties, the flow characteristics in the operation of hydraulic models are usually determined through use of the Froude criterion alone. Water is used in the model as in the prototype, since the factor g is generally the same for both model and prototype, these flow characteristics follow the simplified form.

4.4 Objectives of physical modelling

A tentative experimental program will be conceptualized with the following objectives in mind:

- Identify the condition where subatmospheric pressure occurs
- Conduct experiments that accompany the development of the model such that individual processes are isolated and tested in the laboratory, and perform experiments whose measurements will be used for comparison with the numerical model executed in a full simulation mode.

4.5 Model specification

The model is a standard spillway WES designed for $Q_d = 20.83 \text{ l/s}$ of width. The design head for this spillway will be $H_d = 10 \text{ cm}$. The spillway is fabricated of plexiglass (Photo 4.1), that is easily formed and shaped and is unaffected by water. The design of the spillway shape was based on U.S Army, WES corps of engineers (Fig. 4.1). The dimensions of the model for the small scale (1:80) are $b = 298 \text{ mm}$ wide and 320 mm high (Figs. 4.1, 4.2). The model was located in a flume with inlet box of 3.28 m long and a tailrace box 6.90 m long (Photo 4.2 and Fig. 4.4). In an attempt to simplify the structure, the side flare of the spillway was eliminated with assumption that do not influence the quality of test results. The locations of pressure tapping were arranged along three lines away from the channel axis, $z = 0 \text{ mm}$, $z = 75 \text{ mm}$, and $z = 145 \text{ mm}$ (Fig. 4.3). The similitude parameters of model are:

$$L_r = \frac{L_m}{L_p} = 0.0125$$

$$V_r = \frac{V_m}{V_p} = (L_r)^{1/2} = 0.1118$$

$$Q_r = \frac{Q_m}{Q_p} = (L_r)^{5/2} = 1.7469 \times 10^{-5}$$

$$P_r = \frac{P_m}{P_p} = L_r = 0.0125$$

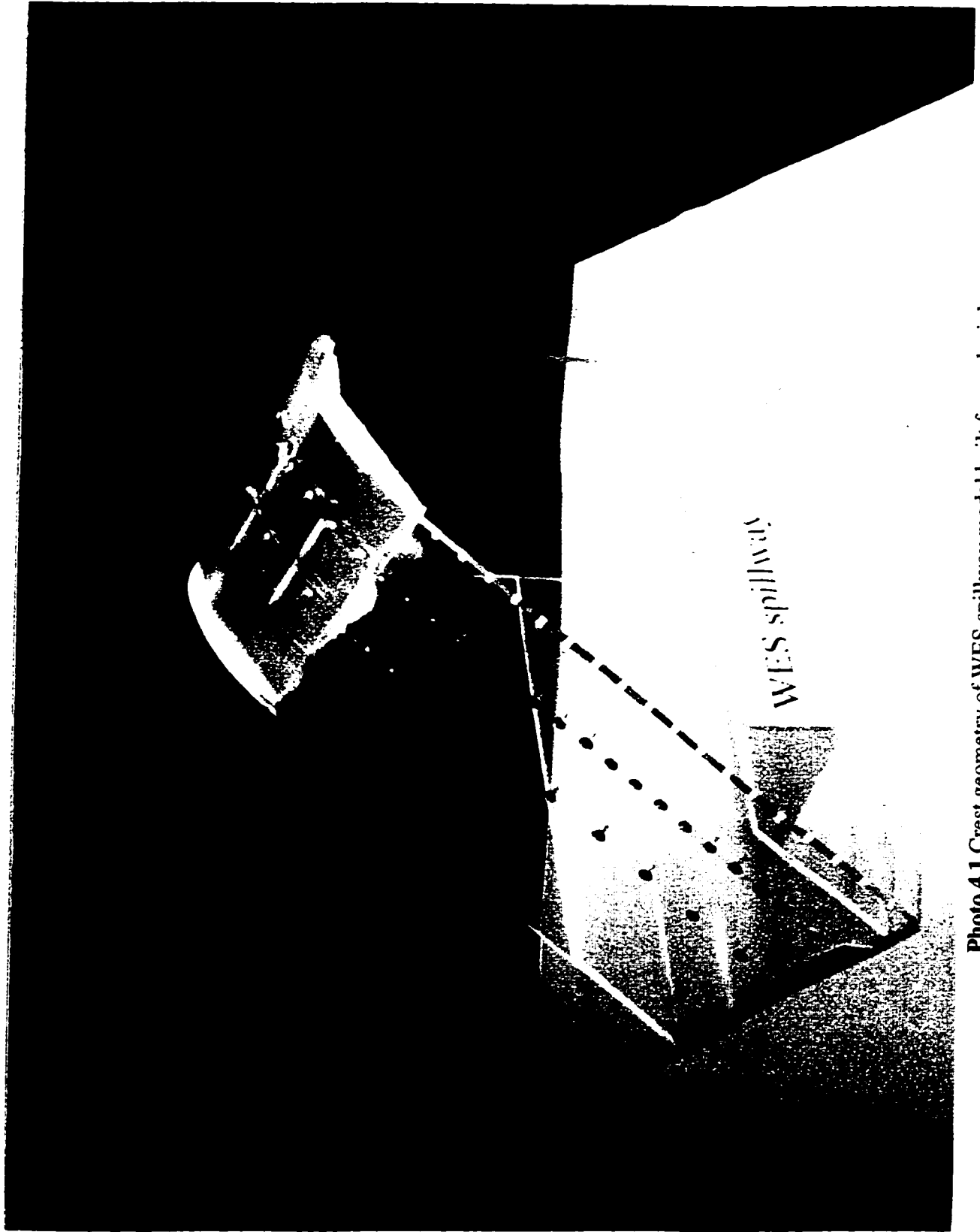


Photo 4.1 Crest geometry of WES spillway model built from plexiglass.

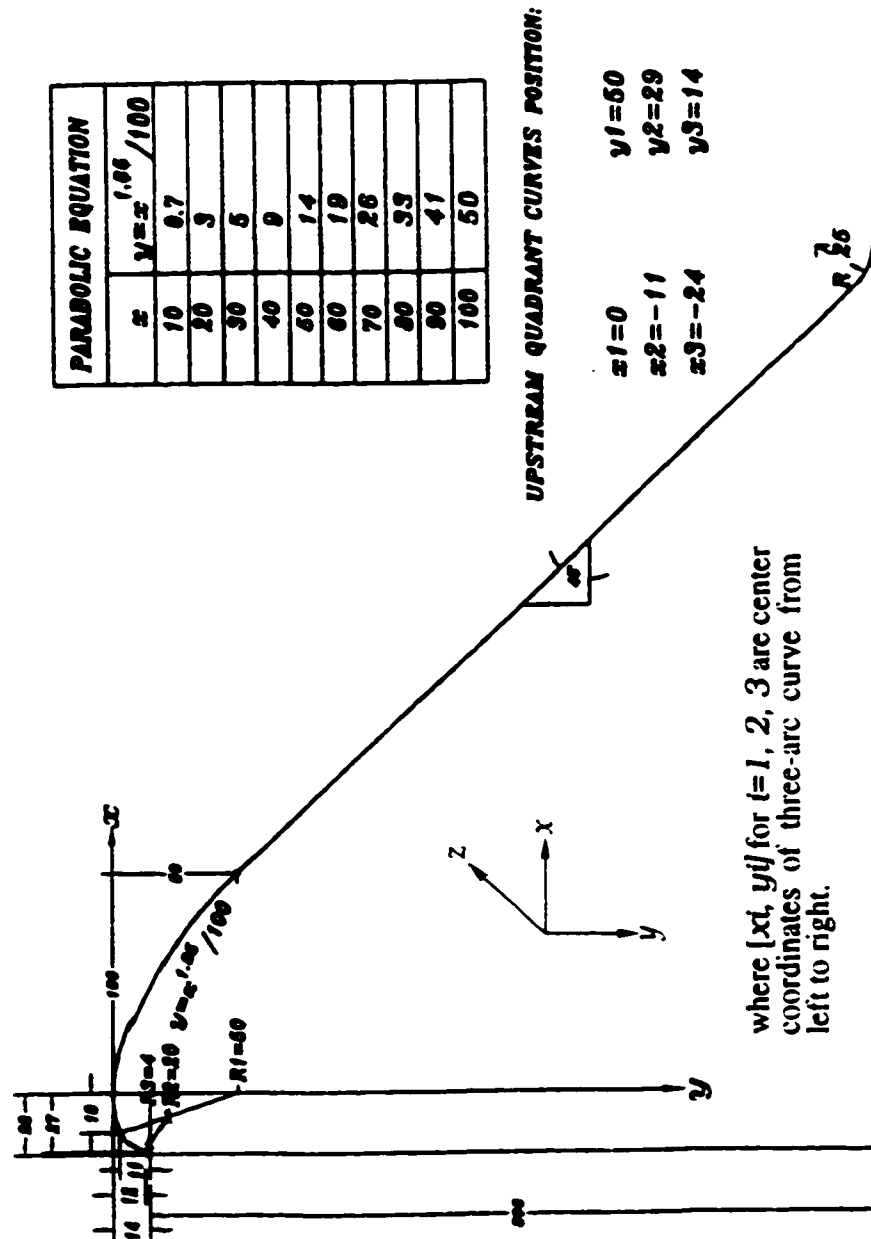


Fig. 4.1 Side view dimensions of experimental model (in millimetres).

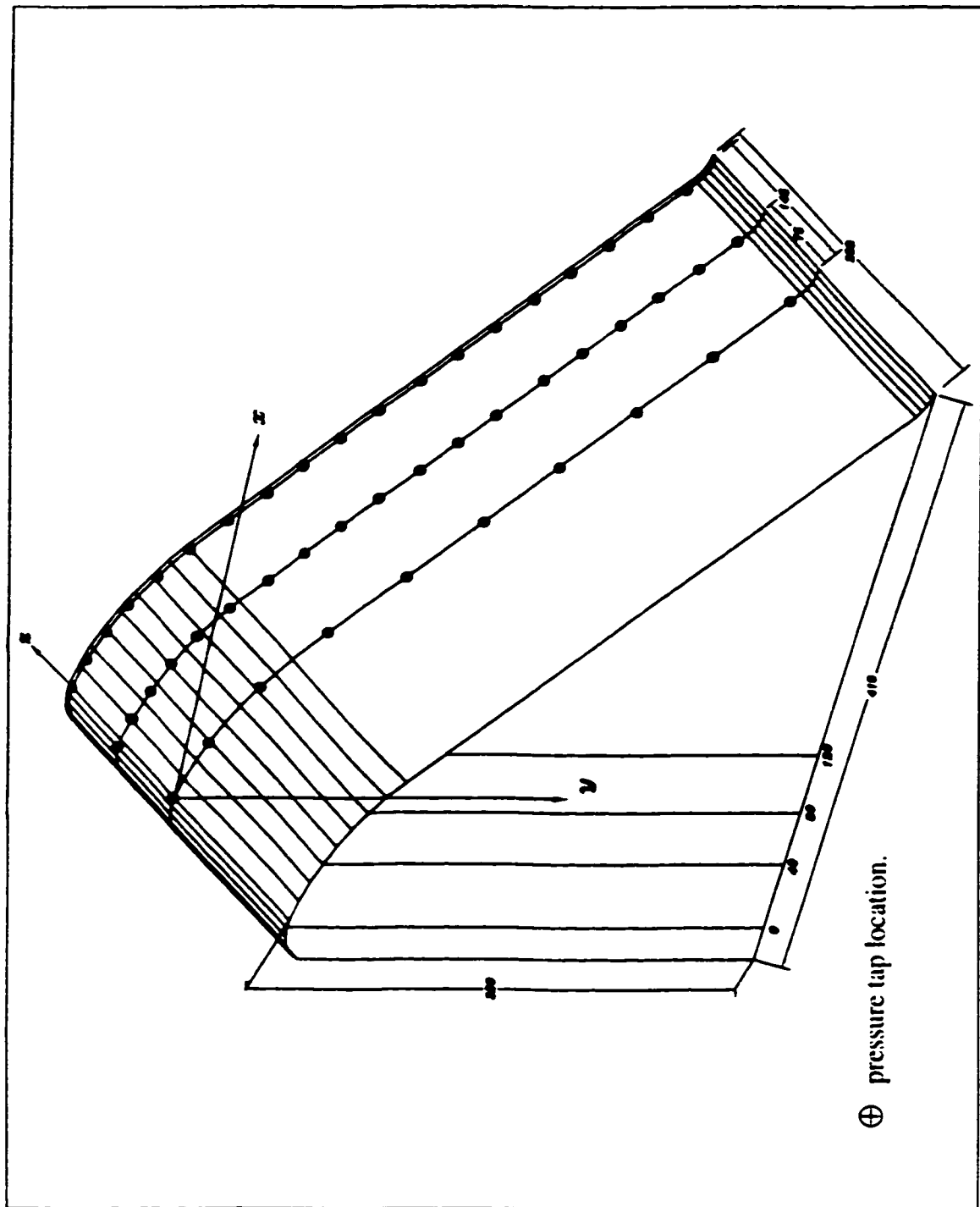


Fig. 4.2 Perspective view of experimental model (in millimetres).

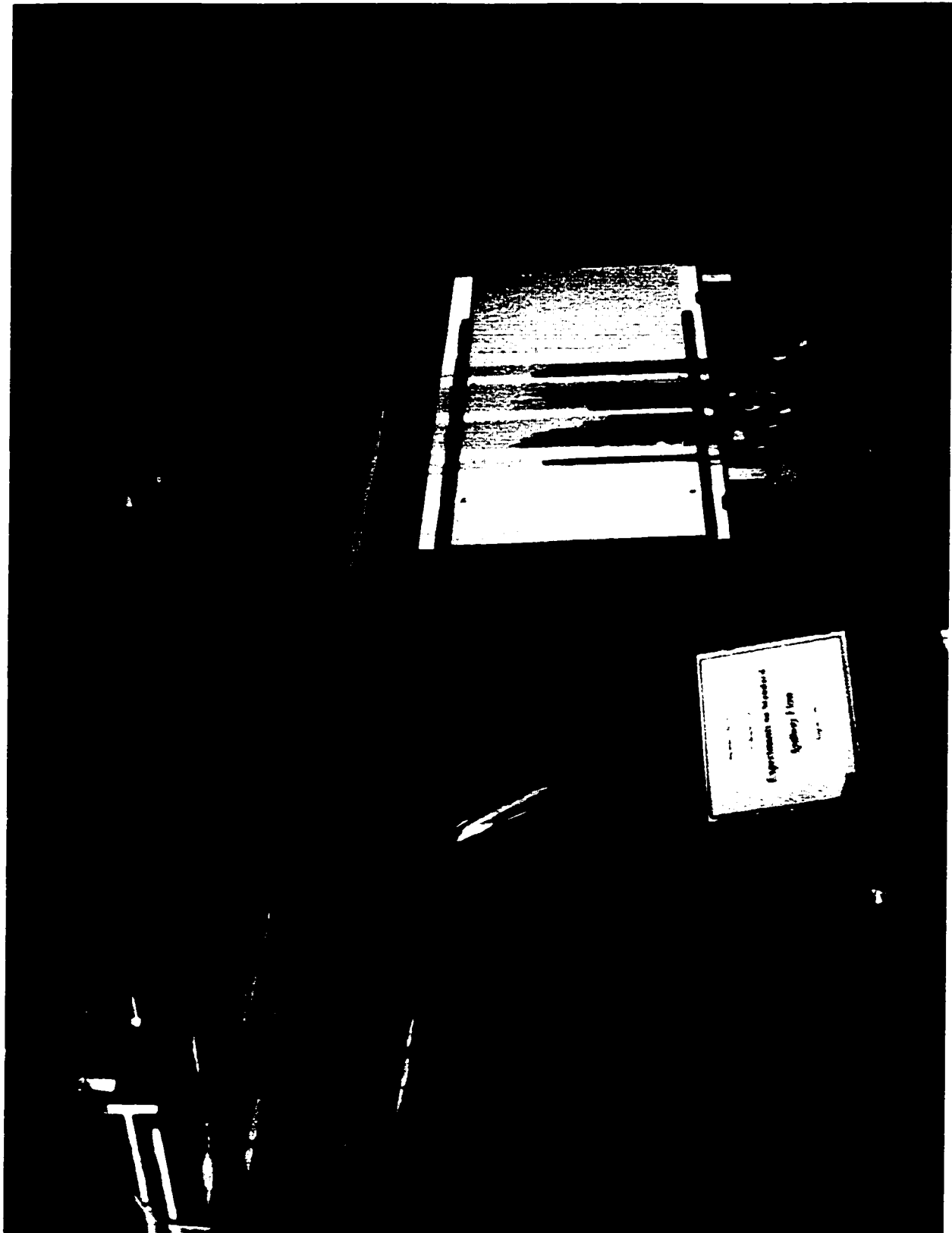


Photo 4.2 Monitoring board and velocity & depth probe set of a spillway model.

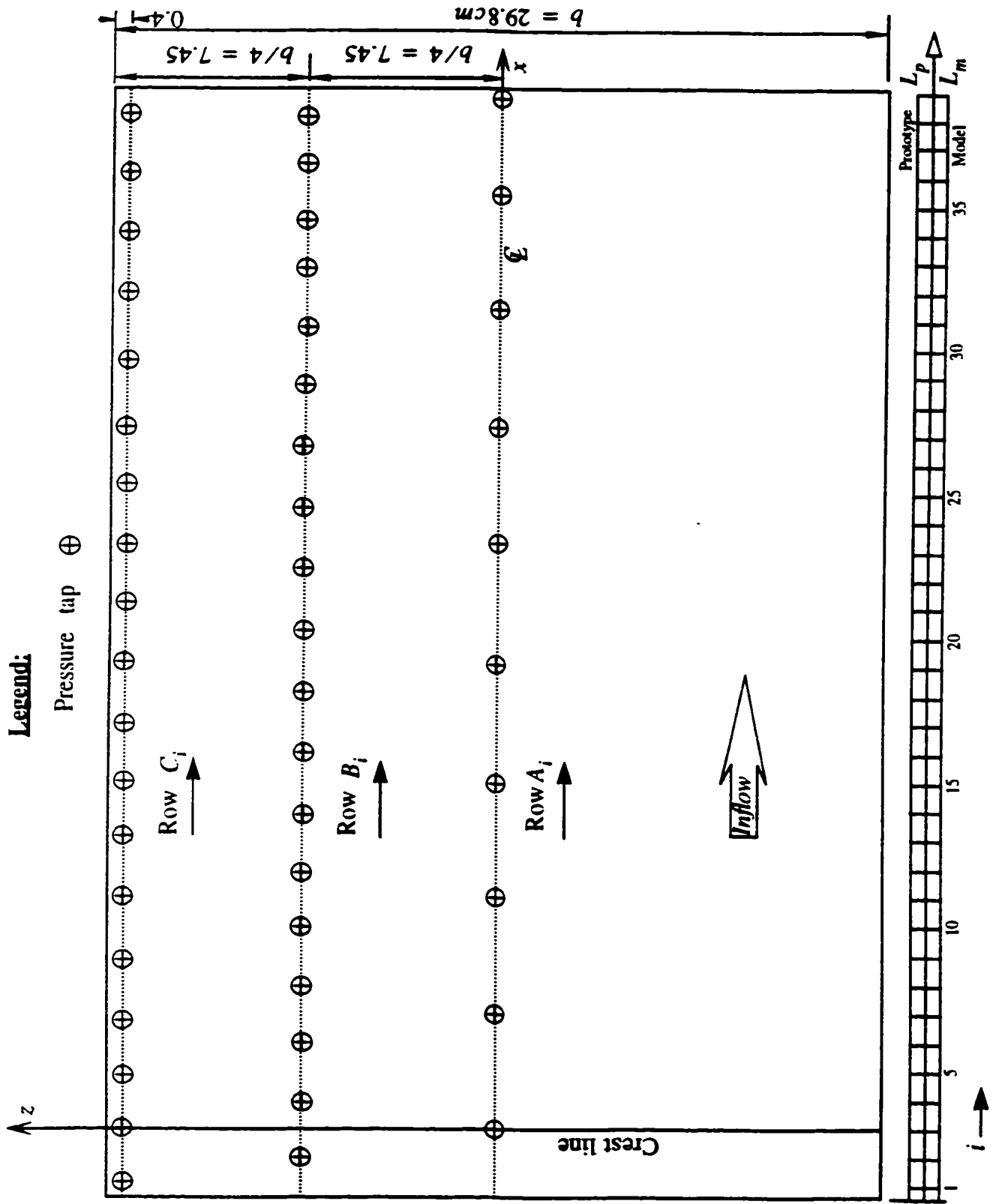


Fig. 4.3 Plan view of experimental WES spillway model (dimensions in centimeters).

4.6 Experimental set-up

The experiments to verify the numerical model were carried out in a $29.8\text{ cm} \times 47\text{ cm} \times 1000\text{ cm}$ flume with a steel frame and glass windows on both sides as necessitated by the thirty-two centimeter height of the model (Fig. 4.4). The flow into the inlet box is conveyed by a 15.24 cm diameter cast-iron pipe that is controlled by a gate valve. A v-notch weir placed at the end of the flume was used to rate the flow.

The approaching condition to the spillway was improved by a honeycomb and floats, to produce a laminar flow and stable free surface at the upstream of the model. The established flow lines entering the approach channel appear to be representative of the prototype condition with a flow from the reservoir.

A portable trolley carrying a point gauge was placed on two rails fixed along the flume top (Photo 4.3). The global coordinate system (x-y) was located at a distance $S = 3H_d$ far from the top of the spillway at a point where the free surface doesn't draw-down and has a constant total energy head of E . At a flat-bed section of the channel (i.e., the section 298 cm from the inlet box), the water depth y was measured using the point gauge to give the energy head $E = y + q^2/2gy^2$.

The point gauge was also used to measure the water depth at every 1 cm horizontal interval along the centreline of the WES model.

A manometer board was elevated 40 cm above the base of the flume, to house the tygon tube connecting the piezometer taps along the centreline of the WES spillway model to the piezometers (Photo 4.3). Along the centreline of the WES spillway, 0.32 cm diameter copper piezometer tappings were fixed at 4 cm horizontal intervals (Fig. 4.3); these were connected by plastic tubes with 0.64 cm (internal diameter) to vertical piezometer of $2\bar{r} = 0.64\text{ cm}$ external diameter glass tubes.

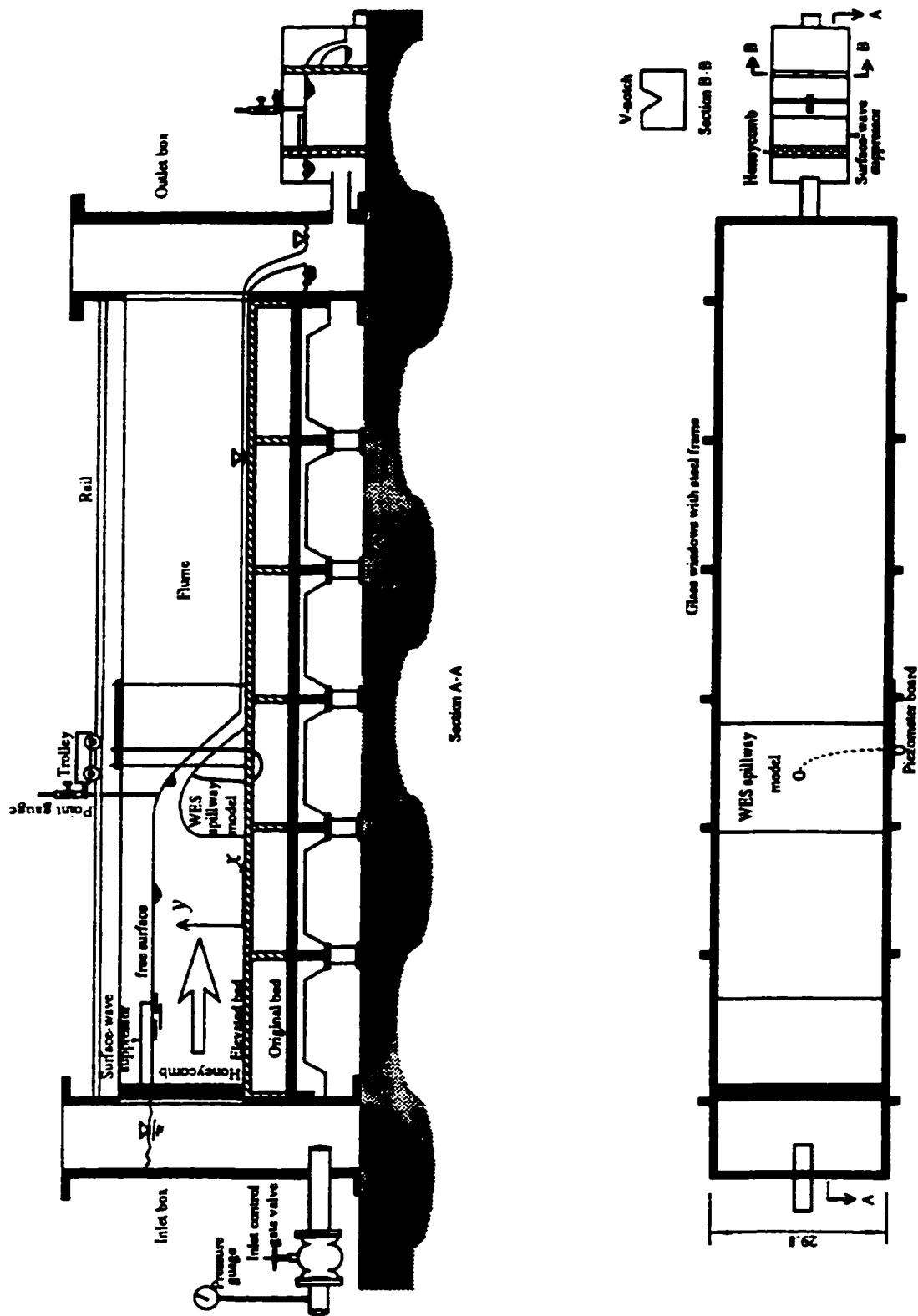


Fig. 4.4 Experimental set-up.

4.7 Methodology of measurements

The procedure for gathering data from detailed observation for the respective head $H/H_d = 0.5, 1.0$, and 1.33 was as follows:

1. Allow the flow into the flume and set the flow rate to give the supercritical flow downstream of the spillway.
2. Note the initial and the final reading of the V-notch's head after each water release.
3. Measure the water surface profile, the velocity at the grid points and bed pressure over the spillway, and
4. Measure the water temperature and atmospheric pressure for calculating P_v and the viscosity.

Detailed observations were made for the approach conditions. The spillway crest was calibrated, and necessary measurements were obtained.

4.7.1 Calibration of the crest model

During the investigation, the WES spillway crest was calibrated to relate the discharge to the reservoir pool elevation.

The specific discharge over the WES spillway crest increased with the depth of the approach flow over the spillway crest:

$$q = \frac{Q}{b} = CH^{1.5} \quad (4.12)$$

where:

Q = Volume flow rate over crest

b = Lateral width of spillway

H = Depth of approach flow over spillway crest

C = Experimentally determined coefficient which is a function of $\frac{H}{H_d}$, where H_d is the design head. The value of C for standard spillway is calculated from:

$$C = C_d \sqrt{2g} \quad (4.13)$$

where:

C_d = Discharge coefficient ($C_d = 0.4992$)

g = Gravity acceleration ($g = 9.80665 \text{ m/s}^2$)

From the 30° v-notch weir equation the steady unit-width discharge (at 21° C) was then determined (Figs. 4.4 & 4.5). The flow rate over the weir was calculated using (Bean, 1971):

$$Q = \frac{4}{15} T_h \sqrt{2gh^3} \quad (4.14)$$

where T_h is the width of the water related to the V-notch head. If Φ = the angle between the sides, then:

$$T_h = 2h_y \tan \frac{\Phi}{2} \quad (4.15)$$

and including the coefficient of discharge, the actual flow rate is:

$$Q = \frac{8}{15} \dot{C} \tan \frac{\Phi}{2} \sqrt{2gh_y^5} \quad (4.16)$$

where Q is in cubic feet per second. The value of the coefficient, \dot{C} , to be used in the equation for the V-notch weir is dependent mainly on the notch angle, Φ , and to the head.

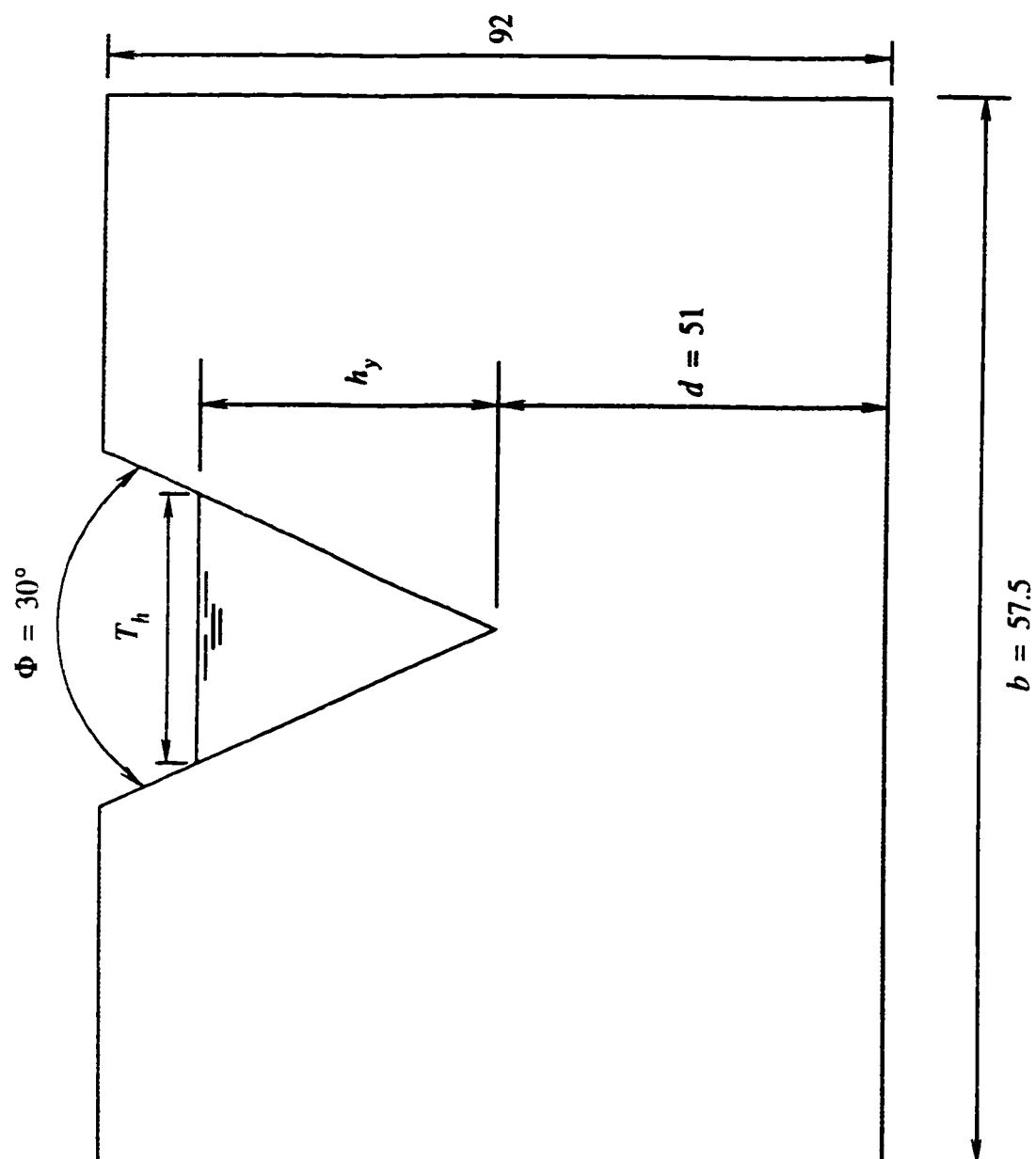


Fig. 4.5 V-notch weir measuring the output flow of flume (dimension in centimeters).

h_y , or rather to the ratio, h_y/d . It was found that the influence of h_y/d on \check{C} becomes negligible when the observed head, h_y , was replaced with:

$$h' = h_y + \Delta \quad (4.17)$$

where the correction term, Δ , was related to the notch angle, Φ . Other parameters are:

h' = Adjusted head of a triangular notch weir in *ft*.

h_y = Height of column of flowing fluid over weir in *ft*.

b = Width of approach channel upstream of a weir in *ft*.

d = Elevation of apex of a triangular notch weir above bottom of approach channel in *ft*.

Q = Volume rate of flow in *cfs*

Φ = Angle included between sides of a triangular notch weir in degree

Δ = Adjustment to be added to observed head of a triangular notch weir in *ft*.

Thus, Eq. (4.20) becomes:

$$q = \frac{8}{15} \check{C} \tan \frac{\Phi}{2} \sqrt{2gh'}^5 \quad (4.18)$$

Values of \check{C} and Δ are given by the diagram (Bean, 1971) and for a 30° V-notch, they are $\check{C} = 0.587$ and $\Delta = 0.007$ *ft*.

By equating Eq. (4.18) and Eq. (4.12), the discharge coefficient $C_d = q/(\sqrt{2g}H_0^{3/2})$ was calculated (Table 4.1). The study results were in good agreement with Chow's coefficients (Chow, 1959).

Table 4.1: Comparison of measured discharge coefficient with Chow results

Oper. Head	Theory	Chow	Spillway
$H/H_d = 0.5$	0.4686	-----	-----
$H/H_d = 1.0$	0.4992	0.501	0.35
$H/H_d = 1.33$	0.5212	0.523	0.34

Therefore by substituting C_d and g in Eq. (4.13), gives $C = 2.21$. This is close to the value of C given in Table 2.2 for the design head. Discharge Q could be varied between 23 and 112 l/s/m. These discharges are related to design discharge, for which the discharge coefficient $C_d = 0.4992$, therefore $Q_d = 20.83$ l/s.

4.7.2 Water surface profiles on the spillway

Although theory defines the free surface by the coordinate n normal to the bed, the vertical coordinate z to locate the free surface was measured.

The flow depths y_i , $i = 0, 1, 2, \dots$ on the spillway were measured vertically for three operating heads H , by mounting the point gauge. A level point gauge arrangement was used for measurements in the approach channel which is the curved section of the spillway. Photo 4.3 shows a movable point gauge carriage arrangement in the 45° section of the WES spillway model. All free surface readings were measured at $x = i \text{ cm}$, $i = 0, 1, 2, \dots$ using a vertical point gauge, from a common datum coordinated at section $i = 0$, which located at $S = 3H_d$ from the spillway crest coordinate. In the approach channel, the upstream flow depth H_0 at section $i = 0$ was measured as the total head energy for the stagnant point. The experimentation was designed such that at the section $i = 0$, the flow was strictly subcritical (i. e. $V_a / \sqrt{gH_0} < 1$).

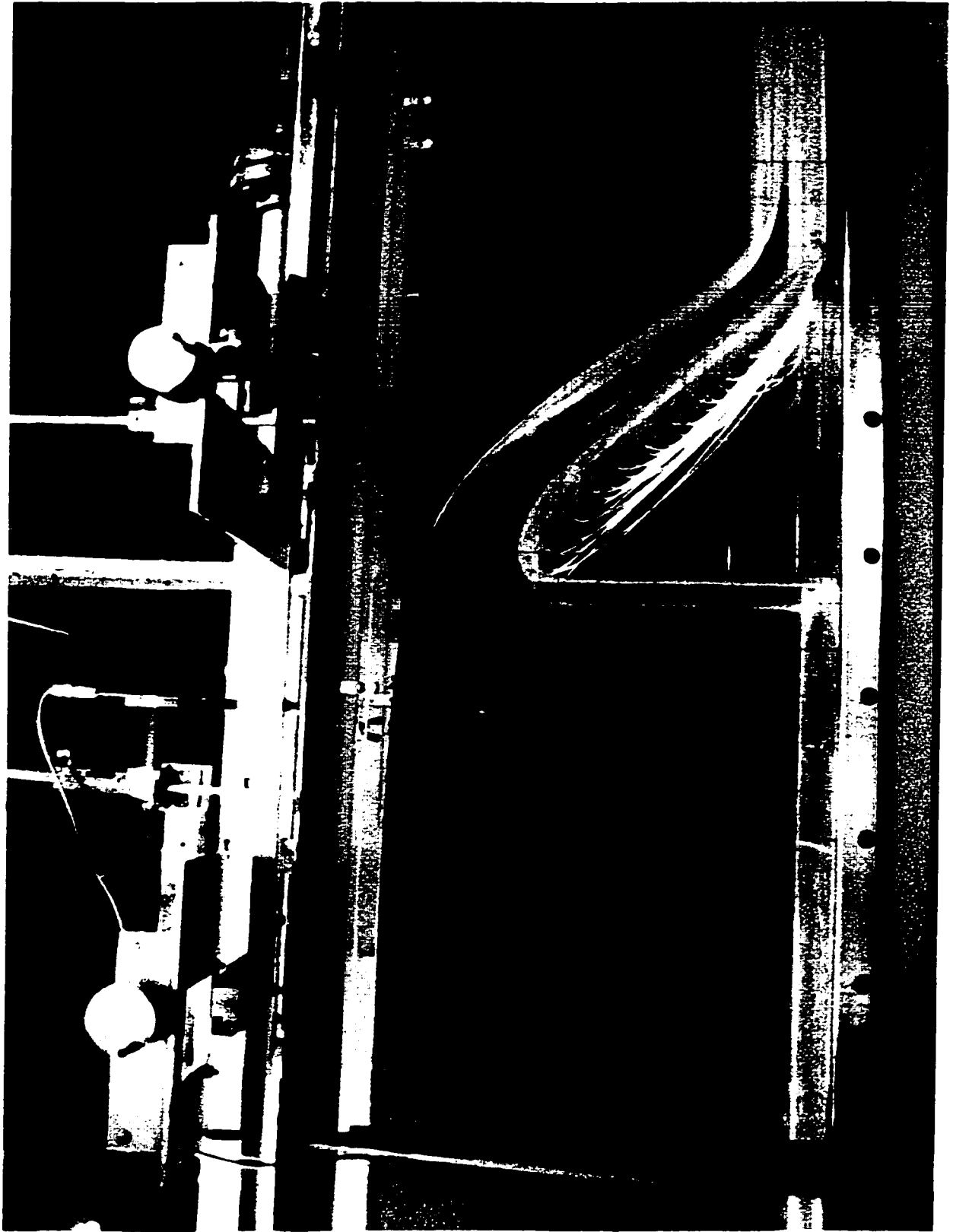


Photo 4.3 Overall view at model spillway, grid points, and recording probe set.

This procedure was repeated for three different value settings along the centerline. 145 mm from the wall. In the downstream concave section of model, the location of the free surface with respect to the datum was measured. The prototype operating conditions simulated in the model are given in Table 4.2. The results of the free surface measurements can be shown in Table 4.3. A non-dimensional graph of the free surface data at $H/H_d = 0.5, 1.0$, and 1.33 is shown in Fig 4.6.

Table 4.2: Model operating conditions

Operating head H/H_d	Discharge $l/s/m$	Headwater Ele. h_1/H_d	Tailwater Ele. h_2/H_d
$\frac{H}{H_d} = 0.5$	23.198	3.72	0.09
$\frac{H}{H_d} = 1.0$	69.890	4.21	0.25
$\frac{H}{H_d} = 1.33$	111.925	4.52	0.41

There is an equation (within experimental accuracy limits) that relates the head to the discharge. It is possible to calculate Q for any H if, Q_d and H_d are available:

$$\frac{Q}{Q_d} = \left(\frac{H}{H_d} \right)^{1.60} \quad (4.19)$$

Table 4.3: Water surface profiles for 3 operating heads

Water surface profiles			
x/H_2	$H/H_2 = 0.5$	$H/H_2 = 1.0$	$H/H_2 = 1.5$
-2.9	0.516	1.006	1.321
-2.8	0.525	1.009	1.326
-2.7	0.530	1.010	1.328
-2.6	0.531	1.009	1.327
-2.5	0.530	1.008	1.327
-2.4	0.527	1.006	1.320
-2.3	0.522	1.004	1.314
-2.2	0.518	1.001	1.308
-2.1	0.513	0.998	1.308
-2.0	0.509	0.995	1.294
-1.9	0.506	0.992	1.287
-1.8	0.503	0.990	1.280
-1.7	0.502	0.987	1.273
-1.6	0.502	0.984	1.273
-1.5	0.502	0.980	1.260
-1.4	0.504	0.980	1.253
-1.3	0.505	0.973	1.246
-1.2	0.507	0.968	1.239
-1.1	0.508	0.963	1.231
-1.0	0.509	0.956	1.222
-0.9	0.509	0.948	1.212
-0.8	0.507	0.938	1.201
-0.7	0.503	0.926	1.188
-0.6	0.497	0.913	1.173
-0.5	0.488	0.896	1.155

Table 4.3: Water surface profiles for 3 operating heads

Water surface profiles			
x/H_0	$H/H_0 = 0.5$	$H/H_0 = 1.0$	$H/H_0 = 1.53$
-0.4	0.475	0.877	1.134
-0.3	0.458	0.855	1.111
-0.2	0.437	0.830	1.084
-0.1	0.411	0.800	1.053
0.0	0.380	0.767	1.018
0.1	0.343	0.730	0.979
0.2	0.300	0.688	0.935
0.3	0.252	0.641	0.886
0.4	0.192	0.588	0.831
0.5	0.135	0.531	0.772
0.6	0.067	0.468	0.706
0.7	-0.07	0.399	0.635
0.8	-0.087	0.324	0.559
0.9	-0.173	-0.243	0.476
1.0	-0.265	0.156	0.388
1.1	-0.362	0.62	0.293
1.2	-0.463	-0.380	0.194
1.3	-0.567	-0.144	0.088
1.4	-0.674	-0.257	-0.022
1.5	-0.783	-0.377	-0.137
1.6	-0.892	-0.502	-0.257
1.7	-1.00	-0.634	-0.380
1.8	-1.105	-0.772	-0.507

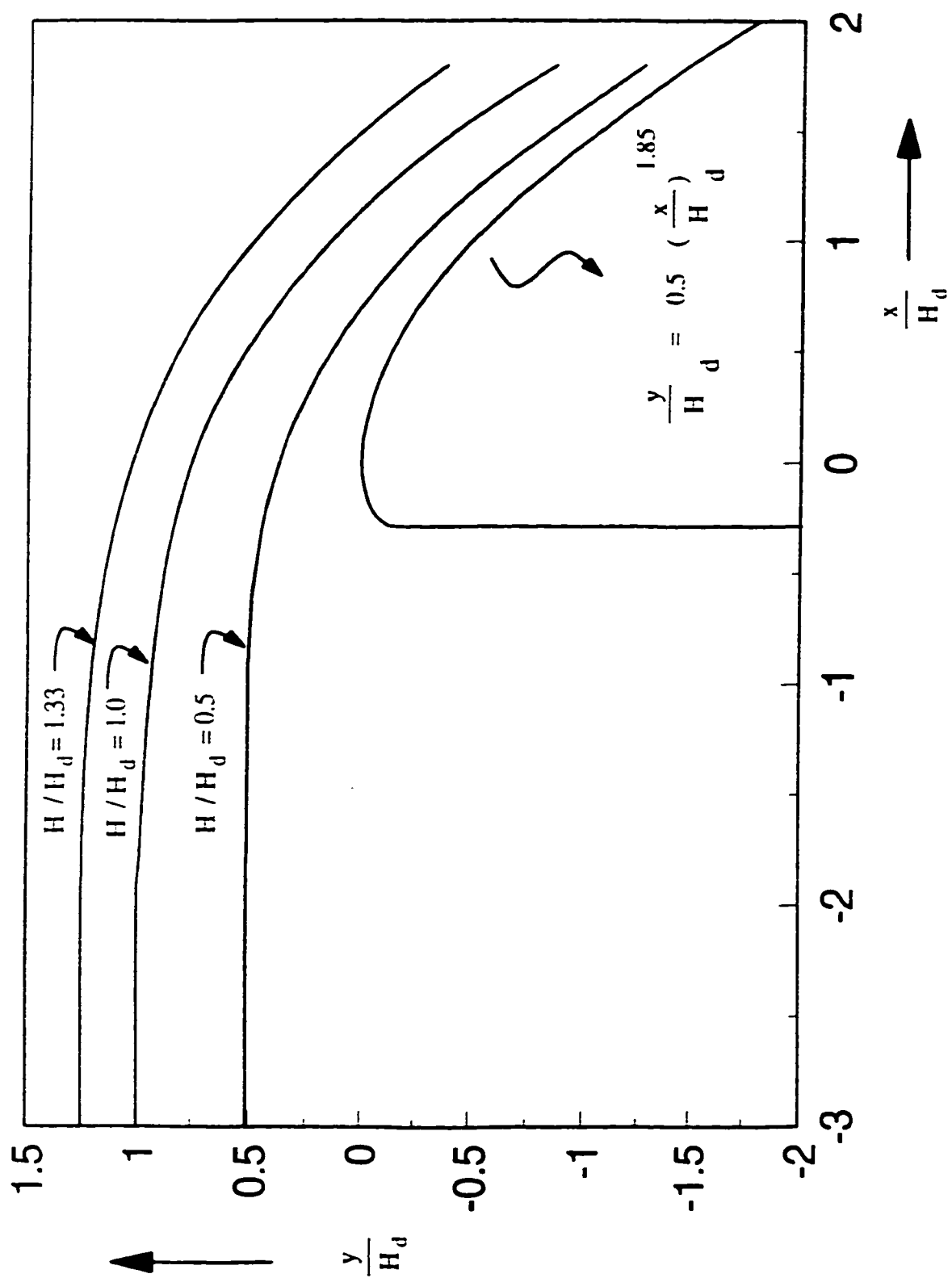


Fig. 4.6 non-dimensional free surface $H/H_d = 0.5, 1.0, 1.33$.

4.7.3 Pressure measurements

Pressure on the spillway was measured in numerous points of the models bed. Twelve taps were installed in the model along WES spillway centerline (Photo 4.1). The tap coordinates were evenly spaced as viewed in a horizontal projection (Fig. 4.3). Since a model is two dimensional, measurements were done in the centerline (row A_i) and they verified in row B_i and C_i . The pressure at $x = 4i$, $i = 0, 1, 2, \dots$ were measured, for flows from 23 l/s/m to the maximum flow of 112 l/s/m .

Photo 4.2 shows the piezometric pressures with a discharge of 69 l/s/m flowing through the model. To make them easier to read, the tubes were filled with colored dyes.

As shown in Fig. 4.7, the recorded piezometric level difference between the steady flow and bottom condition gauged the bed-pressure head $P_0/\rho g$, where the implicit pressure datum corresponds to $P_0 = 0$.

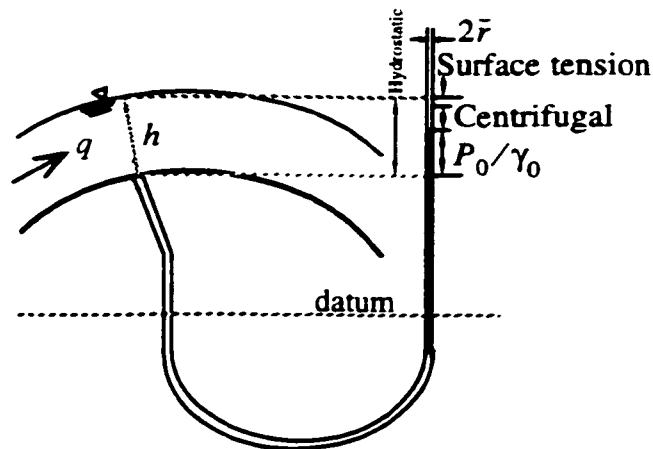


Fig. 4.7 Bed pressure reading.

Another method for determining the pressure for a chute spillway is to calculate the flow profiles for the range of operating discharges. From each profile, the piezometric pressures at various locations on the spillway were calculated:

$$\bar{h} = h_s + h_c \quad (4.20)$$

where h_s is the hydrostatic head in curvilinear flow, h_c and \bar{h} are the centrifugal correction and piezometric head, respectively.

Corrections to these pressures must be made to account for steep slopes, as well as any boundary curvature present (Chow, 1959). The slope correction on steep slopes is:

$$\frac{P_0(x)}{\gamma_0} = d_n(x) \cos \theta \quad (4.21)$$

where $d_n(x)$ is the depth measured normal to flow surface, γ_0 is specific weight of water and θ is bottom slope. If the flow is over a boundary which has a vertical curvature, correction for the centrifugal force in Eq. (4.21) is:

$$h_c = \pm \left(\frac{d_n(x)}{g} \right) \left(\frac{V_0^2(x)}{r} \right) \quad (4.22)$$

$$\frac{P_0(x)}{\gamma_0} = d_n(x) \cos \theta \pm \left(\frac{d_n(x)}{g} \right) \left(\frac{V_0^2(x)}{r} \right) \quad (4.23)$$

where r is the radius of the curvature of the bottom, d_n is the depth of flow and for practical purpose $V_0(x)$ may be measured equal to the average velocity of the flow. The g is the gravity acceleration. The h_c is positive for concave flow, negative for convex flow, and zero for parallel flow.

To further evaluation, the occurrence of subatmospheric pressures at critical locations, served to form the non-dimensional representation of manometric pressures. Results are shown in Fig. 4.8.

Tap B_2 in the curved section of the spillway shows subatmospheric pressure of $\frac{h_p}{H_d} = -0.28$ at 112 l/s/m. It should be noted that subatmospheric pressure fluctuations

of this magnitude tend toward the subatmospheric pressure and hence suggest potential cavitation damage on the spillway surface during periods of high-flow spillway operation.

By reviewing the hydraulic test results, it is clear that although there were no large subatmospheric pressures observation on the spillway, the pressure was so low that it can be a reason for cavitation in velocities of more than 11 m/s .

The location of the pressure taps is presented on Table 4.4 for a complete range of discharges. As the plotted results on Fig. 4.8 show, at most taps for $H/H_d \leq 1$, the pressures are superatmospheric; however, over the spillway for $H/H_d > 1$, pressures dip slightly below zero. The slight dip in pressures over the crest is emphasized, and in addition a dip in pressures can be observed near the crest. It is interesting to note that the pressures on the crest were less than the corresponding hydrostatic pressure. In the convex portions of the spillway, the centrifugal forces were such that the pressure was reduced below the water surface elevation, while the pressures were greater than the hydrostatic pressure for the concave portions. At the joint of the crest curve and tangency, where the spillway chute becomes quite steep, the pressures on the bed were nearly zero. The data in Fig. 4.8 suggests that the pressure conditions in the spillway proper are generally satisfactory for all discharges when $\frac{H}{H_d} \leq 1$. In addition to the centerline taps, other taps were installed 75 mm from the center line.

4.8 Determination of the mean flow velocity along the spillway

The collapse of vapor bubbles is proportional to the mean velocity and this is function of cavitation index. For a fixed pump setting, at section $i = 0$, averaged velocities at $y = 2\text{ cm}$ verticals and $x = 5\text{ cm}$ horizontals were measured using a highly sensitive flowmeter with an internal diameter of 8 mm (Photo 4.3). The flowmeter system

Table 4.4: Measured non-dimensional bottom pressure on the WES spillway

Tap no ^a .	Tap coordinates		Bottom pressure reading $\frac{h_p}{H_d}$		
	$\frac{x}{H_d}$	$\frac{y}{H_d}$	$\frac{H}{H_d} = 0.5$	$\frac{H}{H_d} = 1.0$	$\frac{H}{H_d} = 1.33$
C_1	-0.2	0.033	0.33	0.15	-0.22
B_2	-0.1	0.024	0.27	0.12	-0.28
A_3	0.0	0.000	0.20	0.00	-0.20
B_4	0.1	0.021	0.17	0.08	-0.19
B_6	0.3	0.033	0.15	0.07	-0.18
A_7	0.4	0.070	0.12	0.05	-0.16
B_8	0.5	0.115	0.14	0.085	-0.15
B_{10}	0.7	0.249	0.15	0.11	-0.10
A_{11}	0.8	0.304	0.15	0.11	-0.09
B_{12}	0.9	0.396	0.19	0.12	0.11
B_{14}	1.1	0.548	0.21	0.148	0.18

a. refer to Fig. 4.3.

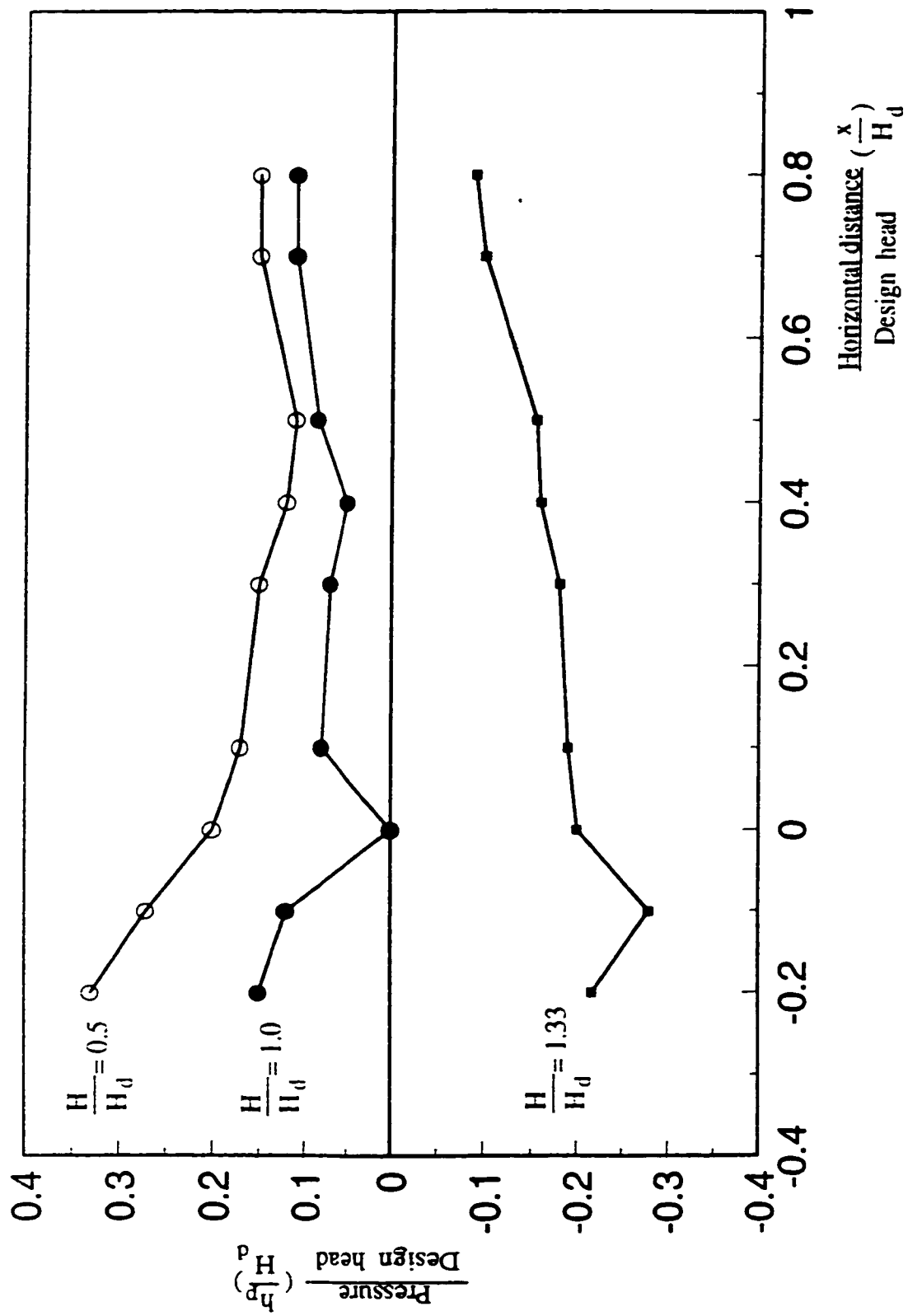


Fig. 4.8 Non-dimensional pressure measured over spillway.

is, responding to velocities as low as 2.5 cm/s . Two low and high velocity probes were used to measure the velocities at upstream and at the downstream face of the spillway. Thereafter, the probe calibration charts were used to obtain actual velocities at these points. The upstream velocity V_a was assumed to be zero. Tables 4.5-4.7 show the results of the velocity measurements, together with other measured hydraulic parameters over the WES spillway. The non-dimensional velocities at these points are shown in Figs. 4.9, 4.10 and 4.11. The horizontal velocity distribution was found to be fairly uniform except for the boundary layer.

Table 4.5: Measured hydraulic parameters over WES spillway for $H/H_d = 0.5$

Parameters	x-distance from model crest (centimeters)			
	0.0	5.0	10.0	15.0
$V_0(x) \text{ [cm/s]}$	70.03	105.04	126.05	140.05
$P_0(x) \text{ [cm]}$	2.0	1.4	2.0	2.35
Parameters	x-distance from prototype crest (meters)			
	0.0	4.0	8.0	12.0
$V_0(x) \text{ [m/s]}$	6.26	9.40	11.28	12.53
$P_0(x) \text{ [m]}$	1.60	1.12	1.60	1.88
$\sigma(x)$	0.67	0.19	0.21	0.20
$\delta(x) \text{ [m]}$	0.0	0.046	0.078	0.105
$V_{0.01}(x) \text{ [m/s]}$	-	6.81	7.44	7.76
$\sigma_G(x)$	-	0.92	0.77	0.68

Table 4.6: Measured hydraulic parameters over WES spillway for $H/H_d = 1.0$

Parameters	x-distance from model crest (centimeters)			
	0.0	5.0	10.0	15.0
$V_0(x)$ [cm/s]	65.82	95.23	119.04	147.05
$P_0(x)$ [cm]	0.9	0.8	1.3	1.70
Parameters	x-distance from prototype crest (meters)			
	0.0	4.0	8.0	12.0
$V_0(x)$ [m/s]	5.89	8.52	10.65	13.15
$P_0(x)$ [m]	0.72	0.64	1.04	1.36
$\sigma(x)$	0.26	0.10	0.13	0.12
$\delta(x)$ [m]	0.0	0.047	0.078	0.104
$V_{0.01}(x)$ [m/s]	-	6.18	7.03	8.23
$\sigma_G(x)$	-	0.93	0.77	0.69

Table 4.7: Measured hydraulic parameters over WES spillway for $H/H_d = 1.33$

Parameters	x-distance from model crest (centimeters)			
	0.0	5.0	10.0	15.0
$V_0(x)$ [cm/s]	77.03	109.24	140.05	180.66
$P_0(x)$ [cm]	-2.0	-1.55	1.60	2.0
Parameters	x-distance from prototype crest (meters)			
	0.0	4.0	8.0	12.0
$V_0(x)$ [m/s]	6.89	9.77	12.53	16.16
$P_0(x)$ [m]	-1.60	-1.24	1.28	1.60
$\sigma(x)$	-0.77	-0.31	0.13	0.10
$\delta(x)$ [m]	0.0	0.05	0.08	0.10
$V_{0.01}(x)$ [m/s]	-	7.08	8.27	10.20
$\sigma_G(x)$	-	0.92	0.77	0.70

The properties of water at 21°C in the experimentation environment are summarized in Table 4.8.

Table 4.8: Fluid properties in experimental environment

Temperature $^\circ\text{C}$	P_v in kN/m^2	ρ in kg/m^3	γ_0 in kN/m^3	ν in m^2/s	T_s in N/m
21	2.5471	997.782	9.78782	9.96347×10^{-7}	0.0726256

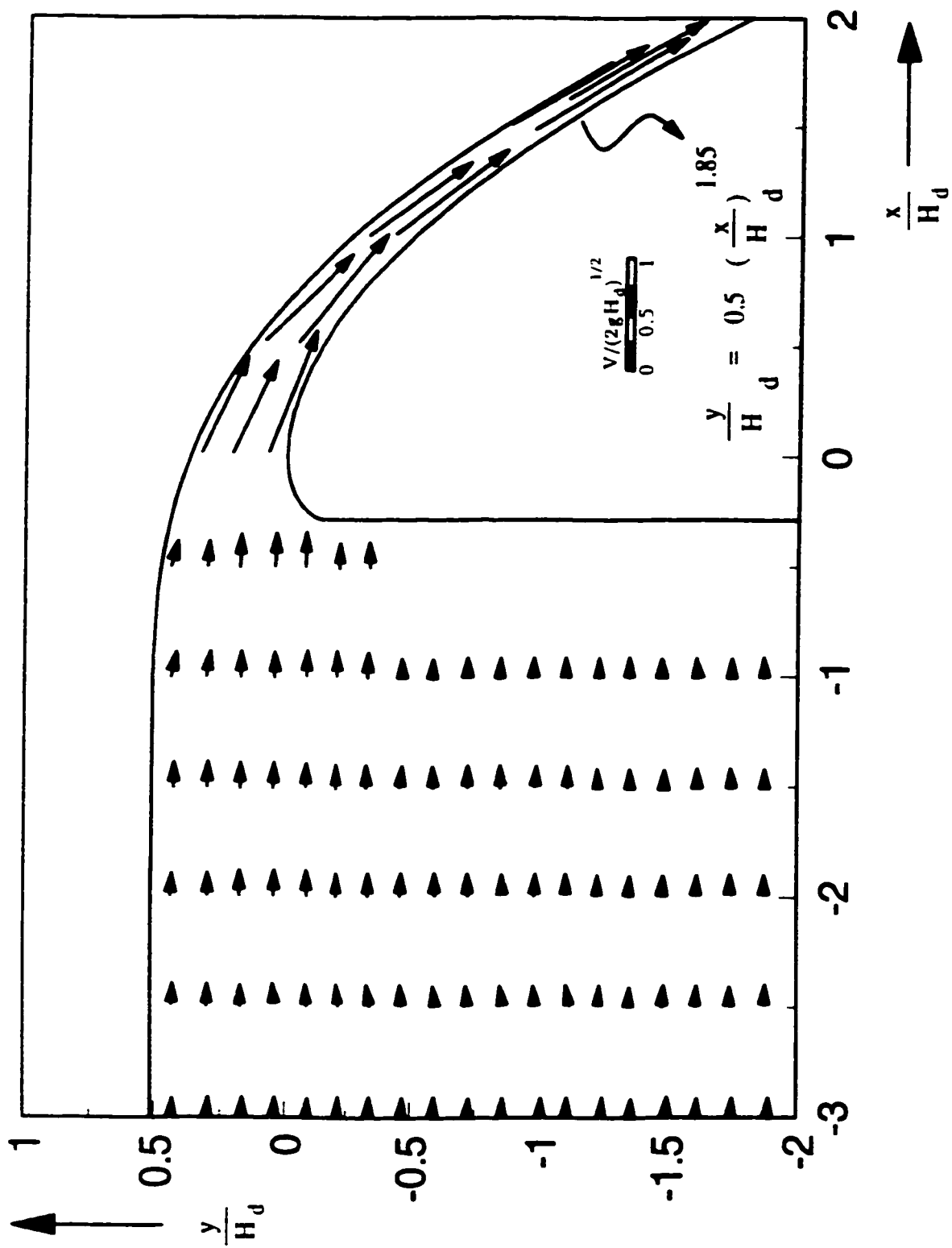


Fig. 4.9 Measured velocity field inside spillway domain for $H/H_d = 0.5$

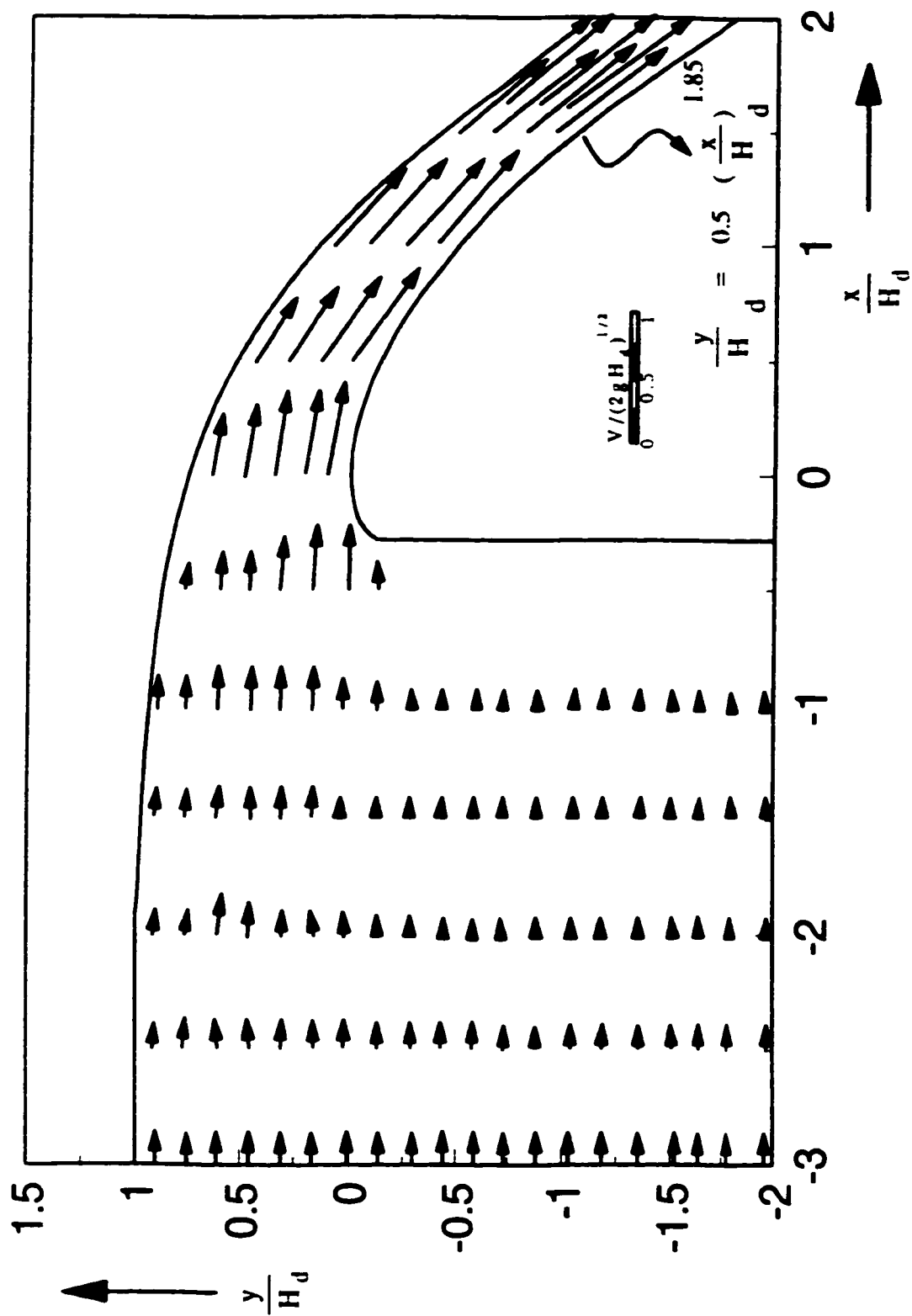


Fig. 4.10 Measured velocity field inside spillway domain for $H/H_d = 1.0$

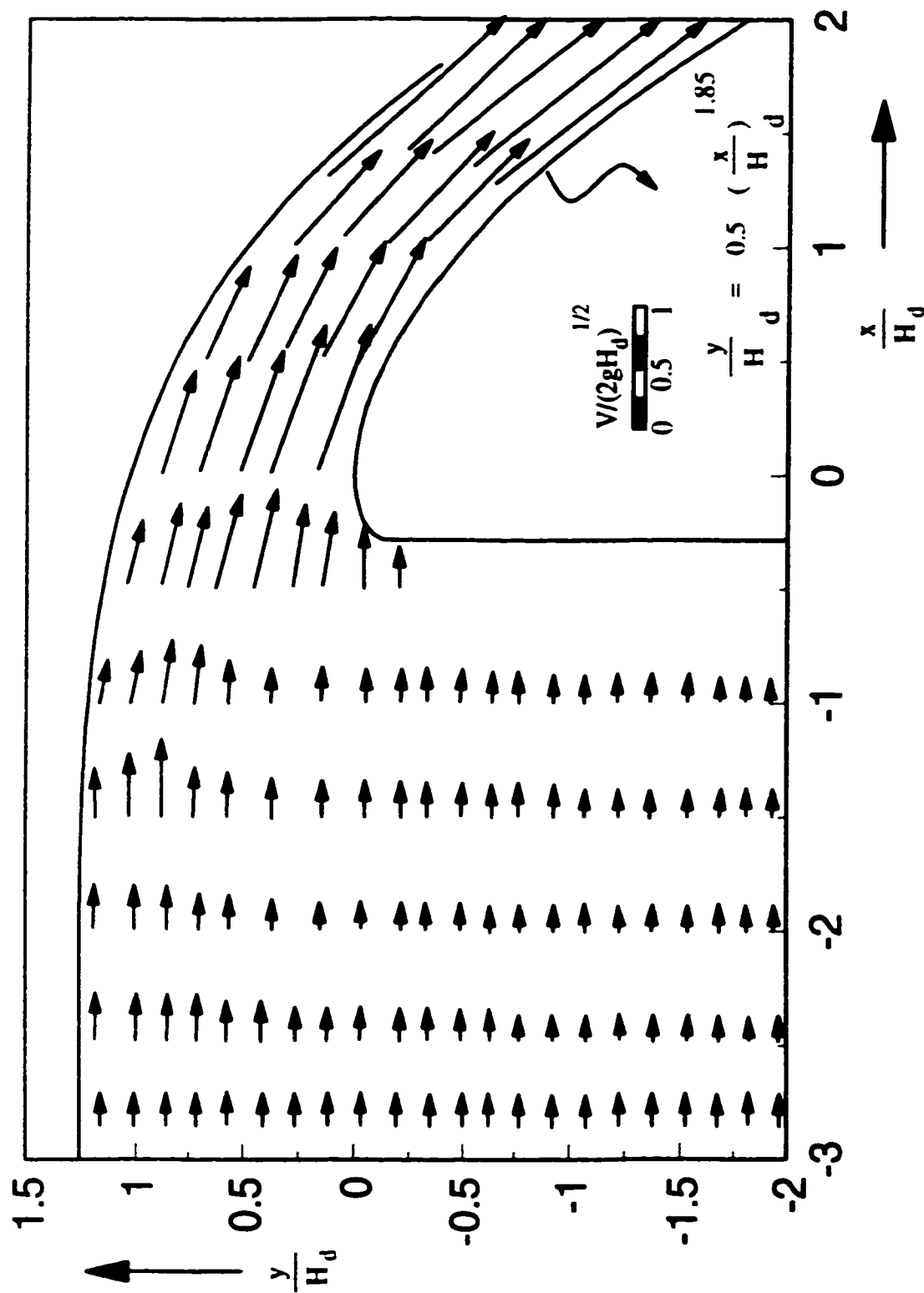


Fig. 4.11 Measured velocity field inside spillway domain for $H/H_d = 1.33$

4.9 Discussion of experimental results

The limit head H depends on the spillway shape (WES spillway shape) and the relative head H/H_d . For $H/H_d \leq 1$, the crest pressure has to remain positive throughout the spillway. However, for $H/H_d > 1$, the head on the spillway is limited, as cavitation damage may occur. The proposed model of this study can determine the bottom pressure along the crest for any H beyond H_d by plotting $P_b/\rho g H_d$ versus x/H_d for different H/H_d , where P_b is the bottom pressure on the spillway. Another useful curve is plotting $V/(2gH_d)^{1/2}$ versus y/H_d for different x/H_d .

The first choice of the boundary conditions giving sufficiently close agreement with the experiment was achieved through numerous computer model trials with different operating heads $H/H_d = 0.5, 1.0$, and 1.33 . By calibrating the spillway for C_d , the discharge value for C_d could be determined. The value of q at any H/H_d other than design head is known from Eq. 4.19 or obtained from the v-notch equation. These discharge values are required for free-slip boundary condition. The study of this problem is summarized by classifying the directions of the search into the following groups:

- Influence of the cell size on the accuracy of calculation

The investigation has shown that for high values of grid points $N = 50$, the solutions for types of boundary conditions H/H_d are very close to the numerical methods.

- Measuring the pressure at grid points over spillways

The reason for the small discrepancy distributed between measured and calculated pressure may be explained by the viscosity effect of water. It can be neglected because of the low viscosity of water.

- Selection upstream condition of H_0

Experimental investigation showed that the draw-down of the free surface occurs very close to the upstream face of the spillway. Therefore, location selection $S = 3H_d$ for measuring H_0 and installation of global coordinates is a good calculation assumption.

- Assumption related to $V_a = 0$

Global system is selected at where draw-down does not yet appear ($S = 3H_d$). Consequently, the energy head $H_a = V_a^2/2g$ can be neglected. This is a traditional assumption that was accepted at the prototype reservoir. Investigation resulted in accuracy of chosen $S = 3H_d$.

- Pressure measurements

The small diameter of the plastic tubes, connecting to pressure taps, may cause error. This error comes from water surface tension. Taking into account the resulting error, the following formula was used:

$$h_T = \frac{2T_s \cos \hat{\theta}}{\gamma_0 \bar{r}} \quad (4.24)$$

where:

h_T = Surface tension height or capillary rise in plastic tubes

γ_0 = Water specific weight

\bar{r} = Tube radius ($\bar{r} = 0.32 \text{ cm}$)

$\hat{\theta}$ = Water-air-polyethylene interface ($\hat{\theta} = 0$)

From Table 4.8, by substituting, h_T , γ_0 , \bar{r} , and $\cos \hat{\theta}$ in Eq. (4.24), the value of

$h_T = 4.6 \text{ mm}$. This value is not negligible and was subtracted from the measured data.

- Air entrainment in the tubes

The slow movement of air through tube requires a long time to test. It must be done completely and carefully. Because small air bubbles confined in water are not visible, the process needs to be repeated several times to get a stable condition for responding manometers with respect to operating head movement.

- Measurement of velocity inside domain

Because this numerical model does not required the velocity value for boundary conditions, measurements of these values in all grid points are not necessary. The measurement of center section were done to verify numerical model.

The cell size influence on calculation accuracy was investigated by the numerical experimentation. The solutions have been obtained with meshes of 54×5 , 54×10 , and 49×15 cells for $H/H_d = 0.5$, 1.0 , and 1.33 respectively. It was demonstrated that the difference between a sufficiently fine grid point in x direction and a sufficiently coarse one is not large, therefore, a coarse mesh $N = 50$ can be used for studying spillway problems.

Chapter 5.0

COMPARISON OF NUMERICAL AND EXPERIMENTAL STUDIES

5.1 General

The results computed with the BFCC method are comparable with experimental flow data.

The BFCC method is a numerical method that can be used to predict crest pressures for non-standard spillways and unusual hydraulic conditions.

5.2 Comparison of Numerical and Lab Models

The validation of the developed BFCC model was performed, for characteristic H/H_d spillway flow values, by comparing results with physical model tests. Comparisons of the two methods suggests that subatmospheric pressures are generally well correlated.

The free water surface position and the distribution of pressure and velocities on a spillway lead to the subatmospheric pressure and the adequate operating head. Furthermore, the internal load on the lining can be calculated and cavitation can be predicted.

The free surface predicted by BFCC is compared with the free surface from physical experiments for the following operating heads $H/H_d = 0.5, 1.0,$ and 1.33 (Fig. 5.1). The small difference between the calculated and the measured free surface confirms a good free surface prediction by the model. It also shows that the inviscous fluid assumption satisfies the flow equations. Numerical non-dimensional pressures with respect to coordinate pressure taps are given in Table 5.1.

The comparison between the bed pressure distribution predicted by the numerical method with the respective pressures measured during the experiment (Table 4.4) for $H/H_d = 0.5, 1.0,$ and 1.33 is shown in Fig. 5.2. The discrepancy between the predicted and the measured bed pressure near the crest is related to coarse grid distributions in the reservoir. This difference does not affect the expected solutions for the bed of spillway.

Based on the experimental data obtained in chapter 4, it has been shown that the BFCC numerical solution of potential flow equations can be used as replacement for the laboratory test on small models.

From pressure distribution a plot of cavitation index was performed (Fig. 5.3).

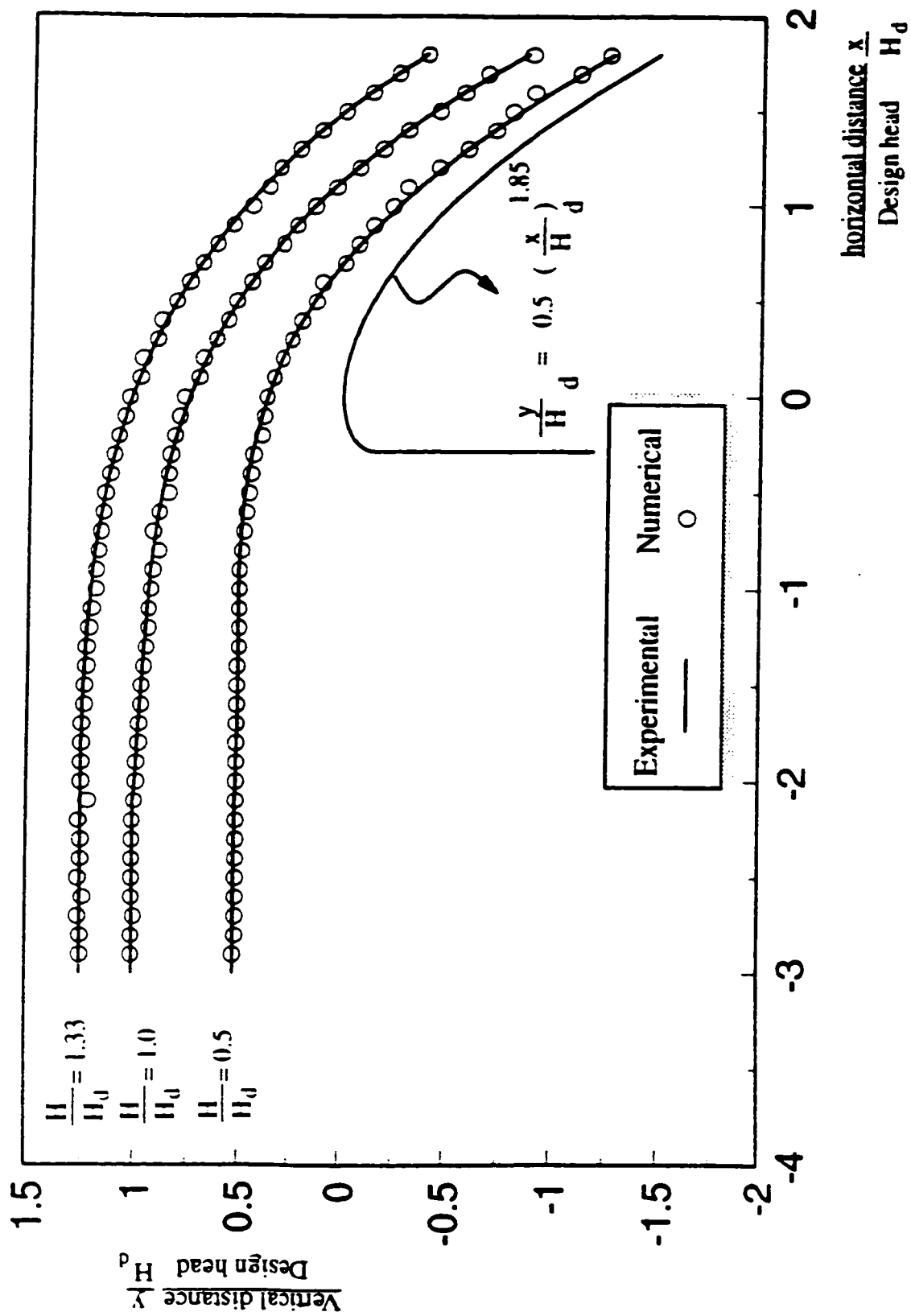


Fig. 5.1 Comparison of numerical and experimental free surface on WES spillway .

Table 5.1: Numerical prediction of non-dimensional bottom pressure on the WES spillway

Tap no.	Tap coordinates		Bottom pressure $\frac{h_p}{H_d}$		
	$\frac{x}{H_d}$	$\frac{y}{H_d}$	$\frac{H}{H_d} = 0.5$	$\frac{H}{H_d} = 1.0$	$\frac{H}{H_d} = 1.33$
C_1	-0.2	0.033	0.46	0.16	-0.18
B_2	-0.1	0.024	0.34	0.11	-0.19
A_3	0.0	0.00	0.23	0.09	-0.20
B_4	0.1	0.021	0.20	0.09	-0.19
B_6	0.3	0.033	0.16	0.09	-0.18
A_7	0.4	0.070	0.15	0.09	-0.16
B_8	0.5	0.115	0.15	0.097	-0.15
B_{10}	0.7	0.249	0.16	0.10	-0.12
A_{11}	0.8	0.304	0.17	0.11	-0.10
B_{12}	0.9	0.396	0.18	0.12	0.15
B_{14}	1.1	0.548	0.19	0.13	0.17

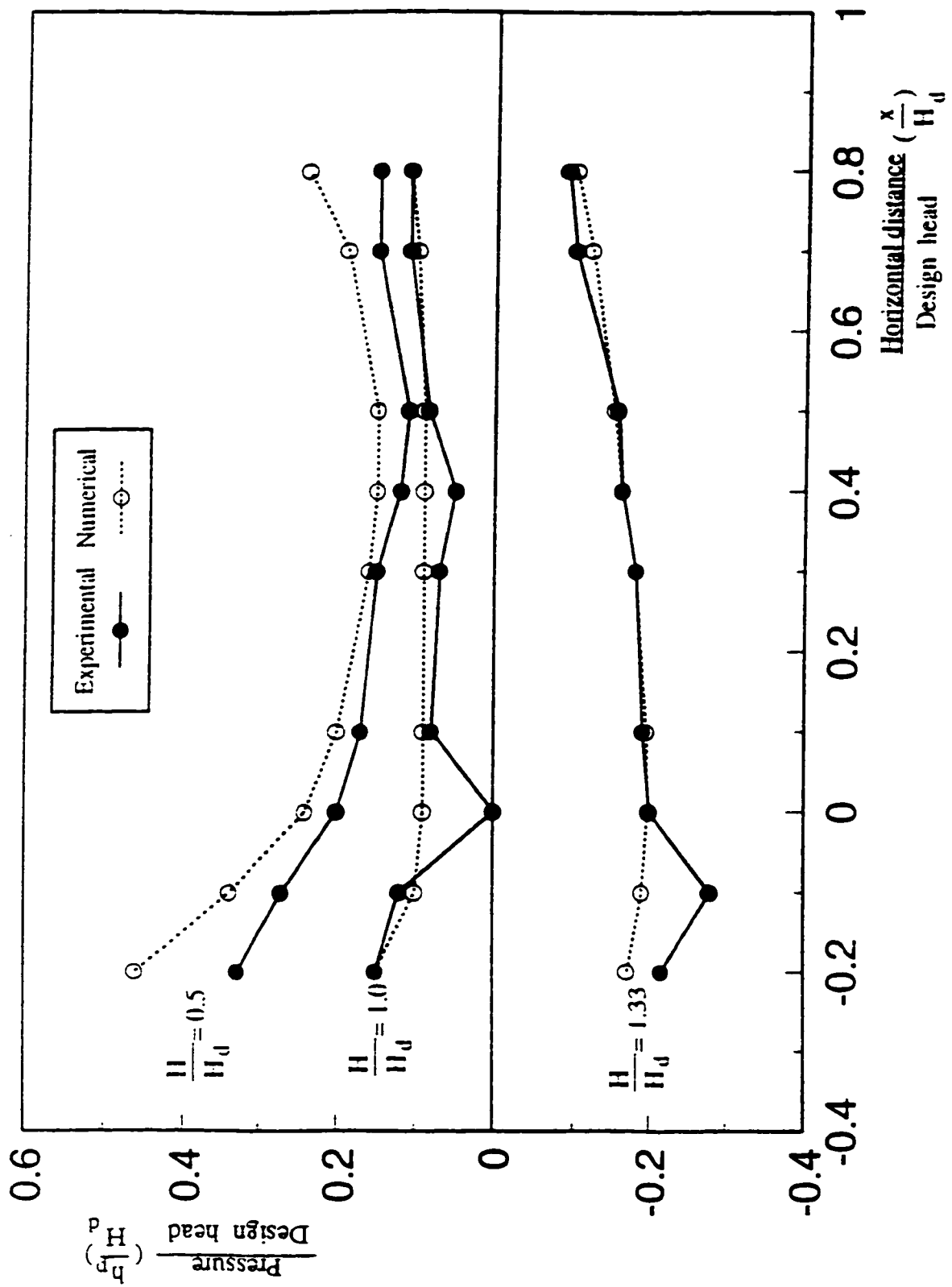


Fig. 5.2 Comparison of numerical and experimental crest pressure on WES spillway.

Table 5.2: Numerical prediction of hydraulic parameters over WES spillway for $H/H_d = 0.5$

Parameters	x-distance from model crest (centimetres)			
	0.0	5.0	10.0	15.0
$V_0(x)$ [cm/s]	72.05	105.06	130.91	142.18
$P_0(x)$ [cm]	2.36	1.50	1.90	2.40
Parameters	x-distance from prototype crest (meters)			
	0.0	4.0	8.0	12.0
$V_0(x)$ [m/s]	6.44	9.39	11.71	12.72
$P_0(x)$ [m]	1.89	1.20	1.52	1.92
$\sigma(x)$	0.77	0.20	0.18	0.85
$\delta(x)$ [m]	0.0	0.046	0.078	0.105
$V_{0.01}(x)$ [m/s]	-	6.92	7.78	7.94
$\sigma_G(x)$	-	0.92	0.77	0.68

Table 5.3: Numerical prediction of hydraulic parameters over WES spillways for $H/H_d = 1.0$

Parameters	x-distance from model crest (centimetres)			
	0.0	5.0	10.0	15.0
$V_0(x)$ [cm/s]	67.90	96.99	120.15	148.29
$P_0(x)$ [cm]	0.98	0.98	1.26	1.74
Parameters	X-Distance from prototype crest (meters)			
	0.0	4.0	8.0	12.0
$V_0(x)$ [m/s]	6.07	8.68	10.75	13.26
$P_0(x)$ [m]	0.78	0.78	1.00	1.39
$\sigma(x)$	0.28	0.14	0.13	0.13
$\delta(x)$ [m]	0.0	0.047	0.079	0.104
$V_{0.01}(x)$ [m/s]	-	6.37	7.11	8.30
$\sigma_G(x)$	-	0.95	0.77	0.69

Table 5.4: Numerical prediction of hydraulic parameters over WES spillway for $H/H_d = 1.33$

Parameters	x-distance from model crest (centimetres)			
	0.0	5.0	10.0	15.0
$V_0(x)$ [cm/s]	78.72	109.74	140.46	182.50
$P_0(x)$ [cm]	-1.98	-1.56	1.62	2.12
Parameters	x-distance from prototype crest (meters)			
	0.0	4.0	8.0	12.0
$V_0(x)$ [m/s]	7.04	9.81	12.56	16.32
$P_0(x)$ [m]	-1.58	-1.24	1.29	1.70
$\sigma(x)$	-0.73	-0.31	0.18	0.11
$\delta(x)$ [m]	0.0	0.046	0.076	0.100
$V_{0.01}(x)$ [m/s]	-	7.23	8.28	10.30
$\sigma_G(x)$	-			

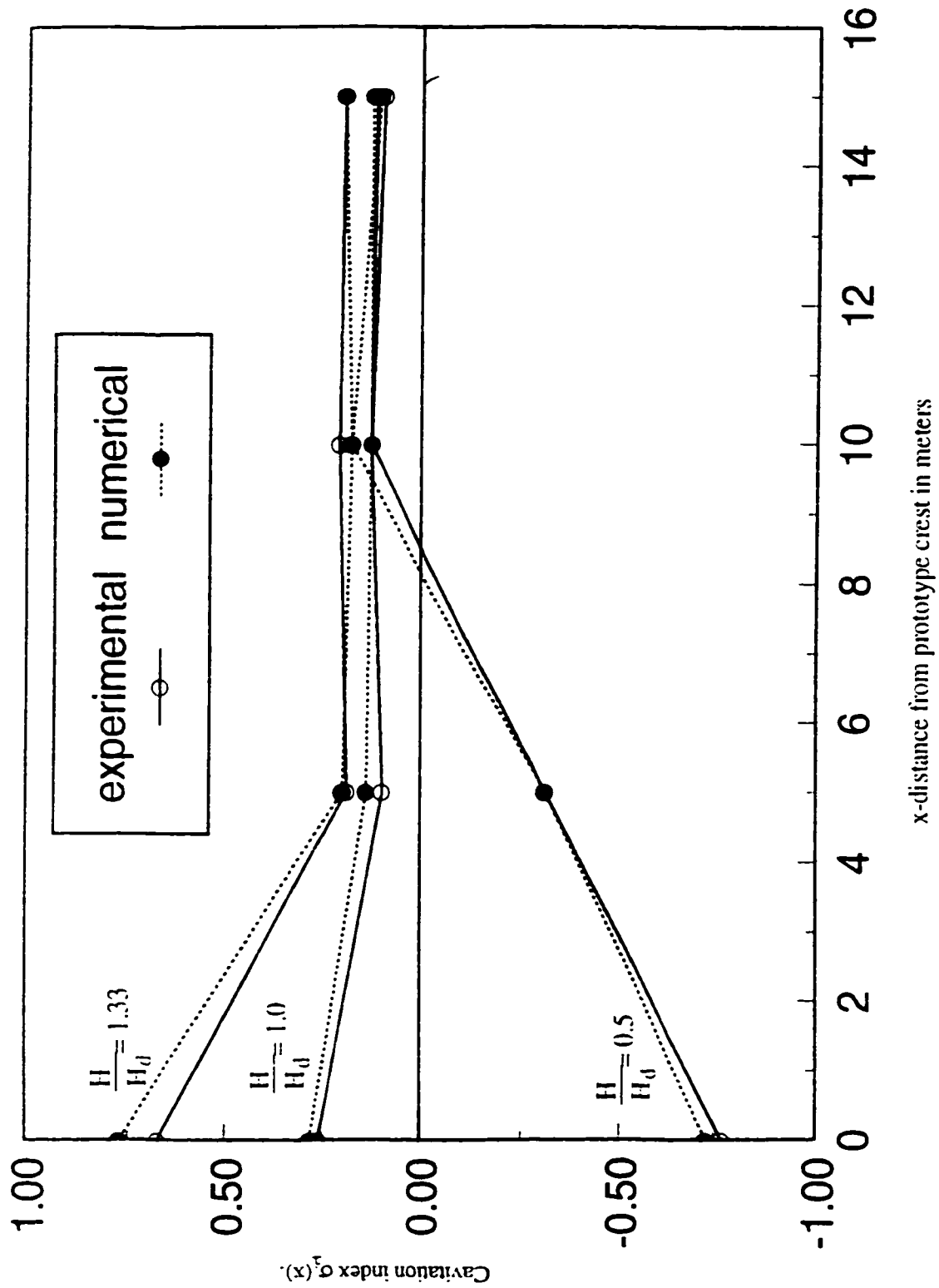


Fig. 5.3 Comparison of numerical and experimental $\sigma_1(x)$.

Again there is a good agreement between numerical and experimental methods.

5.3 Comparison with U. S Army experimentation

The WES experimental model was originally presented by the U. S Army; a smaller scale model was used for this thesis. Three dimensional effects of flow may be appreciable for small 2-D physical models. Therefore, to increase the confidence in the validity of the developed numerical model, results from experimental tests conducted by the U.S. Army on larger models were used. The profile and crest pressure data for the WES spillway model to be used for comparison was obtained from the Corps of Engineers (1952). The results between the BFCC model and the experimental data from the Corps of Engineers are in agreement (Fig. 5.4).

It was previously (section 5.2) demonstrated that the BFCC method is a good tool for predicting the free surface of a small model. The free surface results from small scale investigation are similar to the large scale model results obtained by the U. S Army. This last result verifies that the BFCC numerical two-dimensional model can provide a sufficiently good approximation of actual field flow.

A comparison between the BFCC numerical model and the U.S. Army Engineers Waterways Experiment Station results in its validation for curvilinear flow over spillways. The U. S. Army model is a three dimensional model (including transition section). Despite the fact that the 3-D model has advantage with respect to computational procedure, the 2-D BFCC method is more useful for the preliminary design. The discrepancies between bed pressures at the upstream part are related to distribution of a coarse grid in the reservoir.

With a lower free surface, the pressures on the spillway crest are ensured to be

nearly atmospheric for the design head, and above atmospheric for a lower head. With larger heads, the crest pressures would be sub-atmospheric. Therefore, the presented BFCC numerical model estimates pressure values (same values used in the U.S. Army model) of $H/H_d = 0.5, 1.0$ and 1.33 .

5.4 Comparison with Sivakumaran *et al.* results

The non-linear shallow-flow Saint-Venant equations for open channels have been generalized by Dressler (1978) to account for one-dimensional bed curvature.

Both Dressler and Saint-Venant theories require gradual variations in bed geometry. These theories are not valid for steep slopes.

Sivakumaran and *et al.* (1981) re-derived these equations and applied them to steady shallow flow over a high spillway flow crest and a spillway toe. Their results are valid for large convex curvatures, however, they are not valid for concave curvatures.

Comparing the results obtained with the BFCC model with the Sivakumaran *et al.* results (Fig. 5.4), it can be seen that the developed model predicts accurate results for convex and rapid parts of spillways.

5.5 Discussion and analysis

5.5.1 Discussion on physical and numerical models

While the BFCC model is a significant step forward in the development of numerical methods for predicting flow behavior on spillways, the flow patterns can often defy present analytical techniques. The developed model will indicate the type of flow

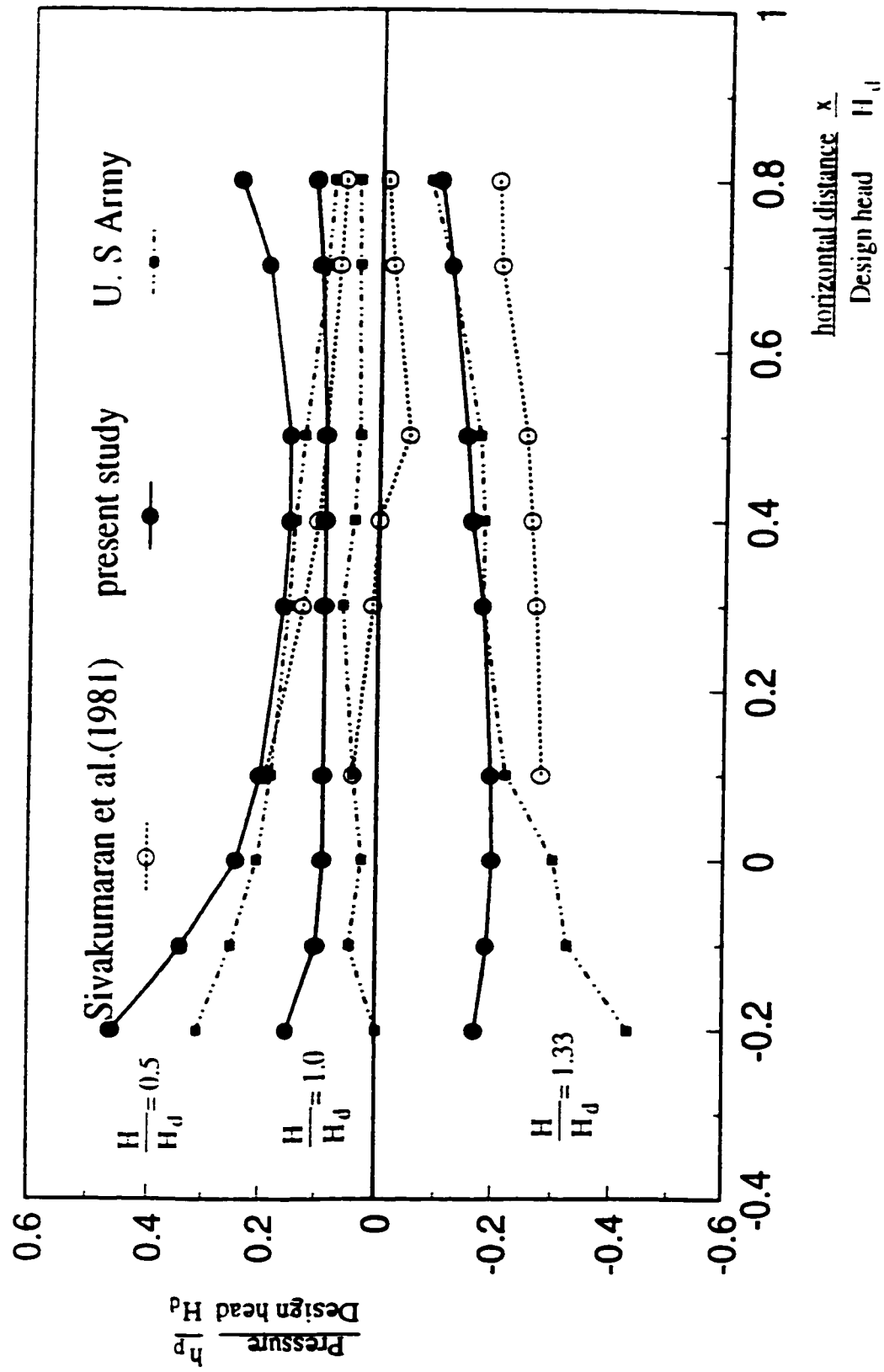


Fig. 5.4 Comparison of present numerical study with U. S Army and Sivakumaran *et al.* studies.

conditions. Subsequently, these flow conditions will be tested with physical models. The combination of both physical and numerical model studies should be used in the future. These present study used physical scale models to determine design criteria for any site which defies analytical treatment and numerical models for other parts of the spillway such as piers, splitters and foundations.

Both physical and numerical models have limitations. Their usefulness of both these methods alone is determined by the following:

5.5.1.1 Physical model

5.5.1.1.1 Dimensions:

Model size is dictated by available funds and the laboratory space available;

Available head and discharge capacity is not always available;

Model scaling laws.

5.5.1.1.2 Practical limitations:

Minimum model scale is governed by viscous effects and hydraulic resistance;

Monitoring methods and data collection;

Modelling of boundary conditions.

5.5.1.1.3 Advantages:

Geometrical similarity to actual prototype

5.5.1.1.4 Disadvantages:

Impossible modification on built model;

Time consuming and costly;

5.5.1.2 Numerical BFCC model

5.5.1.2.1 Numerical limitations:

Simplified governing equations do not represent complex fluid flow;

Laminar flow boundary condition assumptions.

5.5.1.2.2 Practical limitations:

Use of simplified set of equations;

Inaccuracy of assumed relationships;

Lack of empirical data;

Location of boundary conditions.

5.5.1.2.3 Advantages:

Rapid computations and cost efficient;

Design head and dimensions can be altered easily;

Change of spillway shape is adjusted automatically to change in design head.

5.5.1.2.4 Disadvantages:

Accuracy related to grid generation.

The use of numerical modelling will continue to increase. However, the complexity of certain flow characteristics will still require physical modelling.

Numerical models are particularly useful in determining the optimum spillway layout for a range of configurations and flow conditions. For the design of spillways, the costs of conducting a numerical study compared to the physical modelling of each configuration will be a small fraction of the total budget. Numerical modelling techniques are fast and cost-efficient methods that enable the adequacy of a spillway configuration to be quickly assessed. When a spillway proves to be unsatisfactory, it can readily be amended by changing the programs input data. After determining the optimum configuration and flow conditions with a numerical model, a physical model may be built to test the optimal solution.

Numerical schematisation imposes a limit on the extent to which the detailed geometry of a spillway may be represented. A corresponding simulation of flow characteristics must also exist. The accuracy of the numerical model is dependent on the validity of the equations representing the physical behavior of the system under investigation. The comparison between the lab experiment results and the BFCC model results are similar. Therefore, inexpensive computations may often replace expensive physical models in hydraulic engineering for such applications.

In this section, the most important results and general conclusions are summarized to reflect the results of the present investigation. The BFCC model correlates well with experimental results in terms of $H/H_d = 0.5, 1.0, \text{ and } 1.33$. Hence, a high degree of confidence exists in the developed spillway model employed in this investigation. The

difference between computed and measured results are usually neglected for the design of spillways.

When the flow is significantly curved, the BFCC equations are more accurate than the non-linear flow equations derived by Sivakumaran (section 5.4). BFCC applications to high spillways produce free surface profiles, bed pressures and velocities which are significantly close to experimental measurements.

Deeper knowledge of convergence of relaxation processes while reducing the mesh elements is more accurate. The computations of individual velocities and pressure are more accurate when a fine grid is used. However, in practical hydraulics, a fine grid is not required. A fine grid requires lengthy computational time as well as a high speed and/or high memory computer.

By increasing the head over the spillway, the pressure at the crest will decrease. Higher discharges decrease these pressures until either the boundary layer separates from the bed of the spillway or the nappe separates from the spillway. In the present study, these effects have not been dealt with. The maximum range of head considered was therefore limited to 1.33 that of the design head (i.e. $H/H_d = 1.33$).

For an unknown free surface, where there is a double boundary conditions to be satisfied, viz, that ψ is constant, and the velocity is proportional to the square root of the depth below the stagnation pool level, the solution is tentative. For example, we may assume a definite form for the free streamline, solve for ψ , find the velocity and test for the second condition. This procedure would indicate the necessary modification of the free surface, which would ultimately lead to a satisfactory form on which the second condition is also satisfied.

Many model studies use scaling relationships based on only the Froude number. For these cases, the friction losses are usually small and can be neglected in comparison to

the potential changes associated with gravity acceleration. It was shown in section 5.2 that design data regarding pressure and velocity distributions can be accurately predicted with numerical modelling.

When modelling with the Froude number does not give the expected results, physical experiments face the same problems as the numerical methods.

Regarding the two-dimensional flow free surface in large parts of the spillway, the obtained BFCC numerical results are similar to the experimental ones.

The solutions obtained from the BFCC numerical model gives a full description of the flow field. The development of the boundary layer, which is a problem of importance in other fields, is not of immediate importance to this applied research.

The basis of the BFCC numerical model approximation is that boundary layer development is considerably reduced in relatively high accelerated flow. In most cases, viscous effects can be neglected.

The similarity between results from the BFCC model and physical prototypes in cases of modelling with Froude number is usually satisfactory. Differences can occur for either these two cases: 1) when viscous effects are appreciable, 2) when there is a possibility of flow separation. The former results when the model scale is not large enough; then results must extrapolated from other geometrically similar models. The latter occurs when $H/H_d > 3$. A spillway model is scaled using the Froude number still has one advantage over the computational procedure. It reproduces the three-dimensionality of the flow. Therefore, after the BFCC model has generated the proper spillway size, an hydraulic model provides a good approximation of the field flow and where viscous effects can be neglected.

Finally, the present investigations confirmed the applicability of developed BFCC

model for WES spillways that are induced with $H/H_d \leq 1.33$. When the shape of the spillway is not WES, the BFCC approach gives results that require experimental verification.

5.6 Application of the model to spillway design

5.6.1 Design criteria

The developed BFCC model is a computer program algorithm procedure (Fig. 5.5) that can be used for the preliminary design of spillways and related structures as well as to evaluate cavitation potential in spillway chutes.

1. To determine the spillway design discharge and the range of operational discharges.

The following discharges are selected for analysis:

- Spillway design discharge using Eq. (4.12)
- Probable maximum flood discharge
- Annual (or more frequent) peak discharge
- 1:5-year and 1:10-year peak discharge

2. To calculate water surface profiles $y_s(x)$ and flow characteristics using rapidly varied flow analysis for selected discharges, Eqs. (3.14), (3.15) and (3.16) are used. The analysis should be performed for steep slopes as well as possible spillway chute curvatures. If the spillway is gated, partial gate openings should also be considered.

3. To calculate boundary layer development Eq. (2.65) is used.

4. To calculate the flow cavitation index $\sigma(x)$ for selected discharges at several points

on the chute Eqs.(2.61) or (2.62) are used. Typical spillway crest curvature points are the mid-points of long straight representative sections.

5. An allowable cavitation index based on construction finish criteria is obtained from Fig. 1.3. This provides an indication of the expected isolated roughness and the spillway surface roughness.

6. A comparison of flow cavitation index $\sigma(x)$ with σ_A is performed. For different operating heads and locations where $\sigma(x)$ is less than σ_A , a cavitation potential exists on the chute.

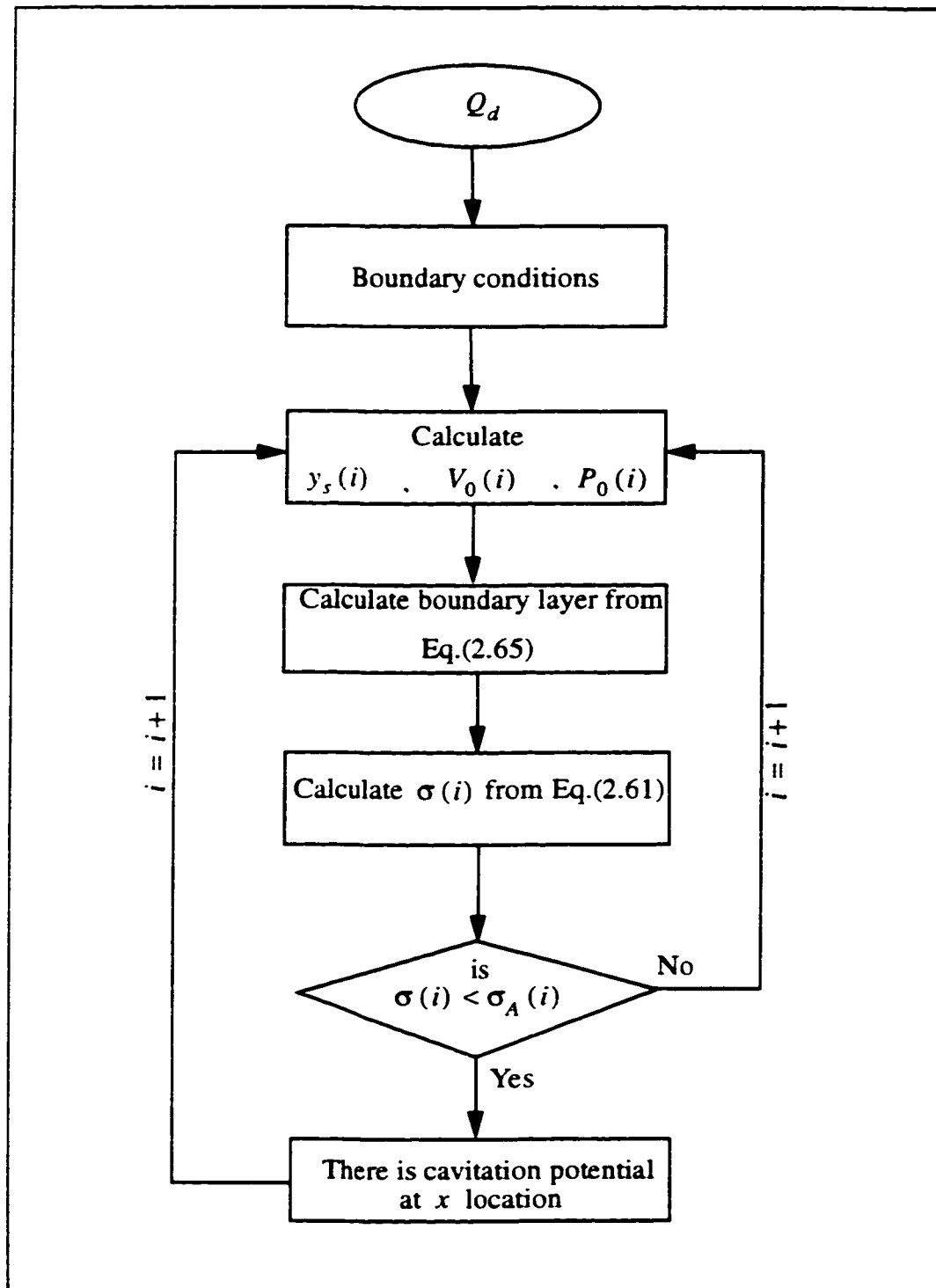


Fig. 5.5 Design criteria algorithm for cavitation detection.

Chapter 6.0

CONCLUSIONS AND RECOMMENDATIONS

6.1 General

The principal objective of the research was to develop and test a numerical model for the prediction of salient flow properties over high spillways. For solving the complex free surface over spillways the BFCC method was developed. To investigate the effects of subatmospheric pressure, attention should be focused on the prime objective of a spillway, to ensure that it is not cavitated by discharge under design head. Presently, state-of-the-art mathematical models are necessary for the design of high dam spillways. The results of this study will be applied directly to the upper head H limit where incipient cavitation appears.

6.2 Conclusions

Spillway construction for dams is expensive. The focus of the research was the development of a cost efficient numerical model. The highlights of the research contribution include:

- i.* Development of a computer program to anticipate subatmospheric pressure on spillways before construction;
- ii.* Determining the appropriate hydraulic simulation model parameters to study cavitation potential on spillways through different design heads;
- iii.* Pressure and velocity calculations on spillways that have been damaged by cavitation.

The potential for cavitation damage can be identified prior to spillway operation. While intended primarily for application to spillways, the BFCC model can also be applicable to flow in partial-filled tunnels or culverts and in the design of supercritical slopes.

The spillway flow was investigated with physical models in the laboratory and with the BFCC model. A subatmospheric pressure was computed with the BFCC numerical method. It was shown that both numerical and experimental work give the parameters affected by the cavitation index.

The BFCC model was used to compare the computed analytical results with actual laboratory measurements. It was demonstrated that the BFCC model improves other numerical models.

For this investigation, attention was given to the spillway crest because it is more sensitive to the available head. In reality, the whole length of a long spillway should be

examined. Due to the spillways steep slope, the pressure can be subatmospheric. This particular problem requires a large scale model.

In this research, the BFCC method with finite differences was developed for solving the curvature free surface in spillways. Numerical free surface results and bed pressures for operating heads $H/H_d = 0.5, 1.00$ and 1.33 were found to be similar with experimental data.

Preliminary experiments indicate that subatmospheric pressure conditions occur for smooth surfaces for heads greater than the design head. Beyond these experiments, the BFCC numerical model clarifies subatmospheric pressure related to $H/H_d \geq 1$. For gated spillways, extreme care must be taken to ensure that proper gate opening sequences are developed in order to guard against asymmetrical flows. Improper gate operations can cause the water flow to be diverted and can lead to asymmetrical flow. This can cause gate vibrations; undesirable flow patterns in the high-velocity chute and/or located cavitation potential; and improper flow distributions entering the flip bucket. Therefore, to reduce these effects, the operating head should be $H/H_d = 1.0$.

The results of the BFCC model can provide a non-dimensional velocity and pressure field plot that can be applied for any spillway scale. A comparison between the pressure head non-dimensional curve at the bottom of the spillway and experimental WES results on high overflow spillways validates the BFCC model's output.

By mapping the physical domain of the spillway geometry, computations can be carried out efficiently. An important feature of the BFCC model is that it can be used if the structure has cavitation potential before construction.

The BFCC method is not meant to replace physical model studies that reproduce three-dimensional behavior and are geometrically similar to the prototype. However, time and cost of physical model studies can be significantly reduced when used in conjunction

with the developed BFCC method. This numerical tool is also a cost efficient tool for checking existing spillway design.

The similarity between experimental and numerical results indicates that the BFCC potential flow method can be used with success to predict hydraulic parameters. The only deviation was between the velocity profiles caused by the boundary layer development at the bottom of the spillway.

Based on the performed experimental and numerical studies, the following conclusions concerning spillway flow characteristics can be made:

- i.* The free-surface profiles obtained with the BFCC numerical model and the physical model experiments are similar. This similarity indicates that viscous effects are negligible at the free surface.
- ii.* The minimum pressure points produced by a spillway flow at a particular head is dependent on the boundary configuration. For standard spillways, the minimum pressure point occurs at the point of maximum curvature.
- iii.* The minimum pressure curves on the spillway surface developed by the BFCC model can be used to design spillways that will operate without cavitating through the entire range of expected heads.

Spillway design calculations are complex due to rapid spillway flow. Subatmospheric pressures often arise during the release of a large volume of water. The BFCC numerical model can help the dam engineer determine the necessary spillway wall heights required to contain extreme flood discharges safely. However, it is expected that the discharge passing through a reservoir would be less for crest piers rather than if the overflow were unobstructed by piers.

The developed BFCC model predicts the large volume discharge effects and

extends the knowledge about this significant problem. The above-mentioned topic forms a continuing spectrum of research efforts in this vital field of engineering.

This investigation showed that supercritical flow behavior should first be examined numerically. This technique has advantages in terms of flexibility of application and economy of calculation.

BFCC computations, confirmed by experimental results, showed that the stipulated maintenance procedures must be capable of guaranteeing gate operations whenever required. Periodic operation of every gate, to test the operating head on the spillway is necessary.

The benefits of the developed BFCC model are summarized as follows:

- BFCC model determines design criteria for preliminary studies,
- BFCC model determines incipient cavitation index for all flow cases.
- BFCC model is adapted to a WES standard spillway shape.

The aerators should be designed for the third region in Fig. (1.1). The position of these aerators (when $\sigma(x)$ is zero or negative) is given by the BFCC model.

6.3 General recommendation for spillway design

With current research developments, more definitive statements related to cavitation will be possible. Therefore, the designer will be able to predict any prototype behavior with precision and confidence.

Subatmospheric pressure was the primary cause of damage for the following

reasons:

1. Flow velocity

Cavitation damage occurs at lower velocities. The exact lower limit depends on temperature and pressure.

2. Surface irregularities

The construction of a sufficiently smooth concrete surface free from undulations protects against cavitation for high flow velocities.

3. Crest shape

4. Water management.

Spillway designs can be done based on the two following velocity limits:

6.3.1 Velocities $V < 30$ m/s

1. At least 60 percent of atmospheric pressure over the crest is ensured for the design flow (allowing for the altitude of the dam) to prevent cavitation downstream from the crest.
2. Uniform cross sections are provided where possible.
3. Sudden transitions or short radius curvatures are avoided.
4. Smooth surfaces are provided.
5. Recesses for ports, slots, etc., are shaped according to WES standards.
6. Incipient cavitation index is determined for all flow cases to detect cavitation-prone conditions.

6.3.2 Velocities $V > 30$ m/s

1. Same as section 6.5.1 except as noted below:
2. A chamfer of $20H:1V$ (accepted irregularities) for all isolated roughness is specified for the spillway. This corresponds to an allowable deviation from the line of slightly under $4\text{ cm}/m$. Care should be taken as to how this is achieved in the field. The flow cavitation index corresponding to this chamfer is 0.22 (Fig. 1.3).
3. Aeration devices at gate slots, along the spillway chute and before the spillway bucket are provided. The location of the first aerator would be where the flow cavitation index $\sigma_A(x)$ equals 0.22.
4. If feasible, large-scale (1:10-1:15) model testing is performed. Or else, a smaller scale model (1:25) would be acceptable provided the Weber number in the model is at least 1000.

Physical model studies are necessary not only for high-dam energy dissipaters but also for the spillway approach and spillway proper. The spillway model may or may not include dissipaters, but it must include sufficient approach topography so its effect on incoming flow is reproduced.

Approach flow problems should be studied first in a model study. After determining a satisfactory approach flow, flow distribution effects in the chute must be considered. Potential cavitation problems can also be studied. All problems must be resolved simultaneously; each has a mutual reaction with the others. Finally, the model should be used to develop the required gate operating program. During this phase, gate malfunction must be evaluated in terms of potential damage to the structure. Model scales of 1:50 to 1:100 are common for detailed spillway studies.

6.4 Recommendations for future work

The investigation presented in this work provides new information on the applicability of the BFCC method for flow over spillways under subatmospherical pressure condition. The BFCC model and the physical models used for the results obtained in this study may easily be extended to spillway channel shapes where supercritical flow exists. The presented methodology forms a basis for preliminary designs. For final designs, it is proposed that detailed investigations be carried out for each case. These investigations include a comparison between experimental and field case studies.

Cavitation potential over spillways requires more research. Despite the progress over the last two decades, the understanding of this subject has been limited to experimentation and a few numerical works. While studying the potential of cavitation, the following should be taken in mind:

- Design investigations, operation and model studies for existing dams with high-head spillways should be continuous;
- Model studies and field studies to investigate aeration features and to confirm design aspects should be performed. Separate model studies will be required for detailed design of air entrainment or aerators in order to finalize geometric dimensions;
- Laboratory simulation of temperature and contamination over spillway;
- Three dimensional flow simulation.

Spillway structures are complex to analyze due to the highly three dimensional nature of the incoming flow. The methodology, used for development of the 2-D model, can create the three-dimensional which will allow to solve more complicated flow over

spillways. Guj and Stella (1993) pioneered the numerical solution of the vorticity transport form of the Navier-Stokes equations in the Cartesian system. As an extension to this study, the coupling of the 3-D model with a reasonably simplified model can be considered in the future:

- Survey of the cavitation beside aerators as final design of spillways, and
- Full equation models yields an accurate prediction of cavitation;
- Care should be exercised in specifying the surface material and roughness. On flat, sloped and curved surfaces that can be troweled, overworking can provide a better tolerance, remove undesired irregularities and a better finish. Overworking, however, will result in a softer surface, potential for scaling and microcrakes that can develop into surface crazing cracks. Grinding to remove excess undulation can also be detrimental. Therefore, it is important to conceive the potential field difficulties while selecting the expected roughness values. Data from Fig. 1.3 may be used for selecting an appropriate roughness value.

In addition, it is anticipated that a flow contraction effect would occur depending upon the degree of pier nose streamlining. The flow adjustment around the pier influences velocity and pressure distributions. These alteration should be considered in this model. Various circumstances exist where merging flow streams require consideration in spillway assessment. The reason of the merging flow could be due to the existence of piers or walls relatively close to the spillway gates. This topic can be investigated in future works.

Specialized facilities are required for unusual conditions or for particular tests, especially to achieve large Reynolds numbers. Very often those facilities can not be supported by university laboratories. For this reason, the author suggests the following:

- The use of a fast high memory computer to get quick grid generation results,
- The use of a large-scale model (1/15),
- Then, running the program with the large-scale model data, and
- Evaluate scale effects on cavitation for two alternative model scales (typically 1:20-1:30).

For the enhancement of the BFCC numerical model, some aspects of high-velocity flow and construction require further research. Among these are bulking and effect of piers on flow.

6.5 General recommendation to prevent cavitation damage

- ☐ The principles behind the cavitation phenomenon should be investigated. Because potential for the cavitation damage can be identified prior to spillway operation.
- ☐ The use of special concrete or materials to prevent cavitation damage on a spillway is of limited value for both practical and economical reasons.
- ☐ The maximum velocities¹ restricted to about 30 *m/s* as well as practical construction with specific material will be sufficient to prevent cavitation problems. Gate slots or other sudden changes in the boundary, however, require special attention.
- ☐ Where necessary, aeration can be used together with criteria related to shape and spillway finish appurtenances to minimize the areas subject to low pressures.

1. It was taken as reference velocity for ordinary roughness of spillway surface based on Johnson (1963) study.

Case studies have shown that induced aeration has been consistently successful in preventing cavitation damage.

- ❑ Although current information is sufficient to design aeration devices, universal design criteria for aeration devices are presently not available.
- ❑ If sufficient aeration is present, no upper limit on allowable velocities in spillways is foreseen. Present experience, however, is limited to application of aeration for velocities up to 50 m/s for tunnels and open-chute type spillways.
- ❑ Small-scale model studies and existing experience prototype supplemented with state-of-the-art analysis will allow reasonable evaluation of the cavitation phenomenon. The required configuration and associated hydraulic characteristics of the aerator can be assessed accurately. However, large-scale (1:10-1:15) models are preferred to confirm small-scale model and prototype relationships.

Until recently, the method for preventing cavitation erosion caused by surface irregularities or structural elements were limited to:

1. The use of steel linings
2. The adoption of stringent construction finish criteria

The first method is very expensive and it is applied to localized areas only, such as behind control gates. Although it is generally effective in preventing cavitation damage, the application of steel lining has introduced secondary problems in some instances: for example, failure due to poor surface with an epoxy paint. This paint has a strong surface adhesion, it is smooth and has high cavitation resistance. Prototype tests at flow velocities of 30 m/s have been carried out satisfactorily. However, the behaviour of epoxy paint under thermal stressing is not satisfactory. Also, information is lacking on the long-term behaviour of these paints when subjected to high velocities.

A more recent development is the introduction of air into the flow. The introduction of air into flow has been successfully used with both existing and new construction to prevent cavitation. This method still presents the following advantages:

1. It is inexpensive and relatively easy to incorporate in the spillway structure design.
2. Stringent surface finish criteria and the use of special construction materials are not required.
3. Surface defects do not result in cavitation damage.

Experience with aeration of high-velocity flows is rapidly increasing, but has not yet reached the level of universal standard application. Practical limits of surface finish criteria (typically $20H:1V$)¹ will continue to be specified while providing satisfactory protection against cavitation for flow velocities up to about 30 m/s . However, sufficient evidence exists to indicate that flow aeration will be the primary, if not the only, means of preventing cavitation damage in higher velocity flows.

Flow aeration increases the size, number, and air content of bubbles in the flow. This causes a great reduction in the collapse rate during the final stages of the cavitation process. Also, the cavity size is much greater when the process of collapse is complete, resulting in lower collapse pressures. Furthermore, the compression energy stored in some of the cavities is returned to a kinematic form by expansion of the cavity. Consequently, the bubble may cycle through a series of growth and collapse phases before the motion is finally damped. Thus, air entrainment has a dampening, cushioning effect on the cavitation collapse phenomenon.

Flow aeration can be achieved either naturally or by installing areation devices on the spillway surface. The former condition occurs from the air supply at the surface of the

1. Ratio of 20 Horizontal to 1 Vertical (deviation from design line related to spillway surface).

water. The amount of natural insufflation depends on the flow characteristics. Fully aerated flow occurs when the boundary layer has developed through the entire flow depth up to the surface. However, this condition will be reached only for low specific discharges, when the depth of flow is small. Artificial flow aeration gives better control over the amount of air required. Air is supplied at the flow boundaries by means of aeration devices. Three types and possible combinations thereof are presently in use:

1. Offsets (steps)
2. Slots (grooves)
3. Deflectors (ski jump).

Each of the three types of aeration devices mentioned above has been applied and operated in existing spillway aerators. Particular advantages and disadvantages of their use have been established.

The deflector aerator requires less height than the offset aerator to set up the under jet space of negative pressure for air supply. Also, an increase in flow velocity occurs which introduces a higher aeration intensity. In addition, the deflector aerator could also be installed after spillway construction has been completed. A disadvantage is that this type of aerator installed in tunnels causes fins of flow to occur downstream, resulting in the choking of the tunnel at high aeration. For open-chute spillways, overtopping of the side-walls may occur.

The slot aerator has been in operation for approximately 20 years and experience in design and operation is available. Its advantage is that installation does not drastically change the flow pattern. However, problem with the slots is filling up with water for lower than design discharges which Results lack of aeration.

The deflector aerator has been applied in combination with the slot aerator in high

pressure outlet gates in the United States. Applications of deflector aerators alone and in combination with offsets are not common in North America.

The pure offset type is a good aeration device for new structures, in that it produces fewer disturbances or shock waves than a deflector in the water profile. But, generally, the pressure depression introduced below the water jet is insufficient, because the exposure of the lower part of the nappe to the air is inadequate. In combination with even small deflectors, its performance improves appreciably.

Recent studies have been conducted to analyze the rate at which air is entrained by ramps or air slots. The rate at which air is entrained is dependent on the following variables, at least: geometry, flow velocity, surface tension and air conduit geometry. Geometry of the slot or ramp is undoubtedly of primary importance. Fig. 6.1 illustrates the geometry of typical aeration slots and ramps.

Self aeration is beneficial to prevent cavitation. Protection could cause an increase of flow depth and thus require an increase of chute side walls.

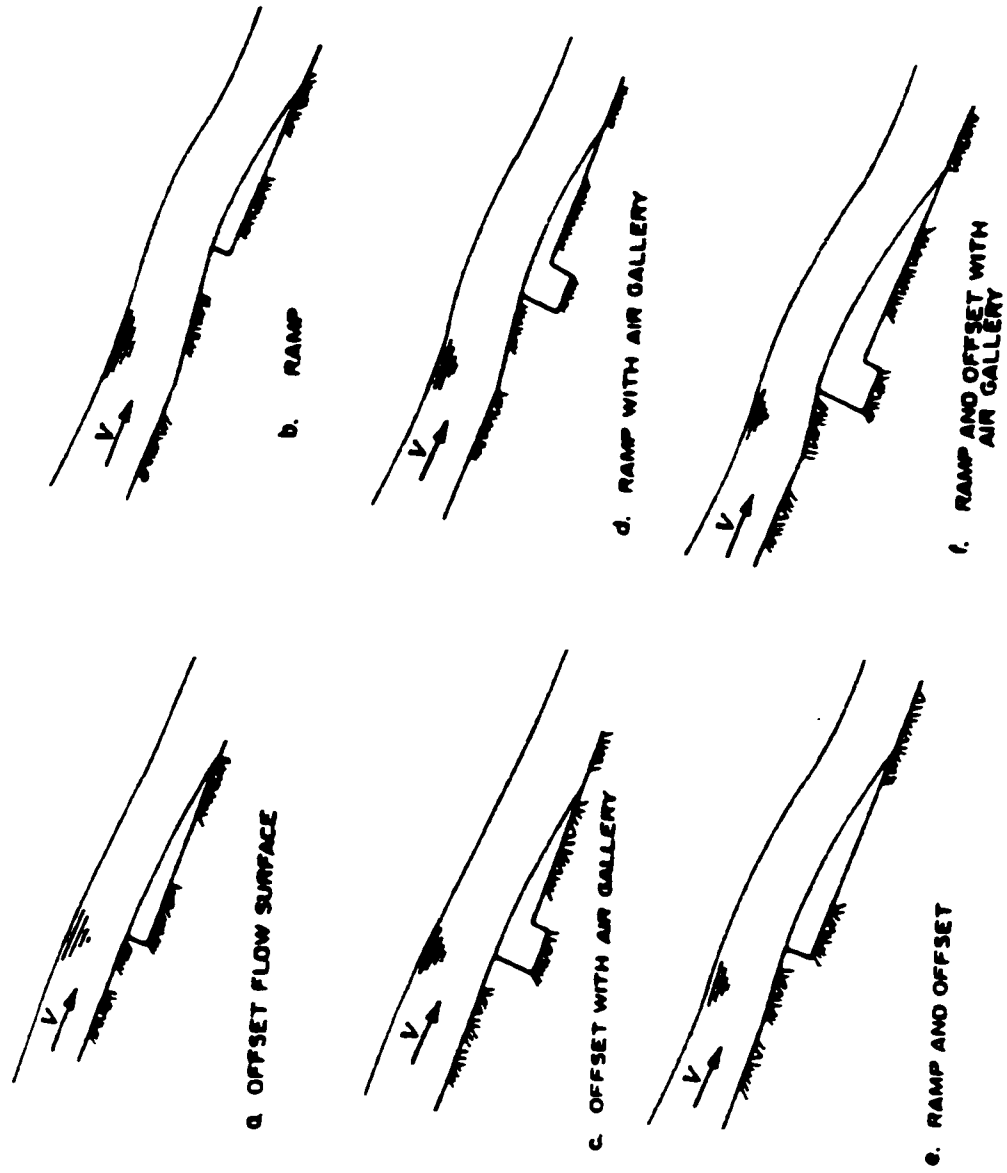


Fig. 6.1 Types of areation facilities (from Novak, 1984).

REFERENCES

1. **Abdallah, S.** (1987), "*Numerical solutions for pressure poisson equation with Neumann boundary conditions using a non-staggered grid*", I and II. Journal of Computational Physics, Vol. 70, pp. 182-202.
2. **Acres international limited** (1983), "Cavitation and aeration for high-velocity flows on spillway structures".
3. **Anderson, D. A, Tannehill, J. C., and pletcher, R. H.** (1984). "*Computational fluid Mechanics and heat transfer*", McGraw-Hill book Company, pp. 502-510.
4. **Ball, J. W.** (1976), "*Cavitation from surface irregularities in high velocity flow*", Journal of the Hydraulics Division, ASCE, Vol.112, No. HY9, pp. 1283-97.
5. **Balloffet, A. F.** (1961), "*Pressures on spillway flip buckets*", Journal of the Hydraulics Division, ASCE, Vol. 87, No. Hy5, pp. 87-98.
6. **Bauer, W.J.** (1954), "*Turbulent boundary layer on steep slopes*", Transaction of the American Society of Civil Engineers, Vol. 119, pp. 1212-1242.
7. **Bean, H.S.** (1971), "*Fluid meters-their theory and application*", Report of ASME research committee on fluid meters-sixth edition. pp. 116-118.
8. **Berger, R. C., and Cary, G. F.** (1990), "*A pertubation analysis and finite element approximate model for free surface flow over curved beds*", International Journal for Numerical Methods in Engineering, Vol. 31, PP. 493-507.
9. **Berger, R. C., and Winant, E. H.** (1991), "*One dimensional finite element model for spillway flow*", Hydraulic Engineering Conference, pp. 388-393.
10. **Berger, R. C., and Stockstill, R. L.** (1993), " *A 2-D numerical model for high*

velocity channels", Hydraulic Engineering 93, pp. 1085-1090.

11. **Bettess, P., and Bettess, J. A.** (1983), "*Analysis of free surface flows using isoparametric finite elements*". International Journal for Numerical Methods in Engineering, Vol. 19, pp. 1675-1689.
12. **Betts, P. L.** (1979), "*A variational principles in terms of stream function for free-surface flows and its application to the finite element method*", Computers and Fluid, Vol. 7, pp. 145-153.
13. **Biringen, S., and Cook, C.** (1988), "*On pressure boundary conditions for incompressible Navier-Stokes equations using non-staggered grids*", Numer. Heat transfer, Vol. 13, pp. 241-252.
14. **Blevins, R. D.** (1984). "*Applied fluid dynamics handbook*", Van Nostrand Reinhold Company, pp. 208-210.
15. **Bradley, J. N., and Peterka, A. J.** (1957), "*The hydraulic design of stilling basins*", Journal of the Hydraulics Division, ASCE, Vol. 83, No. HY5, pp. (1401-1)-(1401-24)..
16. **Cain, P., and Wood, R.** (1981). "*Measurements of self-aerated flow on a spillway*", Journal of the Hydraulics Division, ASCE, Vol. 107, No. HY11, pp. 1425-1444.
17. **Cassidy, J. J.** (1965), "*Irrotational flow over spillways of finite height*", Journal of the Engineering Mechanics Division, ASCE, Vol. 91, No. EM6, part 1, pp. 155-173.
18. **Chan, S.T.K., Larock, B.E., and Herrman, L.R.** (1973), "*Free surface ideal fluid flows*", Journal of the Hydraulics Division, ASCE, Vol. 99, No. Hy6, pp. 959-

974.

19. **Chen, T. C., and Yu, Y. s.** (1965). "*Pressure distributions on spillway flip buckets*". Journal of the Hydraulics Division, ASCE, Vol. 91, No. Hy2, part 1, pp. 51-63, and pp. 193-195.
20. **Cheng, A. H. D., Liggett, J. A., and Liu, P. L. F.** (1981). "*Boundary calculation of sluice and spillway flows*", Journal of the Hydraulics Division, ASCE, Vol. 107, No. HY10, pp. 1163-1178.
21. **Chow, V. T.** (1959). "*Open-channel hydraulics*", Mc Graw-Hill book Company, pp. 360-380.
22. **Colgate . D.** (1977). "*Cavitation damage in hydraulic structures*", international Conference on Wear of Materials held at St. Louis, Missouri, USA; April.
23. **Corps of Engineers** (1952), " *Hydraulic Design Criteria* ", Office of Chief of Engineers., U. S. Army Corps of Engineers. Waterways Experiment Station, Vicksburg, Mississippi.
24. **Currie, I. G.** (1974). "*Fundamental mechanics of fluids*", McGraw-Hill Inc., New York, pp. 311.
25. **Dias, F. , Keller, J. B., and Vanden-Broek, J. M.** (1988), "*Flow over rectangular weirs*", Physics of Fluids, Vol.31, No.8, pp. 2071-2076.
26. **Diersch, H.J., Schirmer, A., and Busch, K. F.**(1977). "*Analysis of flows with initially unknown discharge*", Journal of the Hydraulics Division, ASCE, Vol. 103, No. Hy3, pp. 213-231.
27. **Dillman, O.** (1933), "*Untersuchungen an uberfallen*", Mitt. des Hyd. Inst., Munich, No. 7.

28. **Dressler, R. F.** (1978), "*New nonlinear shallow-flow equations with curvature*" Journal of Hydraulic Research. Vol. 16, No. 3, pp. 205-222.
29. **Ellis, J.** (1985), "*Numerical analysis of Kleider dam spillway*", Journal of the Institution of Water Engineers and Scientists. Vol. 39, No. 3, pp. 254-270.
30. **Ellis, J.** (1985), "*Numerical modelling of spillway flows*", 2nd International Conference on the Hydraulics of Floods and Flood Control, Cambridge, England:24-26 September.
31. **Ellis, J., and Pender, G.** (1982), "*Chute spillway design calculations*", Institution of Civil Engineers Proceedings, part 2, Vol. 73, pp. 299-312.
32. **Falvey, H. T.** (1982), "*Predicting cavitation in tunnel spillways*", Water Power and Dam Construction, London, U. K., August, pp. 13-15.
33. **Falvey, H. T.** (1980), "*Air-water flow in hydraulic structure*", U. S. Departement of Interior, Denver.
34. **Finnie, J. I., and Jeppson, R.w.** (1991), "*Solving turbulent flows using finite elements*", Journal of the Hydraulics Division, ASCE, Vol. 117, No. 11, pp.1513-1530.
35. **Fletcher, C. A. J.** (1991), "*Computational techniques for fluid dynamics 2*", Springer-Verlag, second edition, pp. 47-58.
36. **Foerster, K. E., and Anderson, A.** (1969), "*Model study of the spillway of Karun project*", University of Minnesota, St. Anthony falls hydraulic laboratory, prepared for Harza Engineering Company.
37. **Fox, R. W., and Mc Donald, A. T.** (1992), "*Introduction to fluid mechanics*", PP. 296-301.

38. **Gerhart, P.M., and Gross, R. J.** (1985), "*Foundamental of fluid mechanics*", Addison-Wesley Publishing Company, pp. 582-618.
39. **Guy, G., and Stella, F.** (1993), "*A vorticity -velocity method for the numerical solution of 3D incompressible flows*", *Journal of Computational Physics*, Vol. 106, pp. 286-298.
40. **Hager, W. H.** (1991), "*Experiments on standard spillway flow*", *Proceedings of the Institution of Civil Engineers. part 2*, Vol. 91, pp. 399-416.
41. **Hager, W. H.** (1987), "*Continuous crest profile for standard spillway*", *Journal of the Hydraulic Engineering*, Vol. 113, No. 11, pp. 1453-1457.
42. **Henderson, H. C., Kok, M., and De Koning, W. L.** (1991), "*Computer-aided spillway design using the boundary element method and non-linear programming*", *International Journal of Numerical Methods in Fluids*, Vol. 13, pp. 625-641.
43. **Henderson, F. M., and Escande, L.** (1961), "*Pressures on spillway flip buckets*", *Journal of the Hydraulics Division. ASCE*, pp. 175-178.
44. **Henderson, F. M.** (1966), "*Open channel flow*", Macmillan Publishing Company. pp. 16-18.
45. **Henderson, F. M., and Tierney, D. G.** (1963), "*Flow at the toe of a spillway*", *La Houille Blanche* No. 1, pp. 42-50.
46. **Hoffmann, K. A.** (1985), "*Computational fluid dynamics for engineers*", a publication of Engineering Education System, Austin, Texas. pp. 267-269.
47. **Hsu, H. C.** (1980), "*A method for the solution of free surface gravity flow by finite elements*", *Journal of the Hydraulics Engineering, Beijing, China* 1, pp. 1-13 (in Chinese).

48. **Ikegawa, M., and Washizu, K.** (1973). "*Finite element method applied to analysis of flow over a spillway crest*", International Journal for Numerical Methods in Engineering, Vol. 6, pp. 179-189.
49. **Isaacs, L.T.** (1969), "*Numerical solution for flow under sluice gates* ", Journal of the Hydraulics Division, ASCE, Vol. 95, No. Hy4, PP. 1211-1226.
50. **Jin, T., Lin, C., and Liu, X.** (1980), "*Cavitation inception on gate slots*". Department of Hydraulics, Water Conservancy and Hydro-electric Power Scientific Research Institute, Beijing, China.
51. **Johnson, V. E.** (1963), "*Mechanism of cavitation*", Journal of the Hydraulic Division, ASCE., Vol. 89, No. Hy3. part 1. pp. 251-275.
52. **Lamb, H.** (1932). "*Hydrodynamics*". Cambridge University Press. pp. 579-581.
53. **Lenau, C. W., and Cassidy, J.** (1969), "*Flow through spillway flip bucket*". Journal of the Hydraulics Division, ASCE., Vol. 95, No. Hy2., pp. 633-648.
54. **Liggett, J. A., and Vasudev, S. U.** (1965), "*Slope and friction effects in two dimensional, high speed channel flow*", International Association for Hydraulic Research, Proceedings XI Congress IAHR High Speed Channel Flow, Vol.1. No.125.
55. **Mahab Ghodss Consulting Engineers** (1987), "*Karun spillway re-design project*", Technical Report, Vol. 1, Iran. (in Persian).
56. **Mahab Ghodss Consulting Engineers** (1984), "*Karun model spillway*". hydraulics department, Iran. (in Persian).
57. **Mansour, M. L., and Hamed, a.**(1990), "*Implicit solution of incompressible Navier-Stokes equations on a non-staggered grid*", Journal of Computational

Physics, Vol. 86, pp. 147-167.

58. **Markland, E.** (1965), "*Calculations of flow at a free overfall by relaxation method*", Proceedings of the Institution of Civil Engineers, No.31, pp.6869.
59. **Matthew, G. D.** (1963), "*On the influence of curvature, surface tension and viscosity on flow over roun-crested weirs*", Proceedings of the Institution of Civil Engineers, Vol. 25, pp. 511-524.
60. **Maxwell, W. H. C., and Weggel, J. R.** (1969), "*surface tension in Froude models*". Journal of the Hydraulics Division, ASCE, Vol. 95, No. HY2, PP. 677-701.
61. **Montes, J. S.** (1992), "*A potential flow solution for the free overfall*", Proc. Instn Civ. Engrs Wat. Marit. & Energy, PP. 259-266.
62. **Novak, p.** (1984), "*Developments in hydraulic engineering-2*", Elsevier Applied Science Publishers, pp. 103-105, and pp. 166-180.
63. **O'Carroll, M. J.** (1980), "*Short communications a variational principle for ideal flow over a spillway*", International Journal for Numerical Methods in Engineering, pp. 767-772.
64. **O'Carroll, M. J., and Toro, E. F.** (1984), "*Numerical computations of critical flow over a weir*", Internatinal Journal for Numerical Methods in Fluids, Vol.4, pp. 499-509.
65. **Ransford, G. D.** (1983), "*Pressures on spillway aprons downstream from partly raised crest gates*", Journal of Hydraulic Research, Vol. 21, No. 4, pp. 303-314.
66. **Roache, P. J.** (1982), "*Computational fluid dynamics*", Hermosa Publishers, pp. 327.

67. **Robinson D. I, and Mc Ghee, T. J.** (1993), "*Computer modeling of side-flow weirs*", Journal of Irrigation and Drainage Engineering, Vol. 119, No. 6, pp. 989-1005.
68. **Robertson, J. M.** (1963), "*Cavitation in hydraulic structures: scale effects involved in cavitation experiments*", Journal of the Hydraulics Division, ASCE, Vol. 89, part 1, No. HY3, pp. 167-180.
69. **Robertson, J. M., and Wislicenus, G. F.** (1969), " *Cavitation state of knowledge*", the American Society of Mechanical Engineers, pp. 40.
70. **Rouse, H., and Reid, L.**(1935), "*Model research on spillway crests*", Civil Engineering, Vol. 5, pp. 10.
71. **Sivakumaran, N. S., and Yevjevich, V.** (1987), "*Experimental verification of the Dressler curved-flow equation*", Journal of Hydraulic Research, Vol. 25, No. 3, pp. 373-387.
72. **Sivakumaran, N. S., Hosking, R. J., and Tingsanchali, T.** (1981), "*Steady shallow flow over a spillway*". Journal of Fluid Mechanics, Vol. 111, pp. 411-420.
73. **Sivakumaran, N. S.,Tingsanchali,T., and Hosking, R. J.** (1983), "*Steady shallow flow over curved beds*". Journal of Fluid Mechanics, Vol. 128, pp. 469-487.
74. **Slisskii, S. M., and Kalandrov, I. A.** (1987), " *Calculation of the position of the free water surface on a bend of a free-flow tunnel*", Hydrotechnical Construction (English translation of Gidrotekhicheskoe Stroitel'stvo), Vol. 21, No. 8, pp. 460-465.
75. **Smith, C. D.** (1992), "*Hydraulic structures*", University of Saskatchewan, pp. 52-54, pp. 58 -63. and pp. 67.

76. **Sreetharan, M.** (1990), "*Numerical computation of free surface weir flow using isoparametric finite elements*", Hydraulic Engineering, Vol. 1, pp. 682-687.
77. **Sun, X. X., et al.** (1984), "*Software for numerical solution of the flow over dam spillways*", Inst. of Water Conservancy and Hydroelectric Power Res. , Beijing China. pp. 72-83 (in Chinese).
78. **Thames, F. C.** (1975). "*Numerical solution of incompressible Navier-Stokes equation about arbitrary two-dimensional bodies*", Ph. D. thesis of Mississippi State University.
79. **Thomas, h. h.** (1976), "*Design of large dams Parts I and II*", John Wiley and sons.
80. **Thompson, J. F. Warsi, Z. U. A., and Mastin, C. W.** (1985), "*Numerical Grid Generation: Foundations and Applications*", New York:North-Holland Elsevier. pp. 450-462.
81. **Thompson, J.F., and Warsi, Z.U.A.** (1982), "*Boundary-Fitted coordinate systems for numerical solution of partial differential equations- A review*". Journal of Computational Physics, Vol. 47, PP. 1-108.
82. **Thompson, J. F**(1980), " *Numerical solution of flow problems using Body-fitted coordi nate systems*", Computational Fluid Dynamics, editor W. Kollmann. Hemisphere Pub. Corp. pp. 1-98.
83. **Vanden-Broeck, J. M., and Keller, J. B.**(1986), "*Pouring flows*", Physics of Fluids, Vol. 29, pp. 3101-4296.
84. **Vanden-Broeck, J. M., Dias F., and Keller, J.B.** (1988), "*Flows over rectangular weirs*", Physics of Fluids, Vol. 31, pp. 1835-2738.
85. **Villegas, F.** (1976), "*Design of the Punchina spillway*", International Water and

Dam Construction. Vol. 28, No. 11, pp. 32-34.

86. **Wang, F. J., and Domoto, G. A.** (1994), "*Free-surface Taylor vortices*", Journal of Fluid Mechanics. Vol. 261, pp. 169-198.
87. **Wang, F. J.** (1990). "*Numerical simulation of free surface flows*", Ph. D. dissertation, Columbia University.
88. **Xu, X. X, and Sun X. X.** (1990). "*Flow in spillway with gradually varied curvature*", Journal of Engineering Mechanics, Vol. 116, No. 2, pp. 390-398.
89. **Zaitsev, O. I.** (1991). "*Calculation of the free surface of a flow on a concrete overflow dam or on a chute*", Hydrotechnical Construction (English translation of Gidrotekhnicheskoe Stroitel'stvo), Vol. 24, No. 9, pp. 586-588.
90. **Zhang, H.** (1984). "*Mathematical modeling of two-dimensional hydraulic problems using boundary-fitted coordinates*". M.Sc thesis. University of Montreal.